BOLU ABANT IZZET BAYSAL UNIVERSITY

THE GRADUATE SCHOOL OF NATURAL AND APPLIED SCIENCES

SYNTHESIS AND CHARACTERIZATION OF SOME GARNET MATERIALS USING SOL-GEL PROCESSING

MASTER OF SCIENCE

SEVAL KARAKUŞ

BOLU, AUGUST 2019

BOLU ABANT IZZET BAYSAL UNIVERSITY

THE GRADUATE SCHOOL OF NATURAL AND APPLIED SCIENCES

DEPARTMENT OF CHEMISTRY

SYNTHESIS AND CHARACTERIZATION OF SOME GARNET MATERIALS USING SOL-GEL PROCESSING

MASTER OF SCIENCE

SEVAL KARAKUŞ

BOLU, AUGUST 2019

APPROVAL OF THE THESIS

SYNTHESIS AND CHARACTERIZATION OF SOME GARNET MATERIALS USING SOL-GEL PROCESSING submitted by **Seval KARAKUŞ** and defended before the below named jury in partial fulfillment of the requirements for the degree of **Master of Science** in **Department of Chemistry, The Graduate School of Natural and Applied Sciences of Bolu Abant Izzet Baysal University in 19.08.2019** by

Examining Committee Members	**Signature**
Supervisor Prof. Dr. Ayşe MORKAN Bolu Abant İzzet Baysal University	.....
Member Assoc. Prof. Dr. Mecit AKSU Düzce University	.....
Member Assoc. Prof. Dr. Bahadır ALTINTAŞ Bolu Abant Izzet Baysal University	.....

Prof. Dr. Ömer ÖZYURT .....

Director of Graduate School of Natural and Applied Sciences

To my family

DECLARATION

I hereby declare that all information in this document has been obtained and presented in accordance with academic rules and ethical conduct. I also declare that, as required by these rules and conduct, I have fully cited and referenced all material and results that are not original to this work.

Seval KARAKUŞ

_____

ABSTRACT

SYNTHESIS AND CHARACTERIZATION OF SOME GARNET MATERIALS USING SOL-GEL PROCESSING
MSC THESIS
SEVAL KARAKUŞ
BOLU ABANT IZZET BAYSAL UNIVERSITY GRADUATE SCHOOL OF NATURAL AND APPLIED SCIENCES
DEPARTMENT OF CHEMISTRY
(SUPERVISOR: PROF.DR. AYŞE MORKAN)
(CO-SUPERVISOR: PROF.DR. AIVARAS KAREIVA)
BOLU, AUGUST 2019

In the first part of this study, $Ho_3Al_5O_{12}$ garnets were synthesized as undoped and doped with Eu^{3+}, Mn^{3+}, Fe^{3+} and Cr^{3+} metal ions in different molar concentrations of 0.10, 0.25, 0.50, 0.75, 1.00 by sol-gel technique. In the second part, the synthesis of undoped and doped with Eu^{3+} ion $Dy_3Al_5O_{12}$ and $Tb_3Al_5O_{12}$ garnets was succesfully done through sol-gel process using with 1,2 ethanediol as complexing agent. The two different heat conditions as 800˚C and 1000˚C were applied to the obtained gels for all products. In spite of heating at 800°C was not suitable temperature for the products, the reactions are monitored by sampling after 800˚C. However, all of these products showed that a single phase which has been occured at 1000˚C. The FTIR analysis indicated that the organic residues have flown after 10 hours and the typical vibrational bands of M-O bonds have been seen under $1000cm^{-1}$ for all products. The XRD patterns showed similar hkl values belong to the typical cubic garnet structures and the doping of the metal ions did not cause any change in the crystal structure of the monophasic host garnet materials. The products were found thermodynamically stable upon 900^oC by analyzing TG/DTA curves. The SEM studies showed that the lanthanide aluminum garnets were in the same plate-like shape, independently the nature of the lanthanides or doping agents of Eu^{3+}, Cr^{3+}, Mn^{3+}, Fe^{3+}. The presence of dopants was confirmed by EDX anaylsis. The optical properties of all products were determined by UV-vis/DRS technique.

KEYWORDS: Europium, Holmium, Dysprosium, Terbium, Manganese, Chromium, Iron, Aluminum, Garnets, Sol-gel Method, XRD, FTIR, UV, SEM

ÖZET

BAZI GARNET MALZEMELERİN SOL-GEL YÖNTEMİYLE SENTEZİ VE KARAKTERİZASYONU
YÜKSEK LISANS TEZI

BOLU ABANT İZZET BAYSAL ÜNİVERSİTESİ
FEN BİLİMLERİ ENSTİTÜSÜ
KIMYA ANABILIM DALI
(TEZ DANIŞMANI: PROF.DR. AYŞE MORKAN)
(İKİNCİ DANIŞMAN: PROF.DR. AIVARAS KAREIVA)
BOLU, AĞUSTOS - 2019

Bu çalışmanın birinci bölümünde, katkısız ve metal iyonları (Eu^{3+}, Mn^{3+}, Fe^{3+} ve Cr^{3+}) katkılı $Ho_3Al_5O_{12}$ garnetleri farklı molar konsantrasyonlarda 0.10, 0.25, 0.50, 0.75, 1.00 olarak sol-gel tekniği ile sentezlendi. Çalışmanın ikinci bölümünde, katkısız ve Eu^{3+} iyonu katkılı $Dy_3Al_5O_{12}$, $Tb_3Al_5O_{12}$ garnetleri; 1,2-etandiyol kompleksleştirici ajanı kullanılarak sol-gel metoduyla başarıyla sentezlendi. Bütün ürünler için, 800˚C ve 1000˚C olarak iki farklı ısı şartı, elde edilen jellere uygulandı. 800˚C 'de ısıtma örnekler için uygun sıcaklık olmamasına rağmen, reaksiyon 800˚C sonrasında örnek alınarak izlendi. Ancak, tüm numuneler 1000˚C 'de tek fazın oluştuğunu gösterdi. FTIR analizi, organik kalıntıların 10 saat sonra uçtuğunu ve M-O bağlarının tipik titreşimli bantlarının tüm ürünler için $1000cm^{-1}$ altında görüldüğünü göstermiştir. XRD desenleri, tipik kübik garnet yapılarına benzer hkl indis değerleri gösterdi ve metal iyonlarının katkısı, monofazik konak garnet malzemelerinin kristal yapısında herhangi bir değişikliğe neden olmadı. Ürünler TG/DTA eğrileri analiz edilerek 900˚C'de termodinamik olarak stabil bulundu. SEM çalışmaları, lantanit alüminyum garnetlerin, lantanitlerin yapısından veya dop ajanları olan Eu^{3+}, Cr^{3+}, Mn^{3+}, Fe^{3+} iyonlarından bağımsız olarak plaka benzeri şekilde olduğunu gösterdi. Katkı maddelerinin varlığı EDX anaylizi ile doğrulandı. Tüm ürünlerin optik özellikleri UV-vis/DRS tekniği ile belirlendi.

ANAHTAR KELİMELER: Evropiyum, Holmiyum, Disprosyum, Terbiyum, Manganez, Krom, Demir, Alüminyum, Garnetler, Sol-gel Metodu, XRD, FTIR, UV, SEM

TABLE OF CONTENTS

Page

LIST OF FIGURES

Page

LIST OF TABLES

Page

LIST OF ABBREVIATIONS AND SYMBOLS

Cr:YAG : Chromium doped Yttrium Aluminum Garnet

Cr:GGG : Chromium doped Gallium Gadolinum Garnet

Cr:YSGG : Chromium doped Yttrium Scandium Gadolinum Garnet

DAG : Dysprosium Aluminum Garnet ($Dy_3Al_5O_{12}$)

DLS : Dynamic Light Scattering

DRS : Diffuse Reflectance Spectroscopy

EDX : Energy Dispersive Using X-Ray (Analysis)

Eu:YAG : Europium doped Yttrium Aluminum Garnet

FTIR : Fourier Transform Infrared Spectroscopy

Fe:YAG : Iron doped Yttrium Aluminum Garnet

HAG : Holmium Aluminum Garnet ($Ho_3Al_5O_{12}$)

Ho:YAG : Holmium doped Yttrium Aluminum Garnet

IAG : Iron Aluminum Garnet

IR : Infrared Spectroscopy

LEDs : Light Emitting Diodes

Lu:YAG : Lutessium doped Yttrium Aluminum Garnet

Nd:YAG : Neodmium doped Yttrium Aluminum Garnet

SEM : Scanning Electron Microscopy

Tb:YAG : Terbium doped Yttrium Aluminum Garnet

TAG : Terbium Aluminum Garnet ($Tb_3Al_5O_{12}$)

TG/DTA :Thermogravimetric/Differential Thermal Analysis

UV-vis : Ultraviolet visible

XRD : X-Ray Diffraction

YAG : Yttrium Aluminum Garnet ($Y_3Al_5O_{12}$)

YAM :$Y_4Al_2O_9$,Monoclinic

YAP : $YAlO_3$, Perovskite

YGG : Yttrium Gallium Garnet ($Y_3Ga_5O_{12}$)

YIG : Yttrium Iron Garnet ($Y_3Al_5O_{12}$)

ACKNOWLEDGEMENTS

I wish to express my deepest gratitude to my supervisor Prof. Dr. AYŞE MORKAN and co-supervisor Prof. Dr. AIVARAS KAREIVA for their guidance, advice, criticism, encouragements and insight throughout the research.

I would like to thank Prof.Dr. A. KAREIVA's Sol-gel Group Members for their suggestions and comments and helpfulness and also appreciative for Erasmus Program for having a student & internship experiences, in Vilnius University.

I would also like to special thanks to my mother Saniye KARAKUŞ, my father Ertuğrul KARAKUŞ and my sister Nihal BULUT for their encouragement, patience and all supports of them on whole my educational and special life who offer a nest full of love and confidence.

Thank you very much to my dear friend who was with me in every time during my thesis preparation period of my life.

1. INTRODUCTION

1.1 Garnets

Garnets are substances that are used as precious stones or abbrasive matters since bronze age. They are come under the category of oxide crystals and generates a part of silicate minerals. Although they could have different chemical properties, the physical view of most garnets likely the same yet presence in different colors (Nivaldo J. T., 2014).

The 'Garnet' name comes from a Latin word that granatus. Since, the shape and color of the mineral seems like the red seeds in a pomegranate, German theologian and philosopher Albrecht von Bollstädt (1193 – 1280) was first used the name as garnet (Galoisy, L., 2013).

1.1.1 Resources of natural garnets

Garnet sources are known in Australia, Canada, Chile, China, the Czech Republic, India, Norway, Pakistan, Portugal, Russia, South Africa, Spain, Sri Lanka, Thailand, Turkey, and the Ukraine. Garnet mines and presences are found in 21 states, but the only presently active mines are in northern Idaho (one mine), southeastern Montana (one mine), and eastern New York (two mines) (Evans, J. G. et al., 2006).

1.1.2 History of garnets

Since bronze age, the people uses garnets in different ways depending on its specific properties. Most of garnets are transparent, colorful and durable with its relative hardness around 6.5-7 on Mohr scale. Therefore, there is a sign from ancient Romanian and Egyptian peoples are prefered to use at their ornaments. (Clark, G. & Clark, J. G. D., 1986). Esspecially, red garnets have been using still as jevellery since from biblical times to the present day as known.

1.1.3 Industrial uses of garnets

Commercially abbrasive garnets was first used as coated sandpaper in 1878. United States consumes about 16 percent of global production of industrial garnet for use in abrasive airblasting, abrasive coatings, filtration media, waterjet cutting, and grinding. Therefore, the domestic garnet production has decreased and imports have increased as much as 60 percent of the garnet by time. U.S industrial garnet production for the years 1894-2002 has accelerated increase graph. The main import countries was firstly India, China, and Australia but Canada joined the list of suppliers in 2005 (Evans, J. G. et al., 2006).

Besides, the main significant importance of the garnet type crystals is in high technology industry. Scintilator garnets has become a central issue as to be used in fiber-optic communications, opto-electronical devices, variety of lamps, optical amplifiers, cathode-ray tubes and TV screens, data storages, light-emitting diodes, electroluminescent and medical applications (Kareiva, A., 2011; Hirata, G. et al., 2005; Skaudzius, R.et al., 2012).

As an example of lasers uses of medical application in urology , Ho-YAG laser lithotripsy uses for stone diseases in kidneys with having very big advantages comparing other techniques of other devices such as ultrasound, electrohydrolytic, pneumatic or other lithotripters. (Jou, Yeong-chin, et al., 2005; Jou, Yeong-chin, et al., 2007).

1.1.4 Crystal structure of garnets

The general cubic garnet crystal formula is $X_3Y_2Z_3O_{12}$ where the position is occupied with X dodecahedral site, Y octahedral site and Z tetrahedral site. The symmetry can show slight differences from the main space group which is Ia3d (O_h^{10}) (Armbruster,T., 1992).

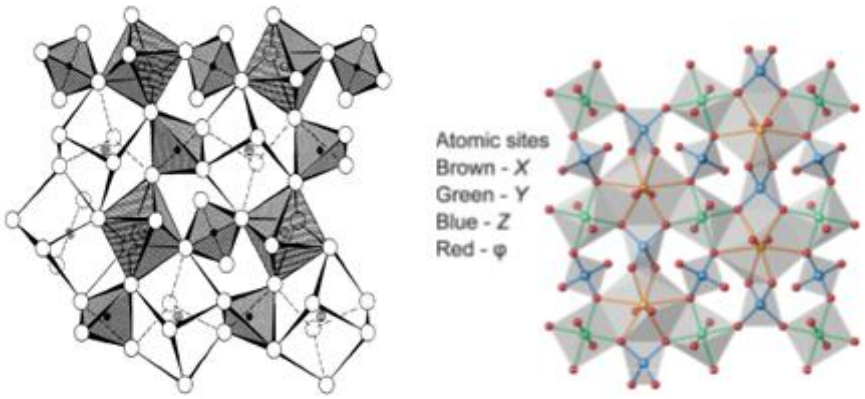

Figure 1. The examples of crystal structures of garnets (Novak, G. A. and Gibbs, G. V., 1971; Bishop, A. et al., 1999).

Silicate garnets (where Z=Si) are divided into two groups as ugrandites and pyralspites.

Ugrandite types are when X = Ca, made up of end-members uvarovrite $Ca_3Cr_2Si_3O_{12}$, grossular $Ca_3Al_2Si_3O_{12}$, and andradite $Ca_3Fe_2Si_3O_{12}$, and intermediate compositions.

Pyralspite types are when X ≠ Ca, with end-members pyrope $Mg_3Al_3Si_3O_{12}$, almandine $Fe_3Al_2Si_3O_{12}$, spessartine $Mn_3Al_2Si_3O_{12}$, and also all intermediate compounds. Garnets of end-member composition are rare. Other rock-forming garnets pertinent to this study are goldmanite $Ca_3V_2Si_3O_{12}$ and knorringite (=hanleite) $Mg_3Cr_2Si_3O_{12}$ (Novak, G. A. & Gibbs, G. V., 1971).

The reason that garnets seems very beautiful to use as jevellery is its crystalline structure.

1.1.5 Types of garnets

Garnets refer to a group of several closely related minerals. Contrary to other minerals with special chemical compositions, the composition of garnets change. There are 6 main garnet groups, each with its own chemical composition and color range. These 6 classifications are almandine,pyrope, spessartine, grossular, andradite, uvarovite.

1.1.6 Variety of garnets

Garnet diversity is increased by adding the elements, whose atomic diameters are close to each other in perovskite crystal structure by no change in unit cells . This diversity brings with different names of garnet supergroups. A classification of the thirty two species of garnet supergroup and such examples for former formulas and end-member formulas are given in tables of introduction part of Grew, E. S. et al (2013) study.

Therefore, using different elements, the garnet crystals can be produced in the laboratory by chemical reactions and can be varied for different purposes (Grew, E. S. et al., 2013).

1.1.7 Garnets as metal oxides

Aluminum oxides form a large and important part of oxide garnets. YAM ($Y_4Al_2O_9$), YAP ($YAlO_3$) and YAG ($Y_3Al_5O_{12}$) are examples of aluminum oxide crystallines (Li, X., 2004). The garnet structured almandine, spessartite, pyrope and grossularite include aluminum element in their cubic system. Esspecially, YAG is investigated by its laser uses to improve. YAG is known also with its the best creep - resistant fiber knit (Wilson, D. M., 2001).

Beside, andradite has iron and iron includes garnets show very specific magnetic properties . From 1970's until today , the scientists have been still producing iron or aluminum garnets to improve their special properties in terms of magnetism and optical studies (Novak, G. A. & Gibbs, G. V., 1971).

1.1.7.1 Magnetism of iron garnets

In 2003, Chul Sung Kim et al. investigated the distirubutions of Fe^{3+} and Al^{3+} ions in different molar ratios of $Y_3Fe_{5-x}Al_xO_{12}$ crystal by synthetizing from sol to have special magnetic nanocrytallines (Kim, C. S., 2003). Similarly, Garskaite, E. et al. (2006) studied on the synthesis of YIG and YAG in terms of formation and magnetization properties . Since, the magnetization has affected to the growth of garnet structure, they have pointed out YIG formation has not proceeded likely the

same YAG crystal formation in exactly the same process application. In another interesting study about magnetism on $BiY_2Cr_xFe_{5-x}O_{12}$, in spite of the presence of chromium ion had no effect on the crystal structure sizes, but the magnetization has influenced. The magnetization is increased when $x<0.1$ and Ms is decreased when $x>0.1$ (Dong, B., 2007). Likewise this studies, many studies are published also demonstrated that garnets are used depending on their magnetic properties.

1.1.7.2 Optical properties of aluminum garnets

Rare-earth doped lanthanide garnets have high optical band gap. As like YAG, LuAG is also known a good host material with high hardness and mechanical stability. Eu doped LuAG with a wide optical band gap of 6.1eV, is used with Xe discharge lamps and plasma displays to give excellent radiation, similarly the other dopants of lanthanides as activators. LuAG doped with Ce^{3+} is such a kind of high efficient scintillator. Also, $Yb_3Al_5O_{12}:Cr^{4+}$ is up and coming high efficient system in tunable laser (Dubnikova, N. et al., 2011).

1.1.7.3 Electrical stability of aluminum garnets

If it needs to give an example to show one more well property of the garnet type crystals; the studies shows also that the electrical activity of YAG can be seen at around 800˚C. This means the crystals shows resistance to electrical current flow until 800˚C, so it is stable material against electric charges (Kuklja, M. M., 2000).

1.1.8 The effects of impurities on crystal structure

The lanthanide Eu^{3+}, Tb^{3+}, Ce^{3+} ions are known their emission spectra for visible radiation region. These doping agents approachs through D_{2h} symmetry to be placed in a crystal structure. As a reason of one site reunion, the energy transfer cannot occured between dopants that causing non-radiative transitions. (Hreniak, D., 2004).

However, the locations of doping metal ions are stable in the crystal cubic system , sometimes such kind of distortions can be seen in the crystal structure because of anti-positioning of metals. Therefore, when the crystal is used for host

lattice of a laser, it may cause to wrong distrubution energy or slipping color centers.

Therefore, the defect formation energies are calculated by Kuklja, M. M. et al. (2000). Another important practical implication is that the defect or distortion can be occured by doping metals into semiconductors (such as $Li_5La_3Ti_2O_{12}:Eu^{3+}$). It can give lead instantaneous peaks of optical absorption edges. Since, oxygen vacancies which are induced by Eu^{3+} act like donor under conductivity band to have more optical absorption energy (Zhang, S., 2018).

1.2 Backward overview

1.2.1 Improving of the synthetic garnets for high technology

In 1978, Guillot and his friends, determined that the molecular field coefficients and the compensation temperatures of Tb, Dy and Ho doped YIG. Doping different metals could be cause the thermal evolution or discontunity of crystal lattice however, the study shows that all the results were overlapped with magneto-optical properties of undoped garnet structure (Guillot, M. et al., 1978).

In 1998, the investigation has been realized that the absorptivity of chromium ions in Cr:YAG, Cr:GGG , and Cr: YSGG in terms of peak power density and the Cr:YAG shows linear transmission neither Cr:GGG nor Cr:YSGG. The steadiness is important specification to use this material in opto-electronic devices (Burshtein, Z. et al., 1998).

Two years later, Ho:YAG was synthetized and excitated to have the absorption and emission spectra and its optical transitional properties are explained by Malinowski M. et al. (2000). Choosing holmium is since it was well known the Ho ions could create laser emissions within limit 2 and 2.9μm from previous studies. Surprisingly, the atomic size of Ho with $[Xe]6s^24f^{11}$ configuration is almost same with Y, which is more lighter than Ho atoms with the likely same physical properties with $[Kr]4d^15s^2$ configuration due to the fact that the effective nuclear charge is increasing with atomic numbers. Therefore, the absorption spectrum of 2% Ho^{3+} doped of YAG is investigated and shared in terms of the electron orbital transitions by having the spectrum patterns, as well.

Also, in this study, the life-time of Ho:YAG have been measured to compare with relative host crystals which contains Ho^{3+} ions and the study shows that the life -time depends on the host crystal. Eventually, after the results are examined , the Ho^{3+} with aluminum garnet has the shortest life-time among relatively similar host oxide crystals (Malinowski, M. et al., 2000).

Eu^{3+} is preferred as luminescent ions as well as Ho^{3+} ions in crystal definition studies. In 2002, Eu:YAG has produced and sintered at 1200˚C by simple combustion method in different amounts using of urea as fuel. The Eu:YAG phosphor nanoparticles showed simple single cubic perovskite garnet XRD patterns in nanoscale particle dimentions (Shikao, S. & Jiye, W., 2001).

By the way, Nd:YAG studies were continuing, which had been done first in 1995. It has been known that Nd:YAG is a good material which has good optical properties within the best ground that is YAG. YAG is a main base magneto-optical crystal that is employed as host material to be dope with Nd. Therefore, the studies are focusing on ways of doping such metals to YAG for improving magnetical or optical properties of the materials are going to be produced in studies, recently.

So, in 2002, there is a good study that is predicted the ceramic type of Nd:YAG is also be able to use as a laser host material instead of well known single crystal of Nd:YAG, as because to obtain more economical lasers.

This paper shows that there is so little difference between ceramic Nd:YAG and single crystal Nd:YAG in terms of output energy of a laser and optical inversition. Until this time, Toshiba Corporation has found the remarkable ceramic nanocrystalline material that has 1.46kW output energy and optical-optical convertion efficiency is 42% , where the single crystal Nd:YAG has 1.72kW energy and the optical-optical convertion efficiency is 49% . Although single crystal laser shows still the best efficiency, the point is that the transparent ceramics are ready to use in industry as well as single crytals in more cheaper way respecting to the way of producing single crystal.

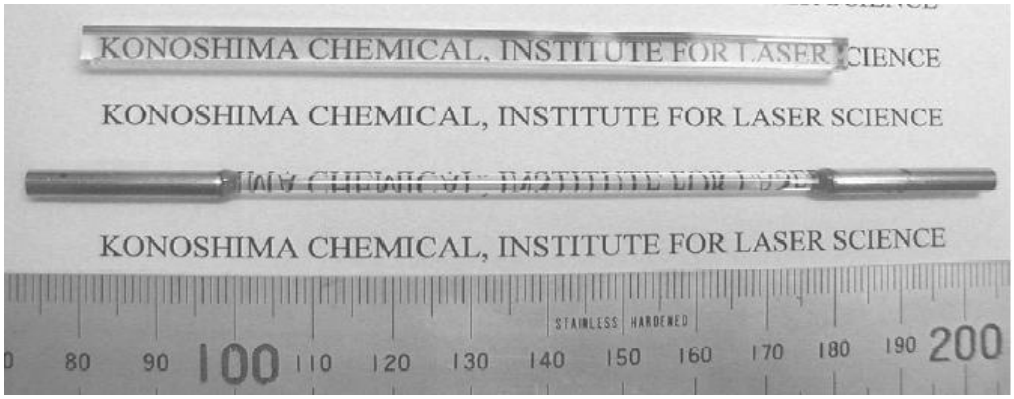

Figure 2. A capture from ceramic type Nd:YAG as a laser rod

The ceramic Nd:YAG was obtained by using aqueous solution to obtain the crystal growth with an easy production method. As stated in the study, the comparison of raman shifts and laser powers of single crystal and ceramic YAG samples indicates that, there is so little difference between single crystal and ceramic Nd:YAG (Lu, J. et al., 2002).

In addition, in 2004, it is tabled that the similarities between single and ceramic YAG, there was almost no difference (Kumar, G. A. et al., 2004).

Then, Chroma M. et al. (2005) stated that synthetic metal-alumunates are be able to synthetize with aqueous sol-gel route with ethane-1-2-diol complexing agent at 1000˚C.

Therefore, transparent ceramic production has got the importance with less expensive aqueous methods than the relative single crystals production.

1.2.2 Importance of production methods

Vaqueiro P. & López-Quintela M. A. (1998) pioneered the first aqueous sol-gel synthesizing method accompanied by citric acid to obtain single phase YAG and they predicted there was no occurance of other oxide phases of $YAlO_3$ or $Y_4Al_2O_9$. In this study, citrate gel method is used and metal-nitrates were used as starting agents. Unlike, to follow a way with glycolate sol-gel method the metal-acetates were selected in this study. Using of metal-nitrates as starting agents was efficient.

The other parameters are also important as much as choosing starting materials. In sol-gel processing, the pH of starting solution, the type of ligand that to be used as complexing agent, the passing time of gelation, and annealing temperature are significant to obtain monophasic crystals at the end of the process (Kareiva, A., 2011).

Likewise, Hreniak, D. & Strek, W. (2002) produced Nd:YAG with sol-gel method, in 1998, YAG:Eu is synthetized by sol-gel method and the single crystal was obtained at 1000°C. However the relevant crystals had been obtained before at higher temperatures than 1000°C with solid state method. According to the advantages of sol-gel method, obtaining the crystal structure needs less energy to be occur (Ruan, S. K. et al., 1998).

In another way of producing of YAG and Eu:YAG has been tried with citrate gel method, in 2002. Zhou, Y. H. et al. (2002) stated that the sintering temperature should be higher than 1200°C with citrate-gel method to obtain more brightness YAG, causing from carbon presence.

Jun-ji Zhang et al., synthetized Tb:YAG with nitrate-citrate sol-combustion method, succesfully by sintering above 1200°C. (Zhang, J. J.et al., 2003a). Jun-ji Zhang et al. (2003) were known that the solid state reaction method requires high temperatures in long time period and ball milling process also causes impurities and defects in needed structure to be obtain (Zhang, J. J. et al., 2003b).

As like pointed out above, many methods has been used to obtain cubic garnet crystals: solid state reaction, sol-gel method, citrate-gel method, co-precipitation, hydrothermal method Zhou, Y. et al. (2002) , sol-combustion Shikao, S. et al. (2001), ultra-sound microwave assisted method Si, W. (2014) and so on .

Comparing both mostly using solid state method and sol-gel method in terms of the synthesis efficiency, one article is published about the differentiates between both to show that the sol-gel synthetized Eu:YAG has lower syntetization temperature than the Eu:YAG synthetized with solid state method. Also, the Eu :YAG synthetized with sol-gel method has lower particle sizes than considering solid -state reaction synthetizated Eu:YAG. The smaller sized particles means having

more crystallinity and more distrubution of activators . Later on, the photoluminesce properties of the produced crystals are compared. The Eu:YAG which is synthetized with sol-gel method shows better photoluminesce properties than that of solid-state Eu:YAG. At the end, it is predicted that the photoluminesce properties depends on the morphology and particle size belongs to synthesis method (Hsu, W. T., 2003). So, it has been shown that the sol-gel method is really better way to synthesis garnet type of photoluminescent crystals than the other methods.

1.2.2.1 The steps to be care in sol-gel method

1.2.2.1.1 Metal-nitrate/Acid ratio

It has conclusively been shown that the metal nitrates - acid ratio has a significant importance of the crystal forming temperature for sol-gel auto-combustion method. According to study of Vajargah, S. H. et al. (2007) , using metal nitrate: citric acid ratio (MA/CA) lower than 1, the crystal formation temperature of YIG was around 800˚C, whereas the metal nitrate: citric acid ratio upper than 1 it causes the crystal formation temperature greater than 900 ˚C.

Despite this , starting with homogeneous amorphous gel at the beginning plays the critical role with following sequent pyrolysis and then, having high-quality gel powders (Leleckaite, A. & Kareiva, A., 2004).

1.2.2.1.2 Complexing agent

By Muliuoliene, I. et al. (2003) , the $Y_3Al_5O_{12}$ (YAG), $Y_3Sc_2Al_1Ga_2O_{12}$ (YSAGG-3212), $Y_3Sc_1Al_3Ga_1O_{12}$ (YSAGG-3131), $Y_3Sc_2Al_3O_{12}$ (YSAG), $Y_3Al_3Ga_2O_{12}$ (YAGG), and $Y_3Sc_{2.5}Ga_{2.5}O_{12}$ (YSGG) are produced with an efficient complexing agent of ethylene glycol by sol-gel method to have sort of alternative laser in-use crystals. After that, among the scientists, who are using sol-gel method to have garnet crystals, using ethylene glycol has been become common trick to obtain ease gelation.

A. Kareiva et al. is also investigated esspecially the complexing agent factor on $Y_3Ga_5O_{12}$ that treated with 6 different complexing agent ; tartaric acid, 1-2 ethandiol, citric acid, EDTA, malonic acid and oxalic acid. $Y_3Ga_5O_{12}$ that

synthetized with the first fourth were homogeneous, however malonic and oxalic acid was not successful and gave different molar ratios of metals with polyphasic crystal yield (Leleckaite, A. & Kareiva, A., 2004).

1.2.2.1.3 Temperature

Sol-gel method never needs extreme conditions in terms of high temperature furnaces comparing with ceramic method for sintering. Most scientist studied at not much higher than 1000˚C to have complex oxide grains . The only disadvantage comes from about the temperature in sol-gel method that the temperature treatment can be cause to be occur of mixtures instead of single phase. Leleckaite, A. & Kareiva, A. (2004) obtained $3LaAlO_3{:}Al_2O_3$ mixture instead of $La_3Al_5O_{12}$.

However, one year later, again Leleckaite, A. & Kareiva, A. et al. (2005) demonstrated that $Y_3Ga_5O_{12}$ can be synthetized with sol-gel method in single phase at 1000˚C. They used tartaric acid as used to be complexing agent and the heat conditions were applied at 1000˚C for 10 hours.

1.2.2.1.4 Summary

In conclusion, sol-gel synthetization is very easy to apply by comparing other methods to have more homegeneous nano-sized structured crystals. In sol-gel method, there is many serious advantages. In begining, sol-gel method starts with high reactive materials and in general, it can be easily apply in aqueous solution to obtain inorganic nanocrystallines. It is good reason to use sol-gel method to have easily composition-controllable sol without need expensive laboratory materials or equipments at around 100˚C. After having sol, the sample is sintered in a furnace at relatively low temperatures, with low cost and low energy in considering to compared of other techniques, at around 1000˚C (Dubnikova, N., 2011).

1.2.3 Literature survey for doping agent ions (Eu^{3+}, $Mn^{2+/3+/4+}$, Cr^{3+}, Fe^{3+})

1.2.3.1 Literature survey for the europium ion (Eu^{3+}) including oxides

Al_2O_3 was doped with europium (Eu^{3+}) by coprecipitation method. All the XRD results shows amorphous structure. SEM images were like expected before and

according to the EDX results the oxygen amount is in remarkable amount. The XRD results shows mostly amorphous lining-up of cubic cells. (Esparza-García, A. E., et. al., 2002).

$Gd_3Ga_5O_{12}$:Eu^{3+}, Tb^{3+}, Er^{3+} structures were synthesized by sol gel method as determined with morphological studies of XRD, TEM and FTIR, succesfully. Therefore, the synthesized crsytals showed the electron transitions of the dopants as expected by additioning of the luminescent ions into the formula. (Pang, M., & Lin, J., (2005).

The luminescent ions which are Eu^{3+}, Tb^{3+}, Tm^{3+}, Er^{3+} and Yb^{3+} doped into Y_2O_3. The morphological investigation is realized by X-ray diffraction and TEM to detect the rounded-shape grains. The luminescent properties and the decay times that related order with the doping concentrations are investigated. These emissions were proper to improving up infrared cards, code-cards and may be bio sensors (Anh, T., et al., 2007).

Eu^{3+} and Tb^{3+} doped cubic garnet $YAlO_3$ is synthesized with sol gel method. Both doping agent sample has short and long lifetime components. The long lifetime component is higher than the equivalent YAG crystal and equivalent ortorhombic $YAlO_3$ (Zatryb, G., et al., 2013).

YVO_4/Y_2O_3 composite phosphor is doped with Eu^{3+} and Bi^{3+} , then the optical properties are examined. After doping, the sample showed green, blue and orange emissions. However, by changing the molar ratios in between YVO_4 and Y_2O_3 the white led light was observed (Wang, D. et al., 2015).

The Eu^{3+} doped lanthanide (Er, Tm, Yb, Lu) aluminum garnets are synthesized with aqueous sol-gel method. The morphological and the optical properties of these samples was examined. The samples were in single phase according to the XRD results and these results are supported by the FTIR spectroscopy results, as well. The morphology investigation is done with TEM and according to the images these particules were in nano-scale range. The most luminescent sample was $Lu_3Al_5O_{12}$, whereas the other samples did not show any luminescent properties (Pavasaryte, L., et al., 2019).

1.2.3.2 Literature survey for the manganese ion (Mn^{3+}) including oxides

The crystal of $CdSiO_3:Mn^{2+}$ was synthesized in different ratios of manganese ions to obtain and take the advantages of high electron transitions of the outermost energy level $3d^3$ of Mn^{2+} ions, which were introduced to the host crystal $CdSiO_3$, with sol-gel method. The sol-gel method was applied in aqueous form. The sol was acidified with HNO_3, dried about 60˚C and finally the samples were calcined at 1050˚C for 10 hours. Later, three other elements were RE (Tb,Nd,Eu) doped into $CdSiO_3:Mn^{2+}$ with the same sol-gel method. All the sample's XRD results are matched with undoped $CdSiO_3$. The samples were obtained succesfully in simgle phase. Then, the photoluminescence and thermoluminescence properties are investigated. The best efficient sample was $CdSiO_3:Mn^{2+}:Eu^{3+}$ in terms of the highest intensive emission energy and the longest emission time, remarkably (Qu, X., et al., 2012a).

$CdSiO_3:Mn^{2+}:Eu^{3+}$ was synthesized and obtained in single phase with sol-gel method. The decay speed of afterglow was compared with solid state produced sample. The results showed that the sol-gel prepared sample particles was slower than the samples are prepared with solid state reaction in terms of the decay speed of afterglow (Qu, X., et al., 2012b).

The phosphate glass was doped with each three Tm^{3+}, Tb^{3+} and Mn^{2+} ions with melting quenching method. Then, the luminescence properties were investigated. The results showed that the molar increasing of manganese ions in samples, increases the efficiency of the luminescent properties of the samples (Zhong, H. J., et al., 2015).

Al_2O_3 was alloyed with an impurity of manganese ions and the optical properties of the aluminum oxide have been examined. Since, the manganese electron shell and the oxygen vacancies, the distortions were occured on the crystal structure with the addition of the manganese ion. Therefore, the decrease in photoluminescence intensity was observed for α-Al_2O_3 (Gasenkova, I. V., et al., 2017).

The aluminum oxide (Al_2O_3) was doped with manganase ions by solution combustion method. According to the manganese ions oxidation state, the crystal structure was changed. The Mn^{2+}/Mn^{3+} ions inside of the crystal caused to the phase transitions of Al_2O_3, however the most of Mn^{4+} ions are exchanged and showed its presence in octahedral Al positions in the crystal structure. (Berezovskaya, I. V., et al., 2018).

1.2.3.3 Literature survey for the chromium ion (Cr^{3+}) including oxides

Pure perovskite structured $YAlO_3$ (YAP) was synthesized and doped with chromium by exchanging with Al of the crystal formula; $YAl_{1-x}Cr_xO_3$, where x=0, 0.035, 0.135, 0.250, 0.500, 0.750. The combustion was existed at around 270˚C and 440˚C of the two-step reaction, respectively. To avoid any occurance of YAM or YAG, the calcination was realized with fast acceleration of the temperature up to 1100˚C, rapidly. In result, complete pureness was obtained of $YAlO_3$ (YAP), perfectly (Blosi, M., et al., 2009).

Al_2O_3 was doped separately with chromium and vanadium. Undoped Al_2O_3, Al_2O_3:V and Al_2O_3:Cr all three samples are investigated by XRD, SEM, electron density distrubutions. All the results were overlapped and doping process was succesful (Thirumalaisamy, T. K., et al., 2011).

According to this structure $Al_{2-x}Cr_xO_3$, chromium was doped into aluminum oxide in 0.1, 0.2 and 0.3 molar ratios. The XRD patterns showed that the doping of chromium does not cause any change in the host crystal of Al_2O_3, however the conductivities were increased with doping amount of Cr. This result was supported by UV results band gap constriction (Badar, N., et al., 2014).

$Y_3Ga_5O_{12}$ pellet was prepared with sol-gel method by doping Cr^{3+} in 8.7% molar ratio. The pellets are sintered in different temperatures of 1000˚C, 1200˚C, 1300˚C and 1400˚C to obtain YGG:Cr samples. The ceramic samples were sintered by getting well when the heating temperature is increased; less porous surfaces and high crystallinity was detected and proved with XRD and SEM results at high tempered pellets. Then, the UV measurement results showed that the emission peaks were at visible region (Zabiliūtė-Karaliūnė, A., et al., 2015).

1.2.3.4 Literature survey for the iron ion (Fe^{3+}) including oxides

Mullite, having the formula $3Al_2O_3.2SiO_2$, was doped with iron by sol-gel combustion method. After 4-hour heating at 800˚C of the undoped sample, the XRD results showed an amorphous crystallinity. The undoped sample pellets heated up again for 4 hours to 1550˚C temperature and the XRD results showed an orthorhombic mullite. The XRD and SEM results showed that after doping iron, the crystallinity was got high and the grain sequences ordering which occurrs smooth surfaces had also become high. However, the Fe^{3+} doped samples were crystallized around 1200˚C which is less than 1550˚C. Addittionally, the density of the iron doped sample increased which supported by SEM images that showed tightly packed grains.(Ilić, S., et al., 2014).

$BiFeO_3$ was synthesized and characterized and later, the $BiFeO_3$ sample was also prepared to be Al doped, according to the crystal formula of $BiFe_{1-x}Al_xO_3$. For doping process, sol-gel method was used, where x=0, 0.1, 0.2, 0.3 and 0.4. The synthesized $BiFeO_3$ sample was used to coated the mica-titania surface. The XRD results of doped samples showed good aggreement with the single phases XRD data of mica and titania. The doping was succesful. Moreover, BiFeO3 was shown a good application onto surface of mica-titania, uniformly according to the SEM results. The morphology was still likely the same with un-coated mika-titania (Yuan, L.,et al., 2017).

$Li[Ni_{0.6}Mn_{0.2}Co_{0.2-x}M_x]O_2$ was synthesized, where x=0 and 0.05 and M= metal ions that are Al, Fe and Sn to obtain good cathode material. The X-ray diffraction patterns matched with the theoretical undoped crystal for all doping agents, consistently (Eilers-Rethwisch, M., et al., 2018).

1.2.4 Some garnet-structured luminescent materials

During the past years, the cubic garnets not only takes place in lasers as focusing agent but also, they are takes place in LED's, as a luminescent phosphor materials, as well. This specially producted bright crystals has given some advantages in-use such as low power energy with obtaining high emissions in case of efficiency and having long life-time (Marius, M. et al., 2014).

More recent attention has focused on the provision of the trivalent lanthanide ion doped garnet phosphors, through their luminecent properties depending on particle size attributions (Vetrone, F., 2005).

1.2.4.1 Ce doped scintillators

There have been a number of longitudinal attractive studies involving Ce^{3+} that reported of its luminescent properties in garnet structured crystals.

$Y_3Al_5O_{12}:Ce^{3+}$ is most known and common crystal as using of yellow emitting phosphor. The electronic transition of Ce is odd $4f^1$ $5d^1$ adsorp the light between 450-470 nm , and emits 510- over 600nm as a broad band. This red-yellow emitter can be use with a blue light emitter LED chip together to obtain white LED (Marius, M. et al., 2014; Katelnikovas, A., 2007).

Therefore, Yi, X. et al. (2014) have Ce:YAG and Ce,Cr:YAG bringed up together with Ce,Cr:YAG prepared in different ratio of Cr^{3+} as to be dual-layer Ce:YAG/Ce,Cr:YAG of blue and red-yellow emitters to have white LED, ideally. The white LED's are prefable due to their long life-time and high efficiency.

1.2.4.2 Eu doped scintillators

Eu^{3+} ions are known as red emitting phoshors, (Hreniak, D., 2004). Eu^{3+} ions in aluminum oxide takes place in low symmetry sites, while demonstrating emission with f-f ($4f^6$) transition (Hirata, G., 2005).

The excitation of Eu can be realized at 273 nm of Eu^{3+}- O^{2-} bond for citrate-gel produced Eu:YAG, however the major excitation peak for this crystal is at 395nm belongs to $^7F_0$-L_6 transition. This excitation peak corresponds to emission peak of $^5D_0$-$^7F_2$ transition that indicates the red emission (Zhou Y., 2004).

However, when Eu^{3+} doped into $Y_3Al_5O_{12}$ and $Lu_3Al_5O_{12}$, green and blue scintillation colors are observed under UV light, respectively (Sugiyama, M., 2012).

1.2.4.3 Dy Doped Scintillators

Li, J., et al. (2013) synthetized of $[(Gd_{1-x}Lu_x)_{1-y}Dy_y]_3Al_5O_{12}$. The findings suggests that the results of fluorescence life-time measurements demonstrated the life-time not much effected depending on concentration of Lu ions however, strongly effected by Dy ions.

1.2.4.4 Tb Doped Scintillators

Tb^{3+} is known as green region emitter and can only occupies with D_{2h} symmetry which blocks energy transferring between dopants thus causes a decrease in luminescence efficiency (Hreniak, D., 2004).

1.2.4.5 Cr Doped Scintillators

The fluorescence properties of Cr^{3+} YAG phosphors with different impurities such as Cr^{3+} ion can be rise by increasing synthesis temperature (Matsubara, I., 2000). At 690 nm, Cr^{3+} shows emission peak corresponds to its ^2E_g-$^4A_{2g}$ transition (Yi, X. et al.,2014).

1.2.4.6 Mn Doped Scintillators

$Y_{2,99}Mn_{0.01}Al_5O_{12}$ is synthetized and luminescence properties are investigated by Singh, V. et al. (2010). According to the photoluminescence spectrum measurements, at 519 nm green emission peak was observed due to $^4T_{1g}$ (G) - $^6A_{1g}$ (S) transitions of $3d^5$ level Mn^{+2} transitions.

1.2.4.7 Fe Doped Scintillators

Actually , there is only a few current study about the photoluminescence spectroscopy of iron garnets. Since, Fe^{3+} ions has bigger atomic size than Y in YAG, also with the bad magnetism effect, it tooks places of oxygen atoms in the garnet structure. Therefore mostly good magnetism properties of YIG and IAG attracts attention. However the studies of luminescence properties of Fe:YAG demonstrates

that the crystal samples has giving such peaks around 407-405 nm (Dong, D., 2005; Garskaite, E., 2006).

1.2.5 Focusing on other impressive studies

The ferrimagnetism of iron garnets is more problematic than aluminum garnets due to the closed shell of Al^{3+} ions with a non-magnetic state in RE aluminum garnets. By focusing on general cubic garnet-type crystals formula of $X_3Y_2Z_3O_{12}$ where X dodecahedral, Y octahedral and Z tetrahedral occupation , the aluminum garnets are prefable for non magnetic applications by replacing both O_h and T_d sites of this cubic garnet structure (Nagata, S. et al.,2001).

The replacement atoms in X position, without disrupting the garnet crystal structure is investigated with replacing Lu atoms by increasing molar concentrations of Y instead. $Lu_3Al_5O_{12}$, $Lu_2YAl_5O_{12}$, $Lu_{1.5}Y_{1.5}Al_5O_{12}$, $LuY_2Al_5O_{12}$ and $Lu_3YAl_5O_{12}$ are synthetized. The comparisons of the physical properties of each material samples showed very smooth and linear increase or decrease. The crystal formation temperature is increased due to atomic size increasing where the Lu atoms exchanged by higher amounts of Y in terms of molar concentration. Also, the heat capacity, heat diffusivity and thermal conductivity are increased in order, while the refractive index is decreased, where the molar concentration of Y is increased in structure (Yasuhunio Kuwano et al., 2004).

$Ho_3Al_5O_{12}$, which is an aluminum garnet crystal, is produced by flux method with a lattice constant (a) = 12.026 Å at room temperature. $Ho_3Al_5O_{12}$ is investigated where Ho^{3+} ions occupies X dodecahedral sites and Al^{3+} ions occupied of both Y and Z (octahedral-tetrahedral sites) to proof the specific heat anomaly at low temperature. Normally, $Ho_3Al_5O_{12}$ shows two sharp specific heat peaks at 0.839K and 0.220K. Nagata, S., et al. (2001) stated that the anomaly may be caused by Ho^{3+} in $^5I_8$ state. (Nagata, S. et al.,2001). The outspread electronic configurations of lanthanides and d-block transition elements offers a variety of electronic transitions due to their different atomic energy levels. This is fruitful to have them using up as fixture material in optical devices due to having different emission energies as colourful lights in different wavelenghts.

2. AIM AND SCOPE OF THE STUDY

In the first part of the study, undoped and Eu^{3+} doped holmium aluminum garnet, dysprosium aluminum garnet and terbium aluminum garnet are prepared in different molar ratios. Moreover, the transition elements which are manganese, iron and chromium are used as doping agents in various molar ratios to synthesize transiton elements doped holmium aluminum garnets, as second part of the study. The sol-gel process is applied to prepare target garnets. The characterization for all products were done by XRD,FTIR,TG/DTA, SEM, and EDX techniques.

The another scope this work, is to investigate the optical properties of undoped and doped lanthanide aluminum garnets using UV-vis/DRS technique.

The following objectives are expected to be achieve:

- To synthesize undoped $Ho_3Al_5O_{12}$, $Dy_3Al_5O_{12}$, $Tb_3Al_5O_{12}$ with sol-gel method.

- To synthesize Eu^{3+} doped $Ho_3Al_5O_{12}$, $Dy_3Al_5O_{12}$, $Tb_3Al_5O_{12}$ crystals in different ratios which are 0.10, 0.25, 0.50, 0.75, 1.00 with sol-gel method by exchanging the lanthanides in these structures $Ho_{3-x}Eu_xAl_5O_{12}$, $Dy_{3-x}Eu_xAl_5O_{12}$, $Tb_{3-x}Eu_xAl_5O_{12}$.

- To synthesize Mn^{3+}, Cr^{3+} or Fe^{3+} doped $Ho_3Al_5O_{12}$ crystals in various ratios as 0.10, 0.25, 0.50, 0.75, 1.00 via sol-gel method by exchanging holmium in this structure $Ho_{3-x}M_xAl_5O_{12}$ where M= Mn, Cr or Fe metal ions.

- To determine the crystal structures of all these samples by XRD analysing to show specific hkl indices of the cubic-celled garnet crystals.

- To define the specific streching lines of all these garnet samples with FTIR spectra investigations.

- To determine the critical reaction steps by DTA/TG measurements in terms of heating temperatures.

- To examine the morphology of the products by SEM and EDX studies.

- To investigate the optical properties of undoped and doped garnets by using UV-vis/DRS technique.

3. MATERIALS AND METHODS

3.1 Chemicals

The following chemicals were used in the synthesis of the products:

Ho_2O_3: (MERCK 99.00% pure)

Eu_2O_3: (MERCK 99.99% pure)

Dy_2O_3: (SIGMA-ALDRICH 99.99% pure)

Tb_4O_7: (MERCK 99.90% pure)

$Al(NO_3)_3.9H_2O$: (MERCK , M= 375.14 $g.mol^{-1}$)

$Mn(NO_3)_2.4.H_2O$: (MERCK , M= 251.01 $g.mol^{-1}$)

$Cr(NO_3)_3.9H_2O$ (MERCK , M= 400.5 $g.mol^{-1}$)

$Fe(NO_3)_3.9H_2O$ (MERCK , M= 403.86 $g.mol^{-1}$)

HNO_3 : (MERCK 1L ~ 1.39 kg, 66.00% assay)

$C_2H_6O_2$, Ethylene 1-2-diol (SIGMA-ALDRICH , M= 62.07 $g.mol^{-1}$)

KBr (heated at 180 ºC before using) , used for preparation of pellets needed by FTIR analysis.

3.2 Instrumentation

3.2.1 Infrared spectrophotometer

Shimadzu Fourier Transform Infrared (FTIR) Spectrophotometer in the region of 4000-400cm^{-1} and Perkin-Elmer FTIR Spectrum 1000 spectrometer in the region 4000-600cm^{-1} are performed to get the FT-IR spectrum analyzation results of the powders.

3.2.2 X-Ray powder diffractometer

The XRD studies were performed on Rigaku Miniflex 2kW DD2759N (200V AC, 30A, 50Hz) and on D8 Bruker AXS powder diffractometer using CuKα1 radiation. The diffraction patterns were recorded at the standard rate of 1.5 2θ / min.

3.2.3 Thermogravimetric - differential thermal analyzer (TG/DTA)

Perkin Elmer STA 6000 Simultaneous Thermal Analyzer and TG-DSC, Netzsch STA 449C Jupiter are performed using a sample weight of about 10 mg in heating rate of 5 °C·min–1 in flowing air (70 $cm^3 \cdot min^{-1}$) at ambient pressure 20-1000 ˚C.

3.2.4 UV-vis/DRS spectrometer

UV studies are performed with Perkin Elmer UV/VIS Spectrometer Lambda 35 and PerkinElmer UV WinLab Data Processor and Viewer Version 1.00.00 is used as software to demonstrate data.

3.2.5 Scanning electron microscope (SEM) and energy dispertive X-Ray(EDX)

The scanning electron microscope DSN 962 and Jeol JSM 6390LV were used to perform the surface morphology and microstructure of the obtained ceramic samples.

3.2.6 Furnaces

Protherm 1600˚C PLF 1SO/5 and Snol Max. 1000 ˚C (1100A, 220V, 50Hz) were used to bake the samples.

3.3 Experimental procedure

The experimental procedure of this experiment has two main structures to sum up the process of manufacturing of the substances. First, $Ho_3Al_5O_{12}$, $Dy_3Al_5O_{12}$ and $Tb_3Al_5O_{12}$ crystals are synthetized and doped with europium which is rare earth element by using oxides of these all metals. Second, $Ho_3Al_5O_{12}$ crystal is synthetized and doped with manganese, chromium and iron which are transition metals by using nitrates of these metals from Ho_2O_3.

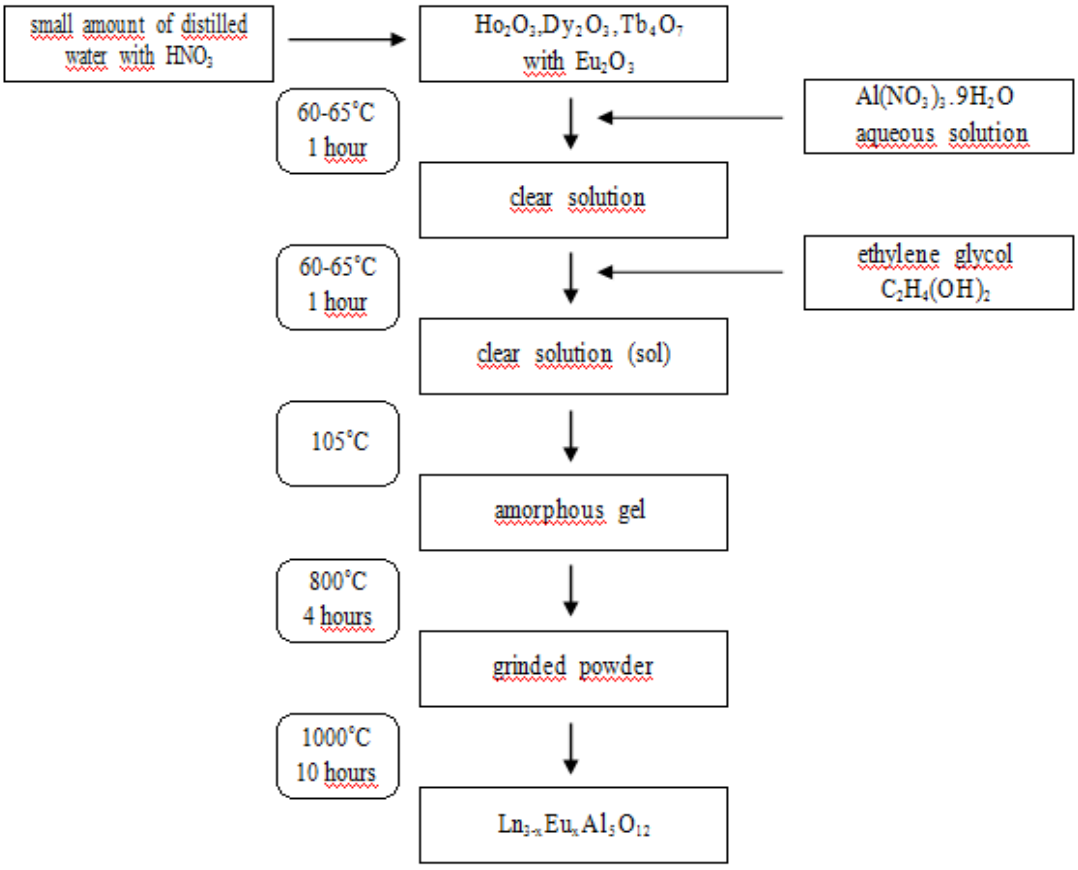

Figure 3. The flow chart of synthetization of the $Ln_{3-x}Eu_xAl_5O_{12}$, Ln=(Ho,Dy,Tb)

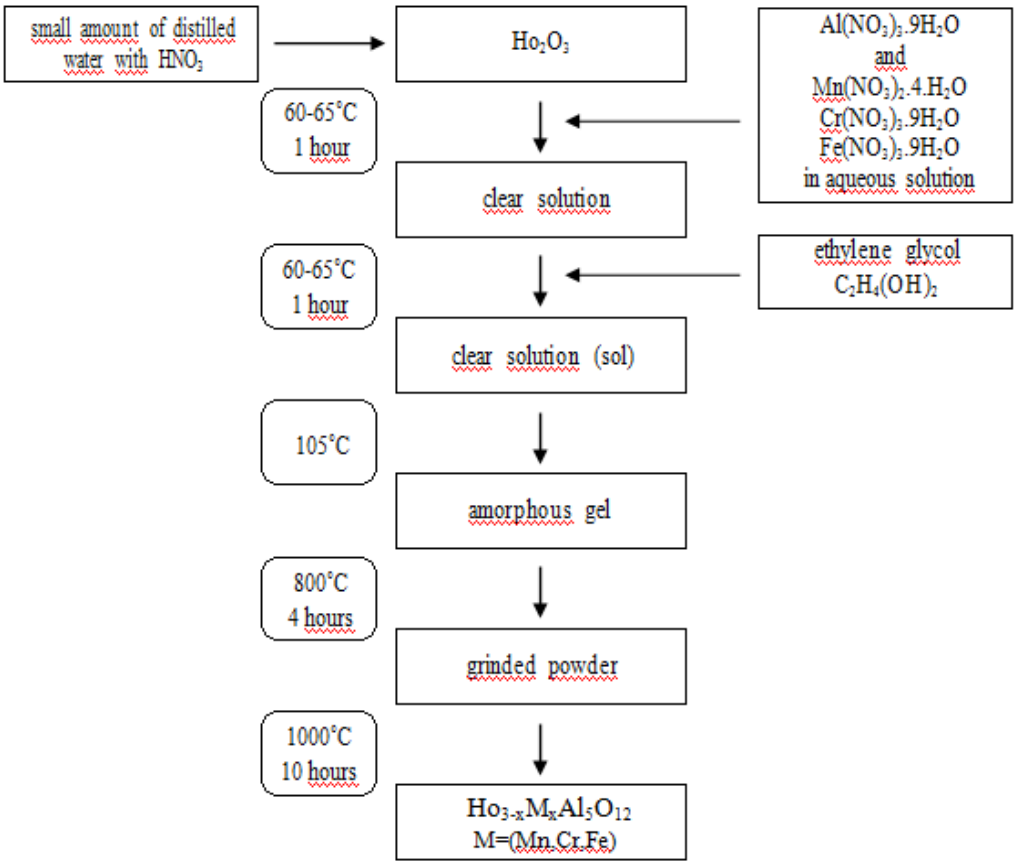

Figure 4. The flow chart of synthetization of the $Ho_{3-x}M_xAl_5O_{12}$, M=(Mn,Cr,Fe)

3.3.1 The synthesis of $Ho_3Al_5O_{12}$ from Ho_2O_3

Ho_2O_3 is heated with nitrous solution of distilled water about 50 mL of the solution in 200 mL beaker that covered by watch glass around 65˚C, which has the calculated amount, stoichiometrically. After the solution pink color changes to be clear, the solution is allowed to evaporate by putting out the watch glass from the top of the beaker. The distilled water about 50 mL is added onto the remained product to dissolve and the solution is evaporated again at 65˚C to flow the acid. Then the solution is heated up to evaporate the water of the solution by avoiding to see the boiling bubbles. After evaporation, $Al(NO_3)_3.9H_2O$ and 100 mL of distilled water are added onto the solution that in stoichiometrical amounts to heat for 1 hour covered by watch glass at 65˚C. At the end of the time, the ethane 1-2-diol (1,2 ethanediol) is added to the solution to get sol and waited for 1 hour by heating of the beaker with

watch glass on the hot plate. Finally , the solution is allowed to evaporation to get the gel product. The beaker is left on hot plate for 20 hours to have it dryer.

This product is taken from the beaker and grinded to put in a convenient crucible means resists to high temperatures. The sample crucible is heated at an oven for 4 hours at 800˚C. The powder product is grinded and put to the oven for 10 hours at 1000˚C.

$$3Ho_2O_3+5Al_2O_3 \rightarrow 2Ho_3Al_5O_{12}$$ (Dubnikova, N. et al., 2010)

3.3.2 The synthesis of $Dy_3Al_5O_{12}$ from Dy_2O_3

To synthesize of $Dy_3Al_5O_{12}$, Dy_2O_3 is taken instead of Ho_2O_3 and all the process is applied in the same method according to the section of 3.3.1.

$$3Dy_2O_3+5Al_2O_3 \rightarrow 2Dy_3Al_5O_{12}$$ (Dubnikova, N. et al., 2010)

3.3.3 The synthesis of $Tb_3Al_5O_{12}$ from Tb_4O_7

To synthesize of $Tb_3Al_5O_{12}$, Tb_4O_7 is taken instead of Ho_2O_3 and all the process is applied in the same method according to the section of 3.3.1.

$$3Tb_4O_7+10Al_2O_3 \rightarrow 4Tb_3Al_5O_{12}+1.5O_2$$ (Dubnikova, N. et al., 2010)

3.3.4 The synthesis of Eu^{3+} doped $Ho_3Al_5O_{12}$ from Eu_2O_3

The stoichiometrically calculated amounts of Eu_2O_3 is put with Ho_2O_3 to the beaker at the begining of the reaction and the process is applied in the same method according to the section of 3.3.1. The amounts of Eu_2O_3 is calculated according to get the molar ratio with $Ho_{3-x}Eu_xAl_5O_{12}$, where x values are 0.10, 0.25, 0.50, 0.75 and 1.00.

3.3.5 The synthesis of Eu^{3+} doped $Dy_3Al_5O_{12}$ from Eu_2O_3

The stoichiometrically calculated amounts of Eu_2O_3 is put with Dy_2O_3 to the beaker at the begining of the reaction and the process is applied in the same method according to the section of 3.3.1. The amounts of Eu_2O_3 is calculated according to get the molar ratio with $Dy_{3-x}Eu_xAl_5O_{12}$, where x values are 0.10, 0.25, 0.50, 0.75 and 1.00.

3.3.6 The synthesis of Eu^{3+} doped $Tb_3Al_5O_{12}$ from Tb_4O_7

The stoichiometrically calculated amounts of Eu_2O_3 is put with Tb_4O_7 to the beaker at the begining of the reaction and the process is applied in the same method according to the section of 3.3.1. The amounts of Eu_2O_3 is calculated according to get the molar ratio with $Dy_{3-x}Eu_xAl_5O_{12}$, where x values are 0.10, 0.25, 0.50, 0.75 and 1.00.

3.3.7 The synthesis of Mn^{3+} doped $Ho_3Al_5O_{12}$ from $Mn(NO_3)_2.4H_2O$

To synthesize of $Ho_{3-x}Mn_xAl_5O_{12}$, Ho_2O_3 is taken and all the process is applied in the same method with a small difference at the step that putting $Al(NO_3)_3.9H_2O$ and $Mn(NO_3)_2.4H_2O$ together to have Mn dopant , according to the section of 3.3.1., in Figure 4. The amounts of $Mn(NO_3)_2.4H_2O$ is calculated according to get the molar ratio where the molar ratio x values are 0.10, 0.25, 0.50, 0.75 and 1.00.

3.3.8 The synthesis of Cr^{3+} doped $Ho_3Al_5O_{12}$ from $Cr(NO_3)_3.9H_2O$

To synthesize of $Ho_{3-x}Cr_xAl_5O_{12}$, Ho_2O_3 is taken and all the process is applied in the same method with a small difference at the step that putting $Al(NO_3)_3.9H_2O$ and $Cr(NO_3)_3.9H_2O$ together to have Cr dopant , according to the section of 3.3.1, in Figure 4. The amounts of $Cr(NO_3)_3.9H_2O$ is calculated according to get the molar ratio where the molar ratio x values are 0.10, 0.25, 0.50, 0.75 and 1.00.

3.3.9 The synthesis of Fe^{3+} doped $Ho_3Al_5O_{12}$ from $Fe(NO_3)_3.9H_2O$

To synthesize of $Ho_{3-x}Fe_xAl_5O_{12}$, Ho_2O_3 is taken and all the process is applied in the same method with a small difference at the step that putting $Al(NO_3)_3.9H_2O$ and $Fe(NO_3)_3.9H_2O$ are put together to have Fe dopant , according to the section of 3.3.1., in Figure 4. The amounts of $Fe(NO_3)_3.9H_2O$ is calculated according to get the molar ratio where the molar ratio x values are 0.10, 0.25, 0.50, 0.75 and 1.00.

4. RESULTS AND DISCUSSION

4.1 The results and discussion of undoped crystals

4.1.1 The studies for $Ho_3Al_5O_{12}$ (HAG)

4.1.1.1 The XRD studies of undoped HAG

X-ray diffraction analysis was used to check the purity and compositional changes of the structure of $Ho_3Al_5O_{12}$ garnets after being doped in different amount of Eu ions. The XRD pattern of $Ho_3Al_5O_{12}$ sample is shown in Figure 5.

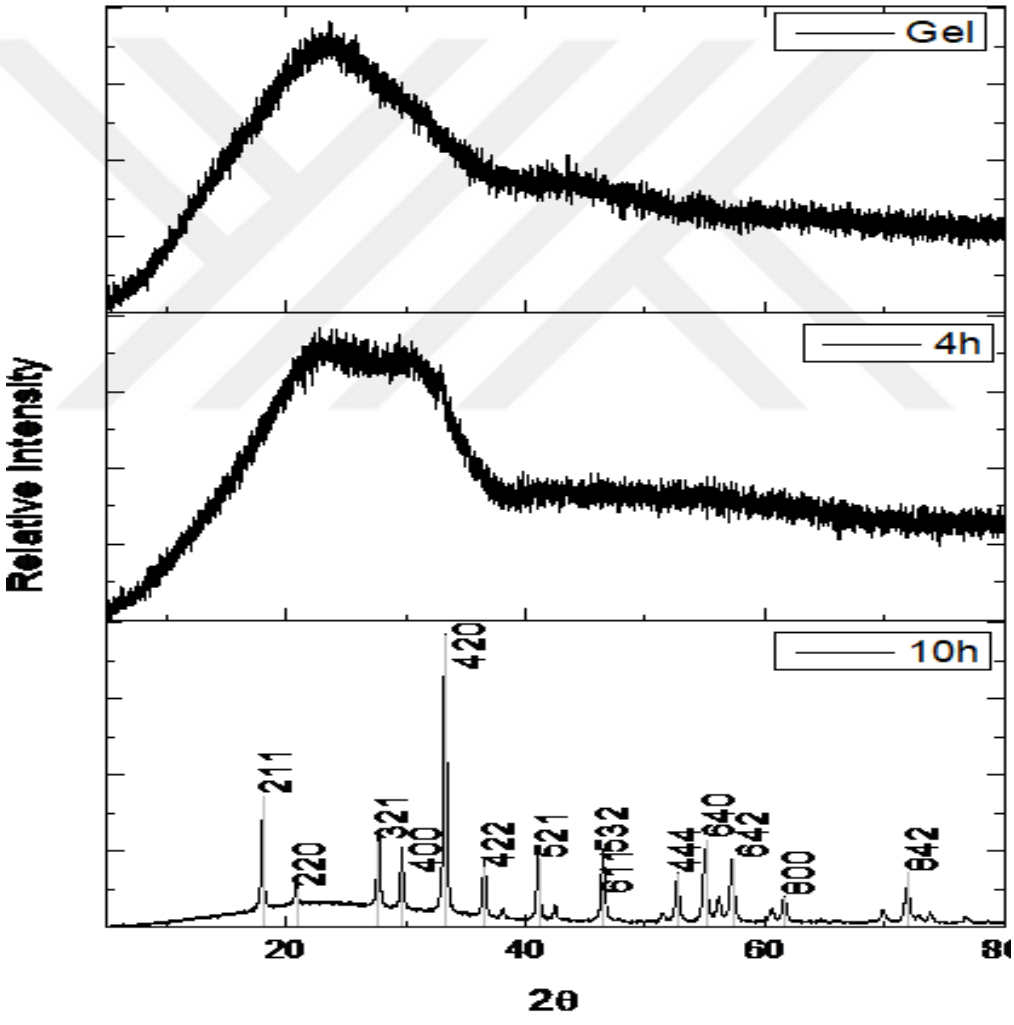

Figure 5. The XRD pattern of $Ho_3Al_5O_{12}$ sample without doping agent

The XRD pattern shown in Figure 5 is in agreement with the reference data for $Ho_3Al_5O_{12}$, ICDD [00-076-0112].

4.1.1.2 The FTIR spectroscopy studies of undoped HAG

FTIR spectroscopy was used for structural characterization of garnets synthesized by the sol-gel method. The infrared spectra of $Ho_3Al_5O_{12}$ without Eu are given in Figure 6.

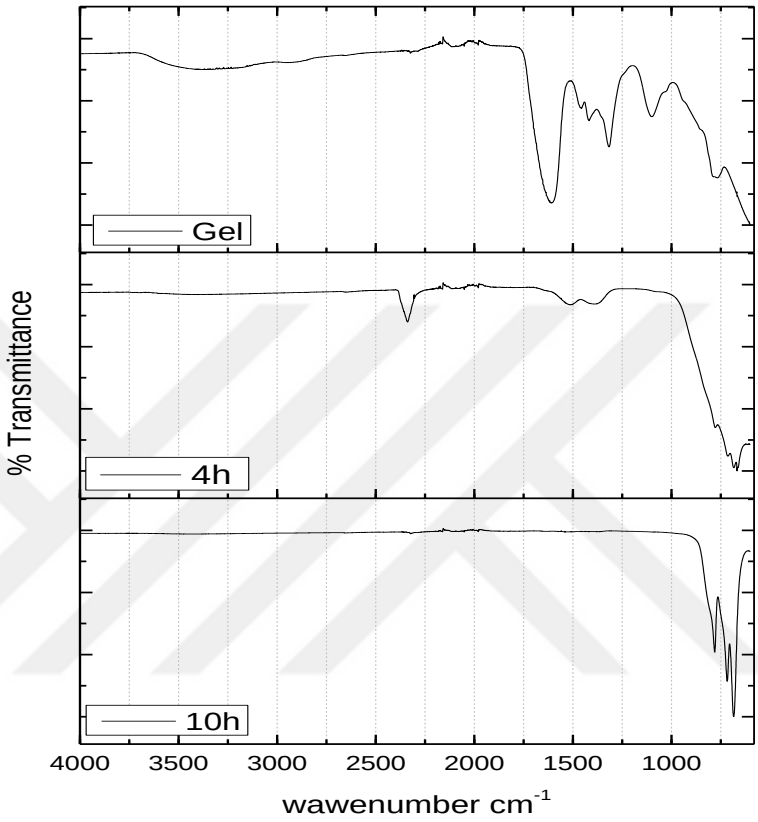

Figure 6. The FTIR spectroscopy of undoped $Ho_3Al_5O_{12}$

It is clearly seen in the Figure 6 that there is no any organic residue after 10h calcination at 1000˚C. The FTIR spectra of synthesized garnets shows typical metal-oxygen (M-O) absorption bands under 1000 cm^{-1} for the garnet-type crystals. The peaks at 771, 686, 644, and 495 cm^{-1} represents typical metal-oxygen bonds.

There is a broad band in the gel form which represents hydroxyl bonds from remain water around 3000-3500 cm^{-1}. Also, the 4 hour-heated sample has a peak around 1100-1600 cm^{-1} which represents C-H and C-O respectively, that may comes from metal-alkoxy groups. (Veith, M. et al., 1999). Also, there is no specific amount of Ho_2O_3 remaining even after 4 hour heating, there is no specific peaks of Ho_2O_3 cm^{-1} at 1527 cm^{-1} and 1122 cm^{-1} (Zinatloo-Ajabshir, S., 2017).

4.1.1.3 Thermal studies (TG/DTA) of undoped HAG

The TG/DTA curves of the $Ho_3Al_5O_{12}$ without Eu both gel form and after heated are shown in Figure 7, a) and b) respectively. The heating was in temperature range from room temperature to 1000°C. The curves are indicated that $Ho_3Al_5O_{12}$ coumpound is thermodynamically stable upon 900°C and there are very small amount of weight loss in these temperature ranges.

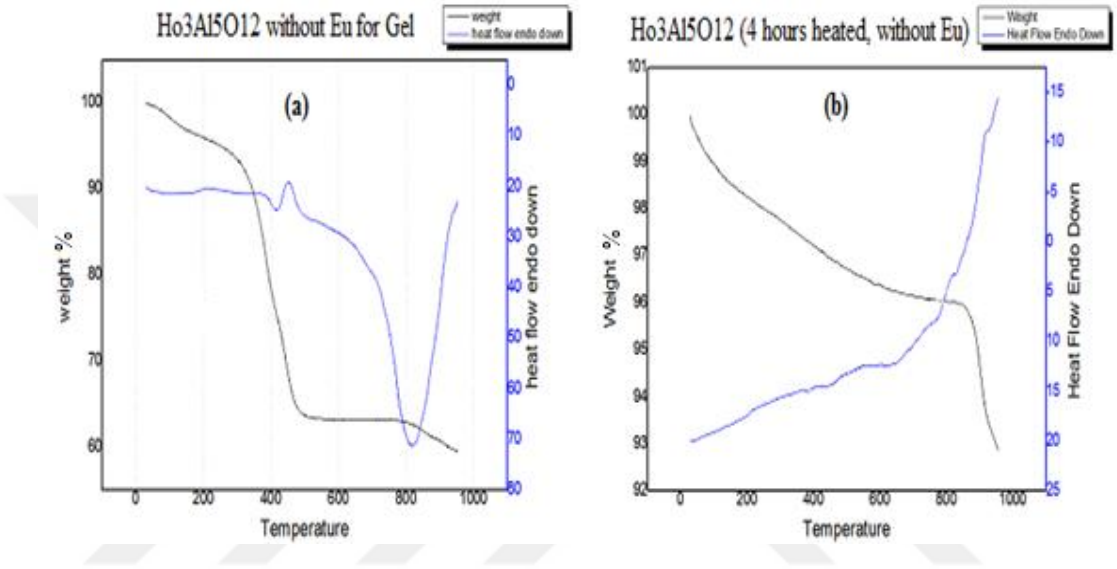

Figure 7. The TG/DTA thermal analysis graphs of $Ho_3Al_5O_{12}$ a) gel form of dried at 100˚C, b) after 4 hours heat treatment

4.1.1.4 The SEM and EDX studies of undoped HAG

The SEM images of undoped $Ho_3Al_5O_{12}$ are shown in the Figure 8. The resolution of the adjacent pictures increases gradually. There can be seen clearly the plate-like shape of holmium aluminum garnet. There are large-grained matrixes and several small granuls on their surfaces. The surfaces are seems smooth. The results shows an extensive particle size dispersion of small granuls. However, as can be seen from the pictures, these small granuls tends to become a huge matrix to form big granuls. This is kind a classic ceramic composition electron microscopy images.

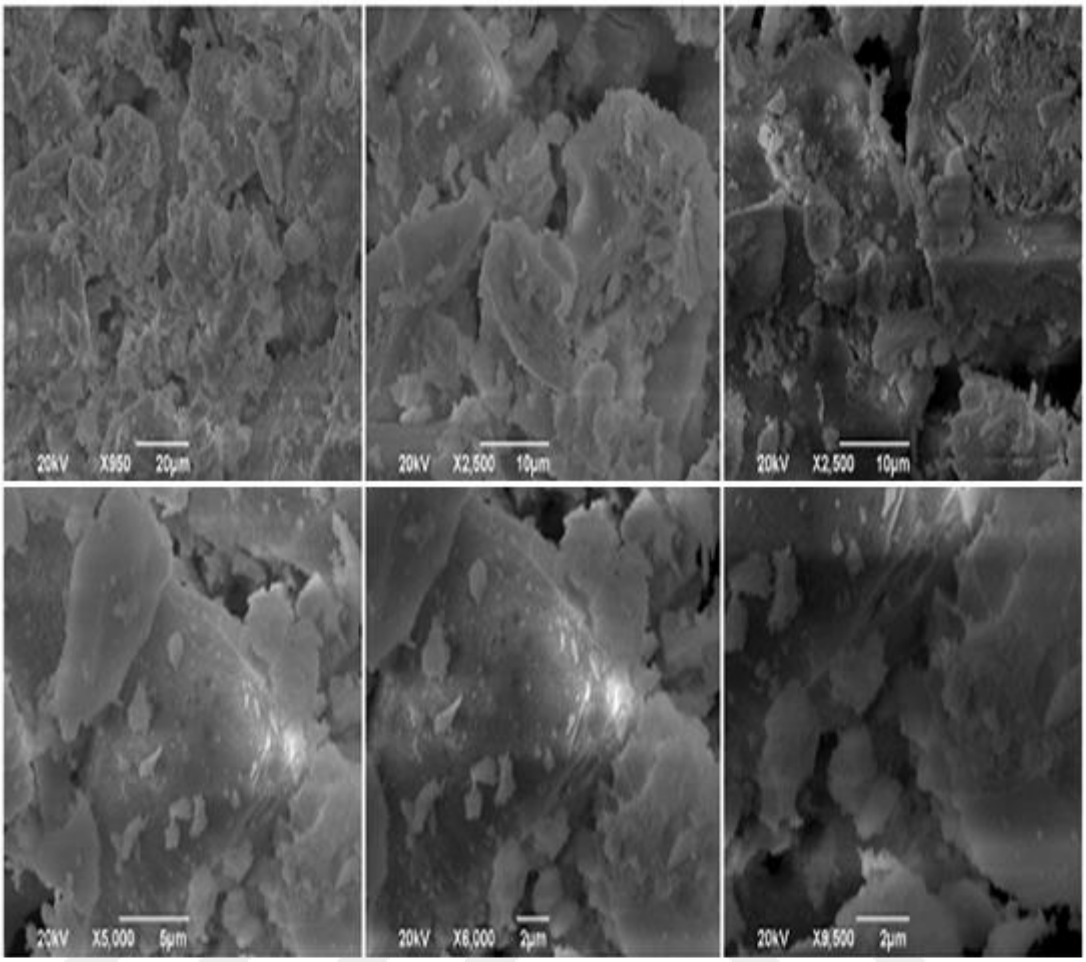

Figure 8. The SEM micrographs of undoped $Ho_3Al_5O_{12}$

The EDX analysis shown in Figure 9 and Table 1 determined that the peak intensities of the typical $Ho_3Al_5O_{12}$ as expected.

Table 1. The EDX analysis of $Ho_3Al_5O_{12}$

Elt.	Line	Intensity (c/s)	Error 2-sig	Conc	Units	
O	Ka	37.94	2.249	18.243	wt.%	
Al	Ka	84.33	3.353	12.667	wt.%	
Ho	La	84.99	3.366	69.090	wt.%	
				100.000	wt.%	Total

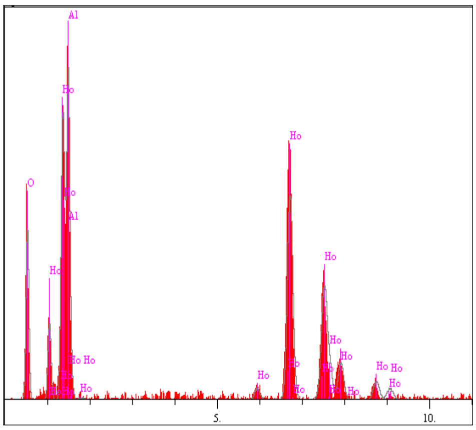

Figure 9. The EDX analysis of $Ho_3Al_5O_{12}$

4.1.2 The studies for $Dy_3Al_5O_{12}$ (DAG)

4.1.2.1 The XRD studies of undoped DAG

XRD patterns for gel , after 4 hours heating at 800˚C and then 10 hours heating at 1000˚C of $Dy_3Al_5O_{12}$ is shown below in Figure 10.

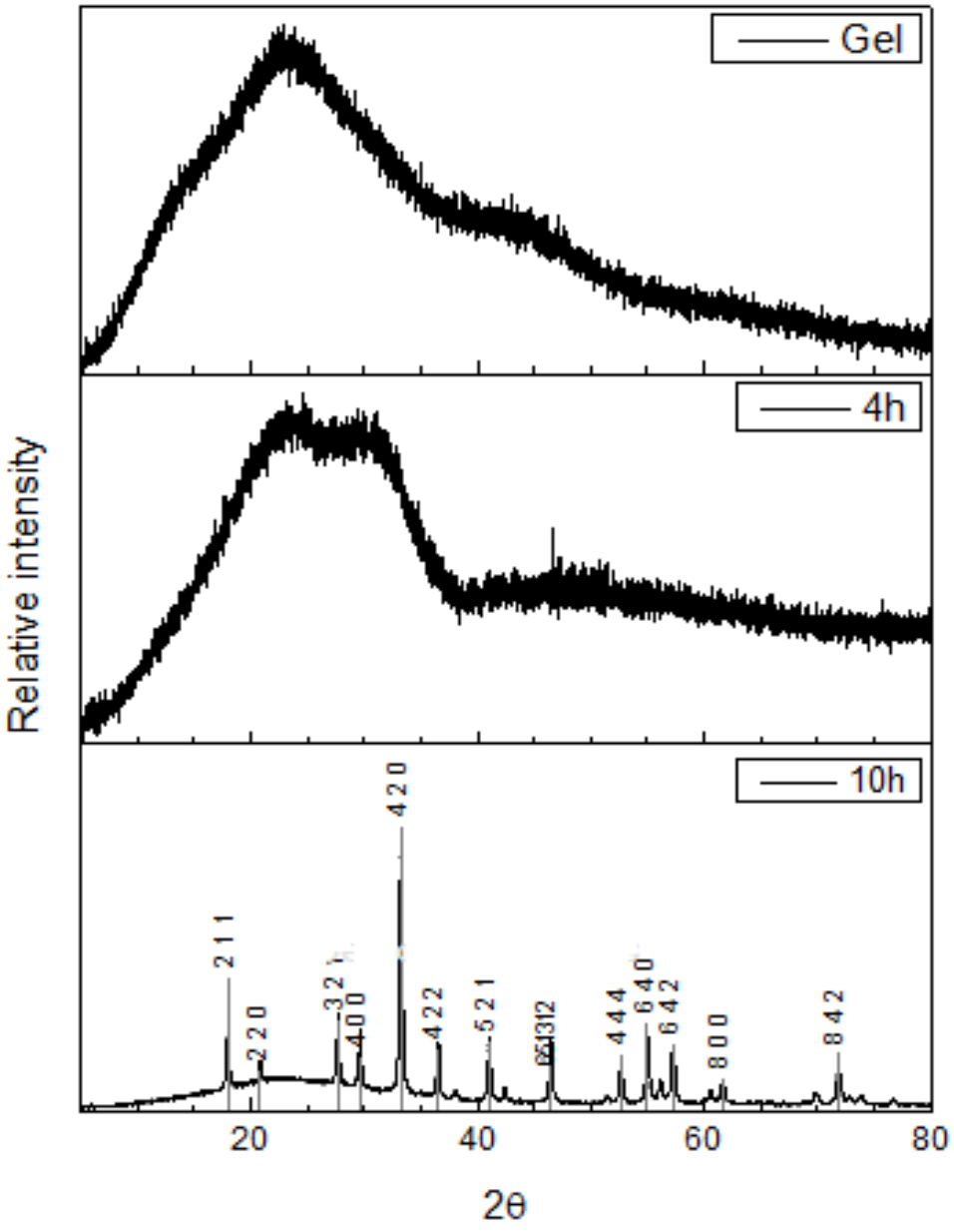

Figure 10. The XRD pattern of $Dy_3Al_5O_{12}$ sample without doping agent

The XRD pattern shown in Figure 10 is in agreement with the reference data for $Dy_3Al_5O_{12}$, ICDD [00-022-1093].

4.1.2.2 The FTIR spectroscopy studies of undoped DAG

Infrared spectrum peaks for gel , after 4 hours heating at 800˚C and then last 10 hours heating at 1000˚C of $Dy_3Al_5O_{12}$ is shown below in Figure 11.

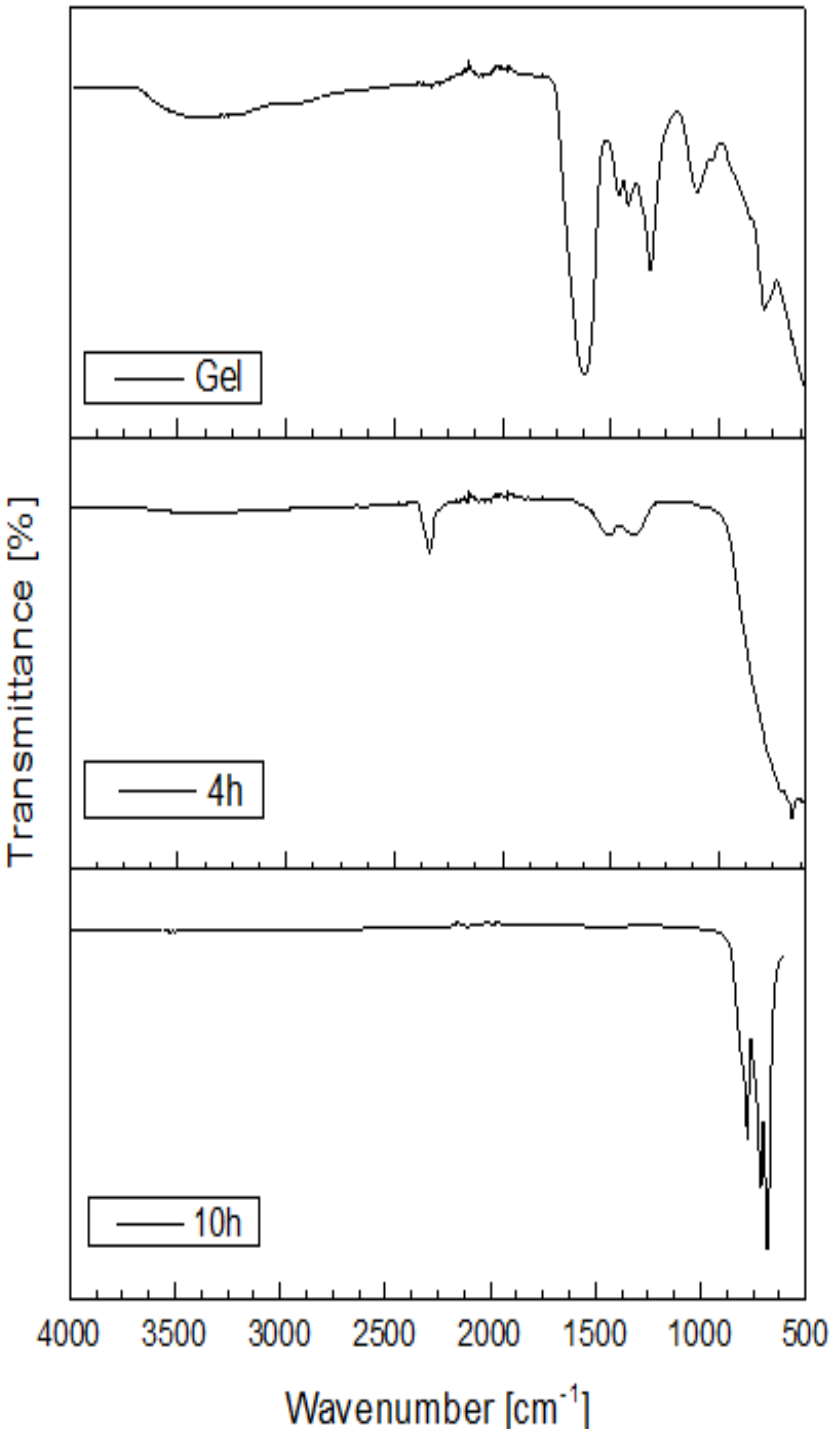

Figure 11. The FTIR spectroscopy of undoped $Dy_3Al_5O_{12}$

It is clearly seen in the Figure 11 that there is no any organic residue after 10h calcination at 1000˚C. The FTIR spectra of synthesized garnets shows typical metal-oxygen (M-O) absorption bands under 1000 cm^{-1} for the garnet-type crystals. The peaks at 771, 686, 644, and 495 cm^{-1} represents typical metal-oxygen bonds. The dodecahedral Al-O bond strechings of specific garnet structure between 900 and 450 cm^{-1}can be seen. There seems no organic bond strechings after 10 hours calcination (Dubnikova, N., 2010).

4.1.2.3 Thermal studies (TG/DTA) of undoped DAG

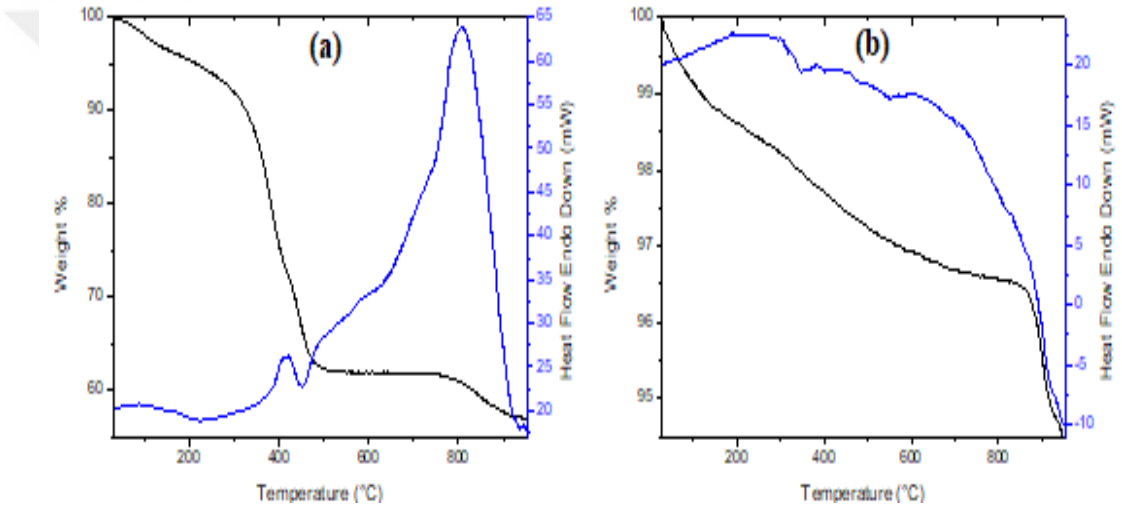

Figure 12. The TG/DTA thermal analysis graphs of $Dy_3Al_5O_{12}$ a) gel form of dried at 100˚C, b) after 4 hours heat treatment

TG/DTA study of gel form of $Dy_3Al_5O_{12}$ shows peaks at around 400˚C and 800˚C . The high amount of weighing lost and reaction steps are occured at these temperatures. The sample agrees 800˚C as to be first heating temperature to up before calcination.

4.1.2.4 The SEM studies of undoped DAG

The SEM images of undoped $Dy_3Al_5O_{12}$ are shown in the Figure 13. There can be seen clearly plate-like shape of dysprosium aluminum garnet. The small grains on the large granul can be seen easily. The small grains have different sizes.

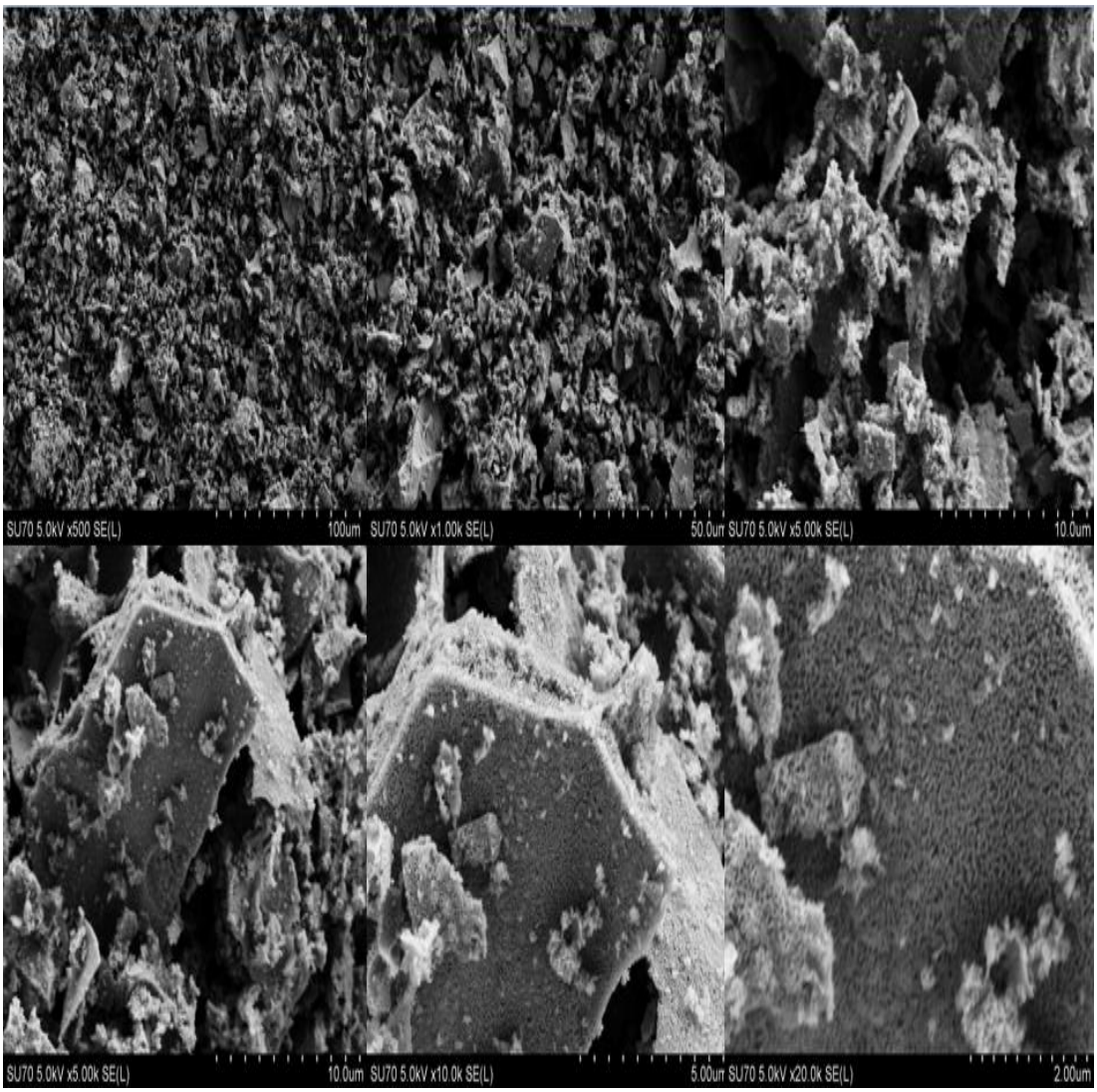

Figure 13. The SEM micrographs of undoped $Dy_3Al_5O_{12}$

4.1.3 The studies for $Tb_3Al_5O_{12}$ (TAG)

4.1.3.1 The XRD studies of undoped TAG

XRD patterns for gel , after 4 hours heating at 800˚C and last 10 hours heating at 1000˚C of $Tb_3Al_5O_{12}$ is shown below in Figure 14. As can be seen from the XRD results in Figure 14, the amorphous structure was lost as the temperature and heating time increased. The crystallinity started to be occur after 1000˚C for 10-hour heat treatment.

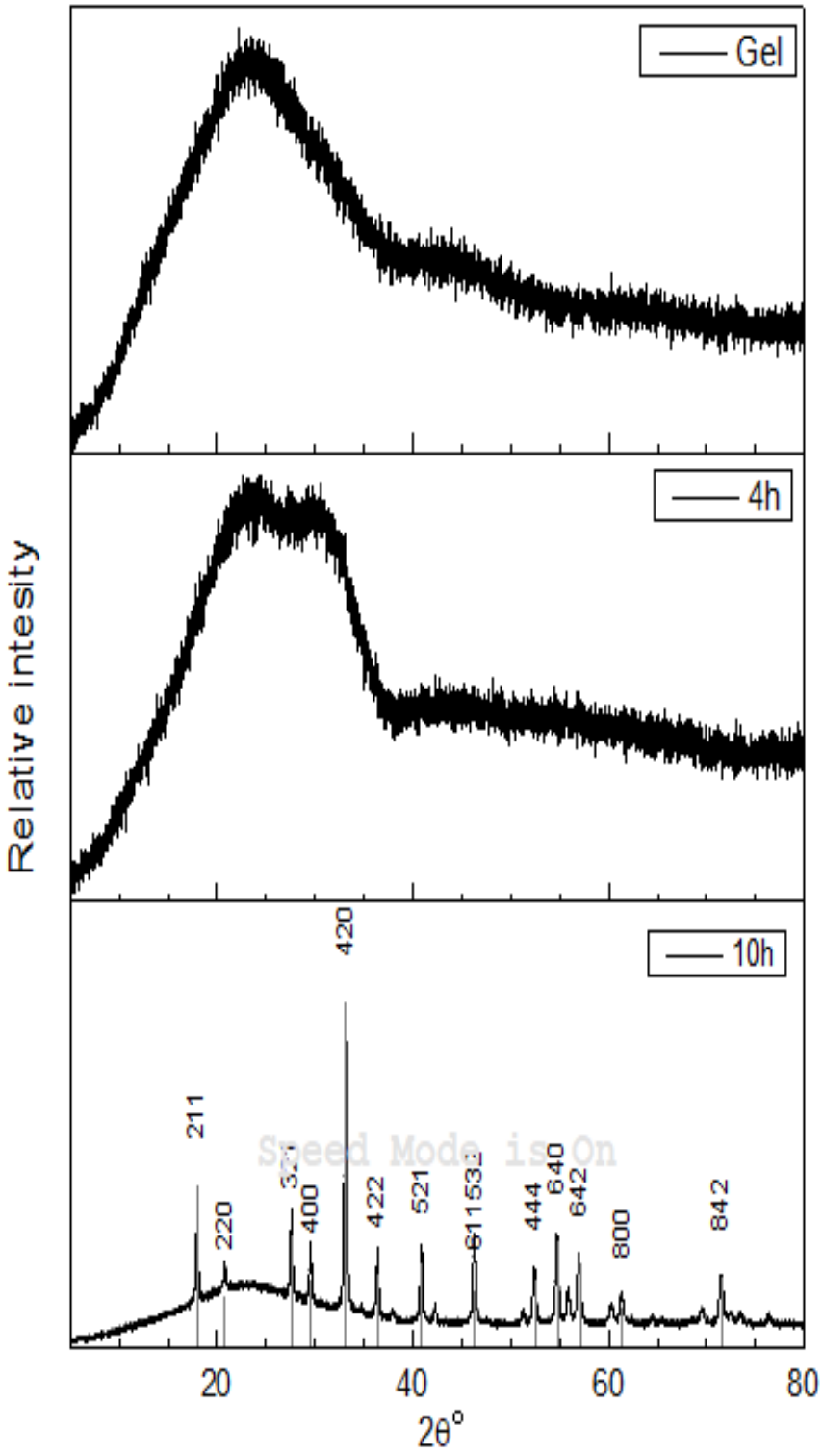

Figure 14. The XRD pattern of $Tb_3Al_5O_{12}$ sample without doping agent

The XRD pattern shown in Figure 14 is in agreement with the reference data for $Tb_3Al_5O_{12}$, JDPDS No. [76-0111].

4.1.3.2 The FTIR spectroscopy studies of undoped TAG

The infrared spectrum peaks for gel , after 4 hours heating at 800˚C and last 10 hours heating at 1000˚C of $Tb_3Al_5O_{12}$ is shown below in Figure 15.

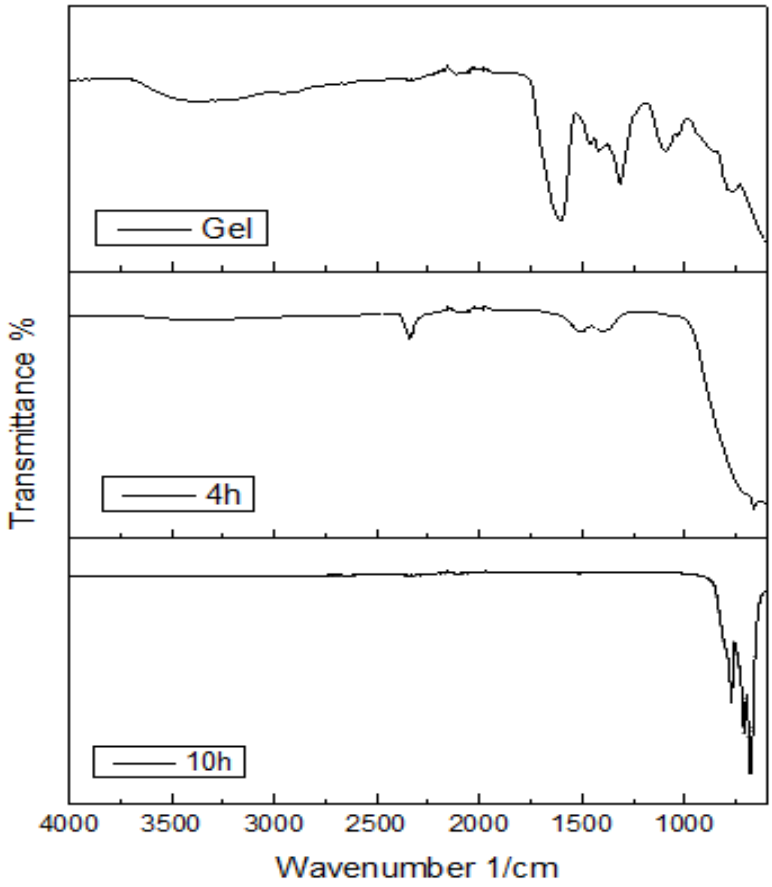

Figure 15. The FTIR spectroscopy of undoped $Tb_3Al_5O_{12}$

It is clearly seen in the Figure 15 that there is no any organic residue after 10h calcination at 1000˚C. The FTIR spectra of synthesized garnets shows typical metal-oxygen (M-O) absorption bands under 1000 cm^{-1} for the garnet-type crystals. The peaks at 771, 686, 644, and 495 cm^{-1} represents typical metal-oxygen bonds. The dodecahedral Al-O bond strechings of specific garnet structure between 900 and 450 cm^{-1}can be seen. There seems no organic bond strechings after 10 hours calcination. (Dubnikova, N., 2010).

4.1.3.3 Thermal studies (TG/DTA) of undoped TAG

After 4 hours heating treatment, according to the TG/DTA result there is a high amount of weighing lost right after 800˚C. Therefore, before calcination at 1000˚C, firstly the samples are heated to 800˚C for 4 hours.

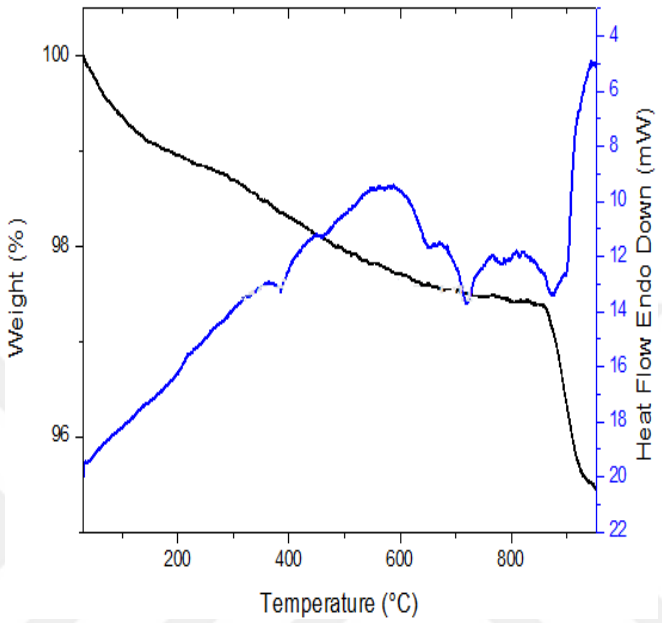

Figure 16. The TG/DTA thermal analysis graphs of $Tb_3Al_5O_{12}$ after 4hours heat treatment

4.1.3.4 The SEM studies of undoped TAG

The SEM images of undoped $Tb_3Al_5O_{12}$ are shown in the Figure 17. It can be seen clearly the plate-like with porous shape of terbium aluminum garnet with small grains. Likewise the holmium aluminum garnet and the dysprosium aluminum garnet images, the small grains are tend to become together to have a big matrix. However, unlike the holmium aluminum garnet and the dysprosium aluminum garnet, the surfaces are not seem so much smooth and actually as can be seen easily, the surfaces has such pores in different sizes. There can be seen the wide particule size dispersion.

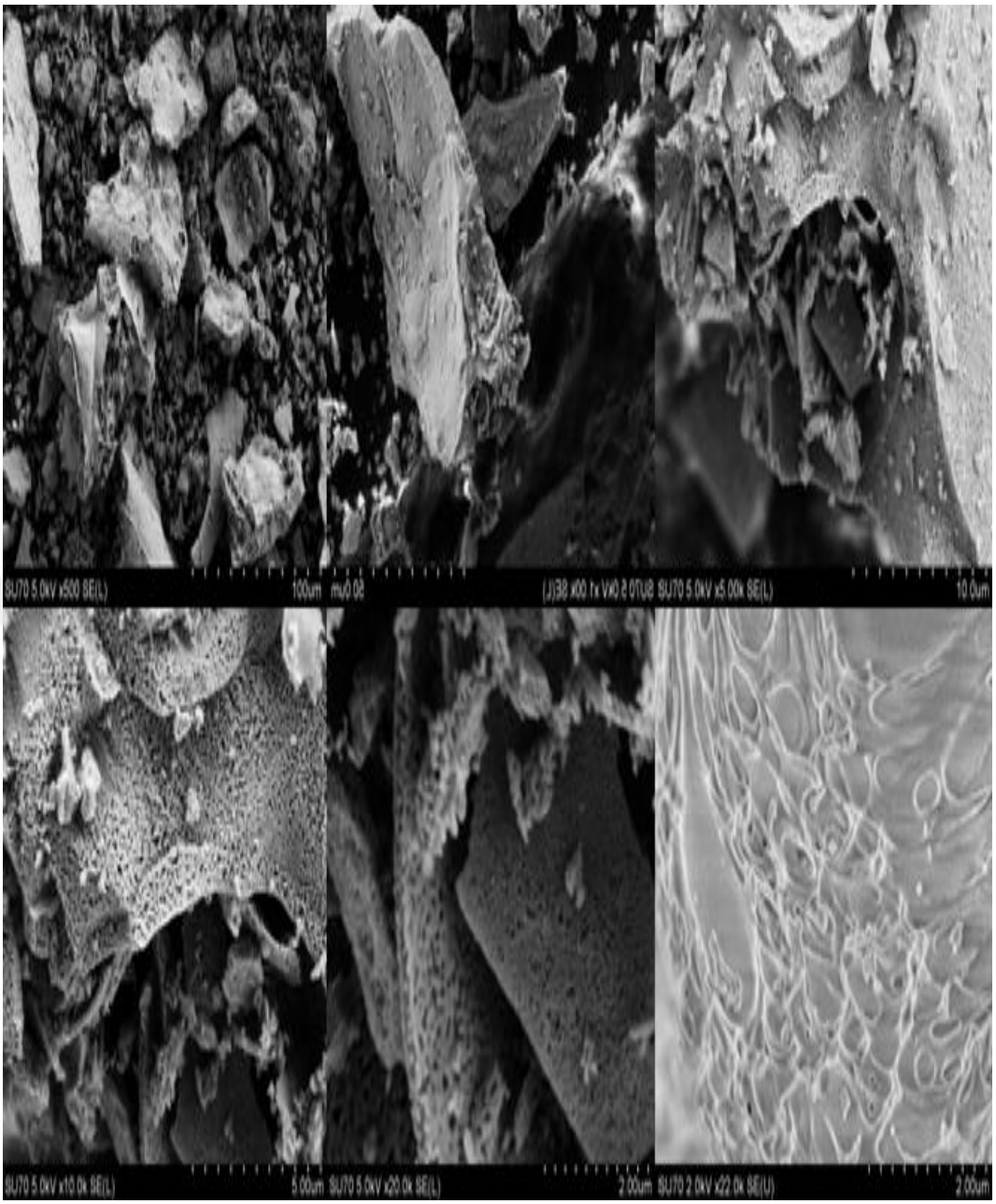

Figure 17. The SEM micrographs of undoped $Tb_3Al_5O_{12}$

4.2 The results and discussion for europium doped materials

4.2.1 The studies for $Ho_3Al_5O_{12}$ doped with Eu^{3+} (Eu:HAG)

4.2.1.1 The XRD studies of Eu:HAG

The XRD patterns of 5 different amount of Eu^{3+} doped $Ho_3Al_5O_{12}$ garnets are shown in figures from 18 to 22.

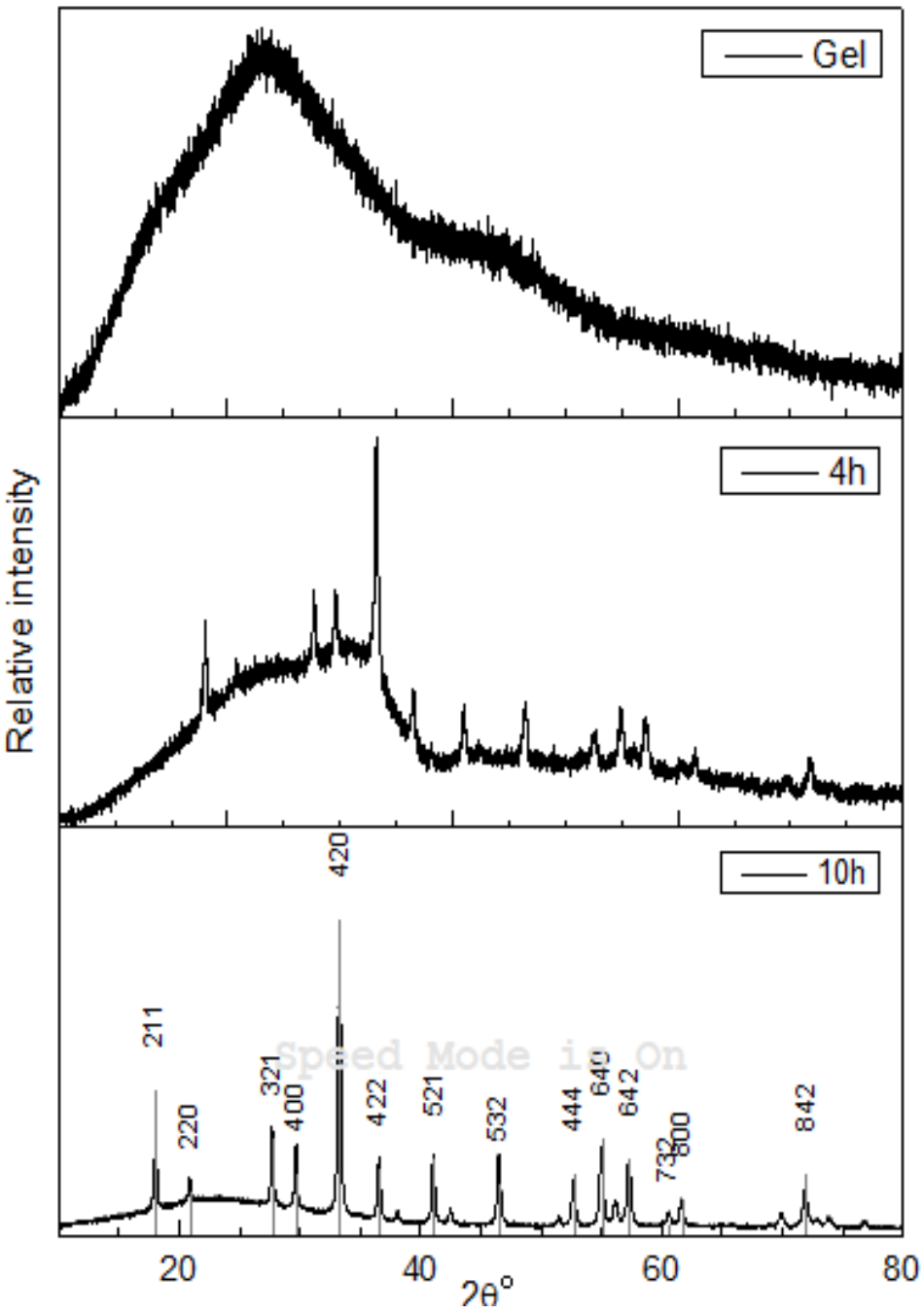

Figure 18. The XRD pattern of 0.10 mol Eu^{3+} doped $Ho_3Al_5O_{12}$

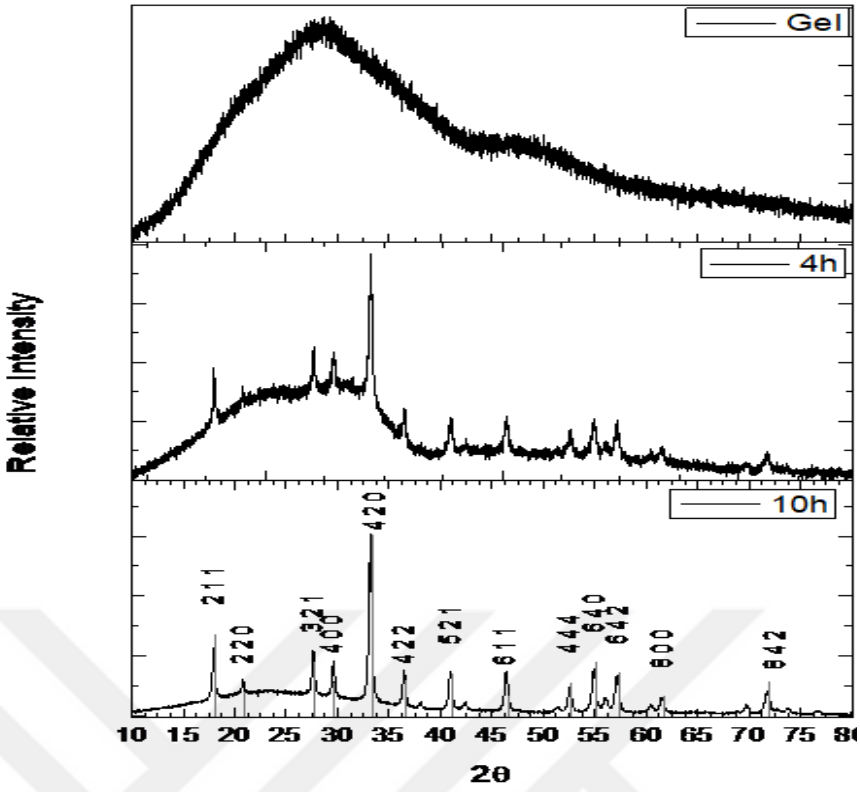

Figure 19. The XRD pattern of 0.25 mol Eu^{3+} doped $Ho_3Al_5O_{12}$

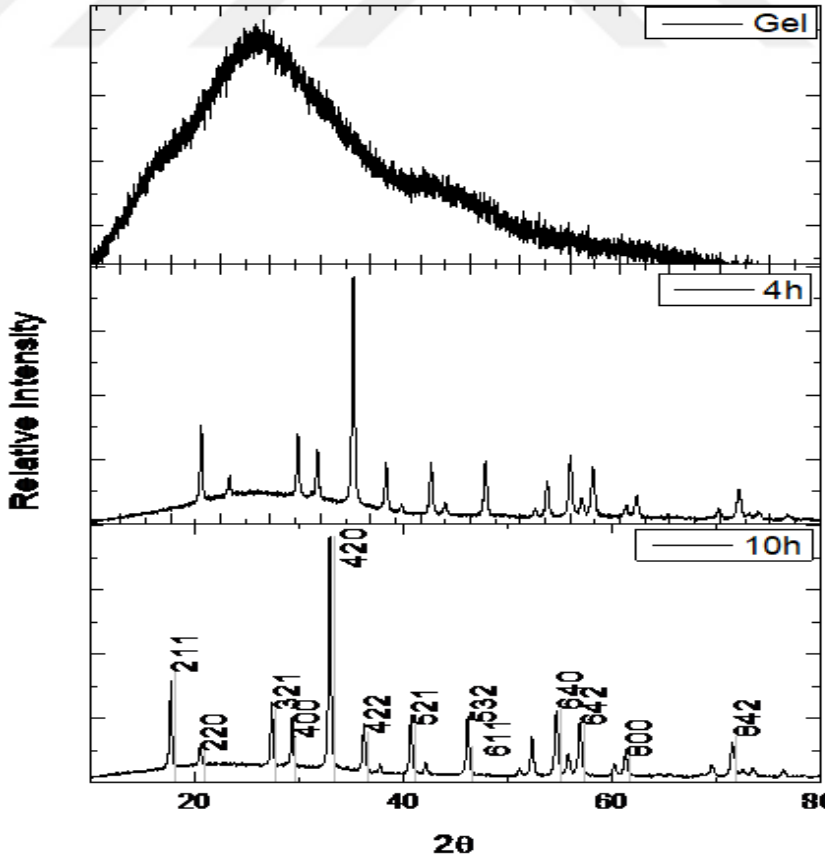

Figure 20. The XRD pattern of 0.50 mol Eu^{3+} doped $Ho_3Al_5O_{12}$

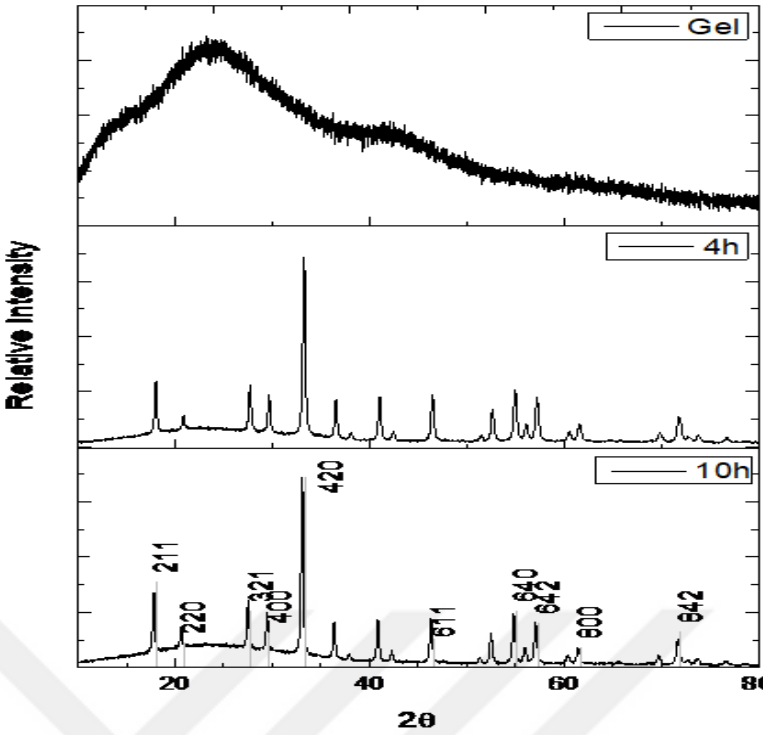

Figure 21. The XRD pattern of 0.75 mol Eu^{3+} doped $Ho_3Al_5O_{12}$

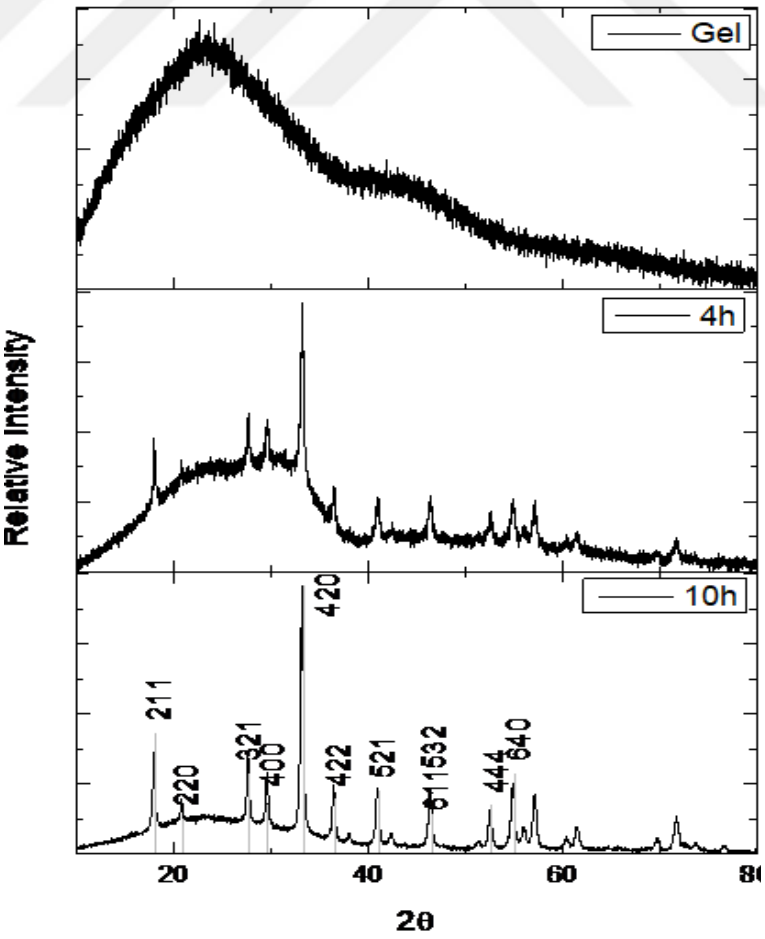

Figure 22. The XRD pattern of 1.00 mol Eu^{3+} doped $Ho_3Al_5O_{12}$

It should be noted that when Eu^{3+} doped $Ho_3Al_5O_{12}$ is shown in the figures 18-22 is synthesized, there is no special condition or change. The lack of impurity peaks shows us that the synthesized garnets doped with Eu are pure and phase stable. The peak positions and relative intensity is also in agreement with the reference data for $Ho_3Al_5O_{12}$ (PDF [04-001-9715]). As can be seen from the XRD patterns, there is no structural change in the garnet after doping with Eu. Thus we can understand this situation as it took place the formation of Eu^{3+} doped $Ho_3Al_5O_{12}$ garnets.

4.2.1.2 The FTIR spectroscopy studies of Eu:HAG

5 different concentrations of Eu^{3+} which were used to obtain Eu^{3+} doped $Ho_3Al_5O_{12}$ garnets then 5 different amounts of Eu^{3+} doped garnets are obtained. These amounts are 0.10, 0.25, 0.50, 0.75 and 1.00 mol Eu^{3+}. FTIR spectra of 0.10, 0.25, 0.50, 0.75 and 1.00 mol Eu^{3+} doped garnet can be seen in figures 23-27.

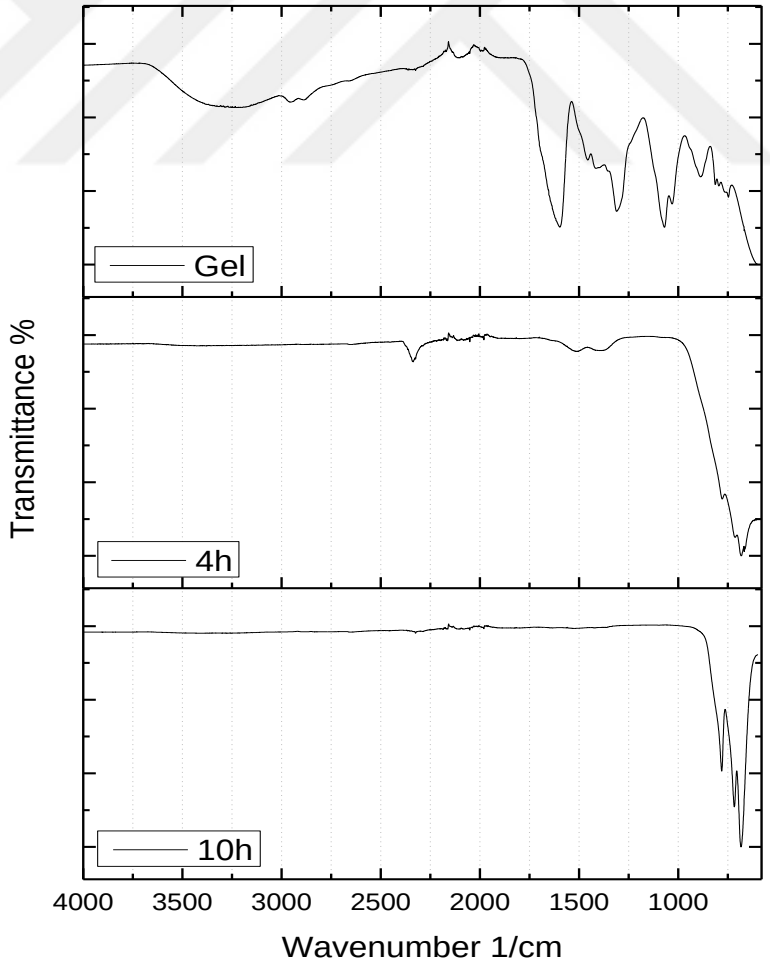

Figure 23. The FTIR spectroscopy of 0.10 mol Eu^{3+} doped $Ho_3Al_5O_{12}$

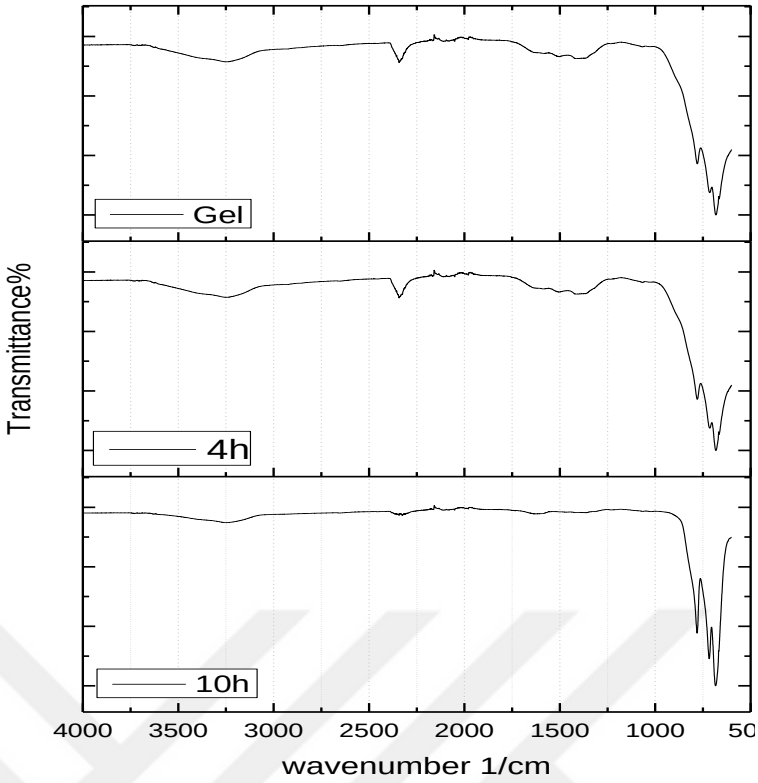

Figure 24. The FTIR spectroscopy of 0.25 mol Eu^{3+} doped $Ho_3Al_5O_{12}$

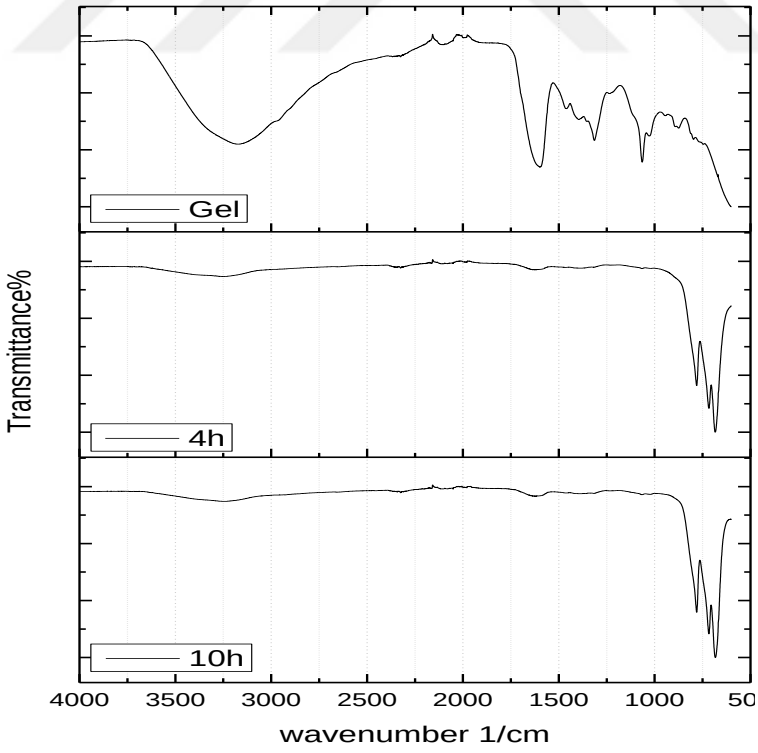

Figure 25. The FTIR spectroscopy of 0.50 mol Eu^{3+} doped $Ho_3Al_5O_{12}$

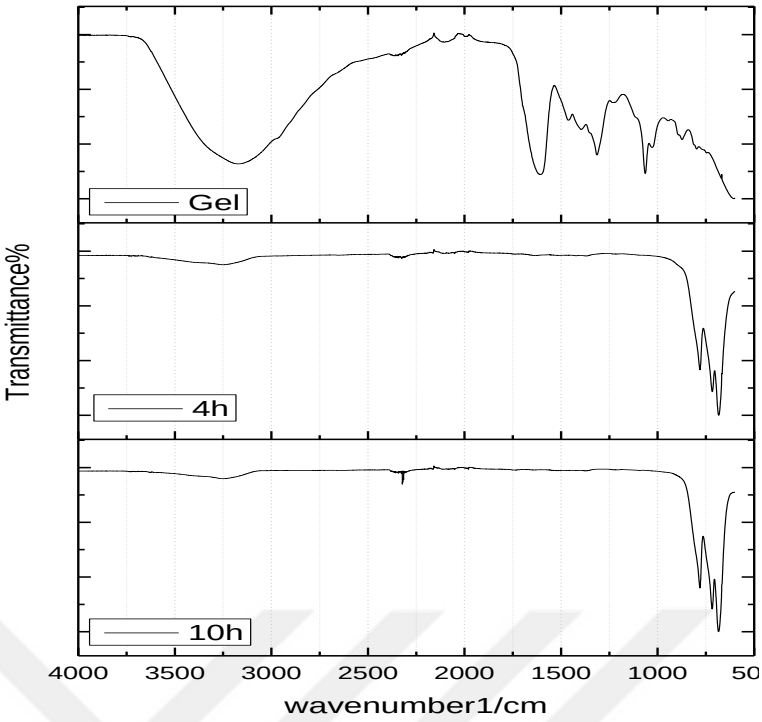

Figure 26. The FTIR spectroscopy of 0.75 mol Eu^{3+} doped $Ho_3Al_5O_{12}$

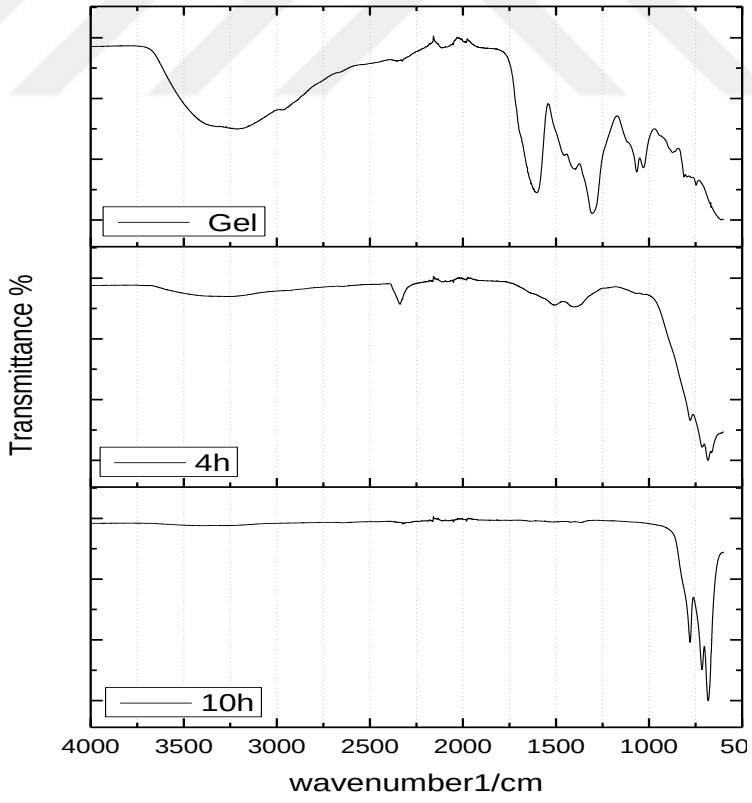

Figure 27. The FTIR spectroscopy of 1.00 mol Eu^{3+} doped $Ho_3Al_5O_{12}$

The FTIR spectra of $Ho_3Al_5O_{12}$ garnets with europium that shown in figure 23-27 were very similar to those shown in Figure 6. The most important feature is that intensive bands are not changed under 1000 cm^{-1} after being doped Eu^{3+} in 5 different ratio. The structure of $Ho_3Al_5O_{12}$ is not changing after the dopant Eu^{3+}. So the metal-oxygen (M-O) bonds in the $Ho_3Al_5O_{12}$ are protected and do not change. Furthermore after the crystallization there is no organic matter in the structure.

4.2.1.3 Thermal studies (TG/DTA) of undoped Eu:HAG

The TG/DTA curves of the 0.10 mol Eu^{3+} doped $Ho_3Al_5O_{12}$ for both gel form and after heated are shown in Figure 28 a) and b) respectively. The heating was in temperature range from room temperature to 1000˚C as like in the holmium garnet without Eu. The curves indicate that this 0.10 mol Eu^{3+} doped $Ho_3Al_5O_{12}$ is also thermodynamically stable up to 900^{o}C and there are very small amount of weight loss in these temperature ranges.

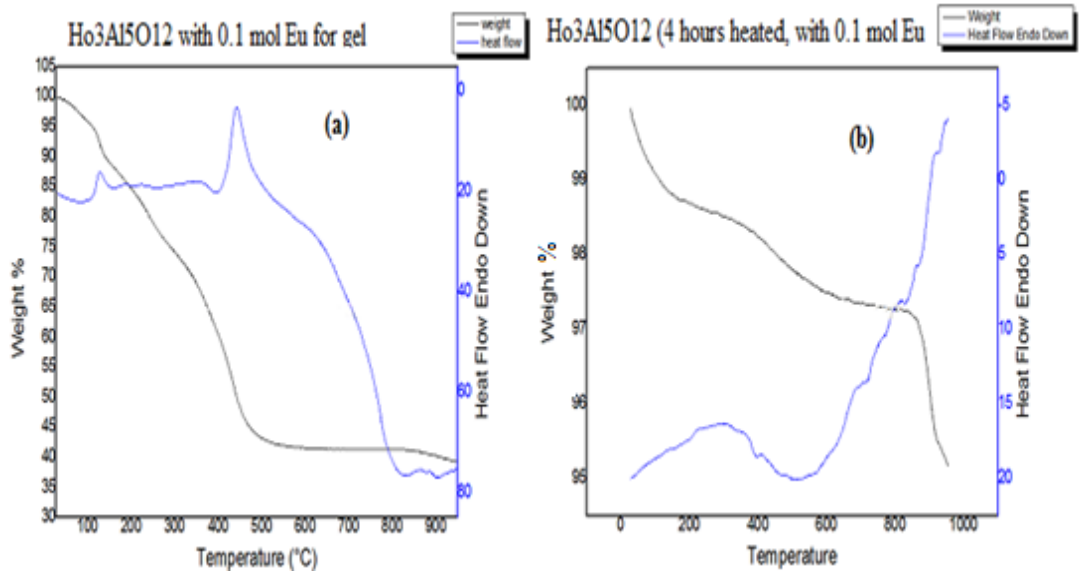

Figure 28. The TG/DTA curves of the 0.10 mol Eu^{3+} doped $Ho_3Al_5O_{12}$ a) gel form of dried at 100˚C, b) after heated 4hours at 800˚C

4.2.1.4 UV-vis/DRS studies of Eu:HAG

The absorbance and reflectance spectra of Eu^{3+} doped $Ho_3Al_5O_{12}$ garnets are shown in figures 29 and 30 respectively. As can be seen from figures all investigated Eu^{3+} doped Ho-Al-O garnet structure compounds show no change after doping. There are 8 peaks in visible and 3 peaks in UV region on spectra. $Ho_3Al_5O_{12}$ garnet without Eu^{3+} has lowest level absorbance between 200 and 900 nm. After the doping Eu^{3+} into the holmium aluminum garnet, it could be waited for the absorbance level is increasing in all wavelengths. In spite, the spectrum lines are mostly parallel for each other, the 0.50 Eu^{3+} doped sample showed highest absorption. This may be caused from atomic size of grain that reached maximum level with doping Eu^{3+} in molar ratio. While, 0.75 and 1.00 Eu^{3+} doped samples has lower absorption than 0.50 doped one, since distortions on crystal structure.

As conclusion it can be told the garnet structures are stable after doping. Red shift is observed increasing with molar doping amount of Eu^{3+}. There is not a big change in the structure and this conclusion is compatible with the results those are obtained from FTIR, XRD, SEM and EDX studies.

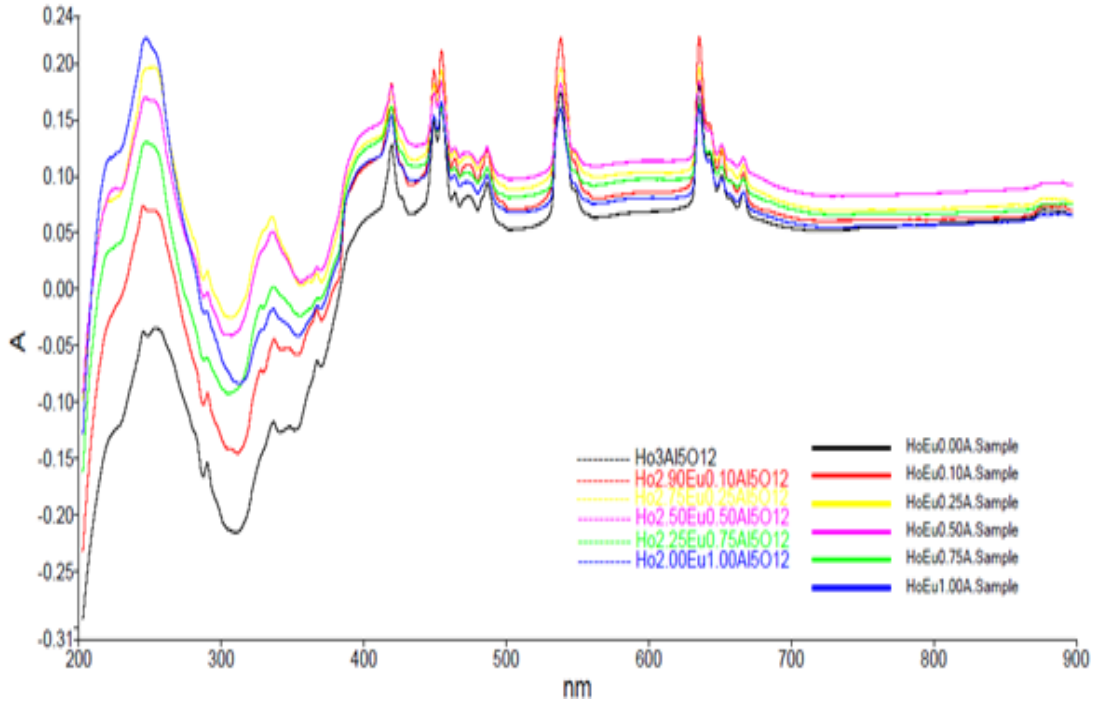

Figure 29. The UV-vis/DRS absorption spectra of Eu^{3+} doped $Ho_3Al_5O_{12}$

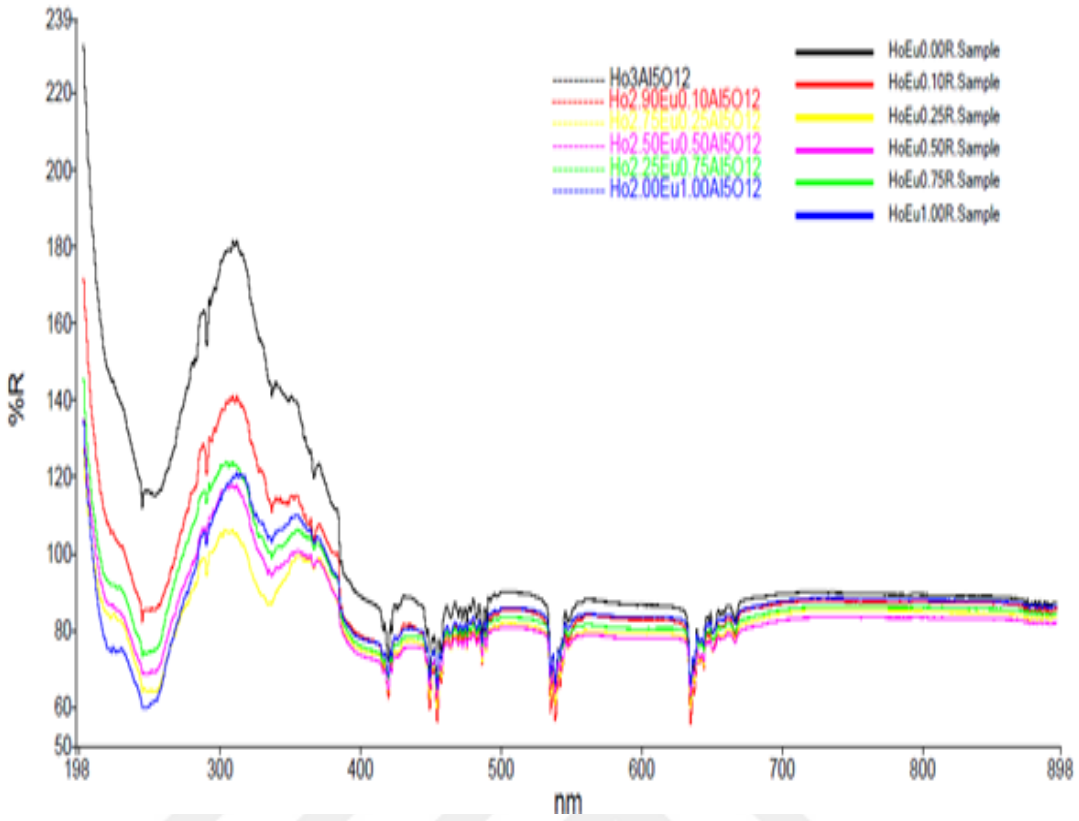

Figure 30. The UV-vis/DRS reflection spectra of Eu^{3+} doped $Ho_3Al_5O_{12}$

4.2.1.5 The SEM studies of Eu:HAG

As a valuable technique for the morphological characterization is SEM for solid materials. The microscopy technique is used to investigate the textural properties of the different amounts of Eu^{3+} doped $Ho_3Al_5O_{12}$. The obtained results are given in figure 31. The garnet particles with different amount Eu^{3+} are similar shaped. There can be seen clearly in the Figure 31 doped Eu^{3+} is covered on the surface of the holmium garnet. The SEM images are consistent with results observed by XRD measurements. Finally SEM results support the conclusions made by XRD and showed that there is not any organic matter left in sol-gel derived garnet and also there is no change in the garnet structure after doping Eu into the structure .

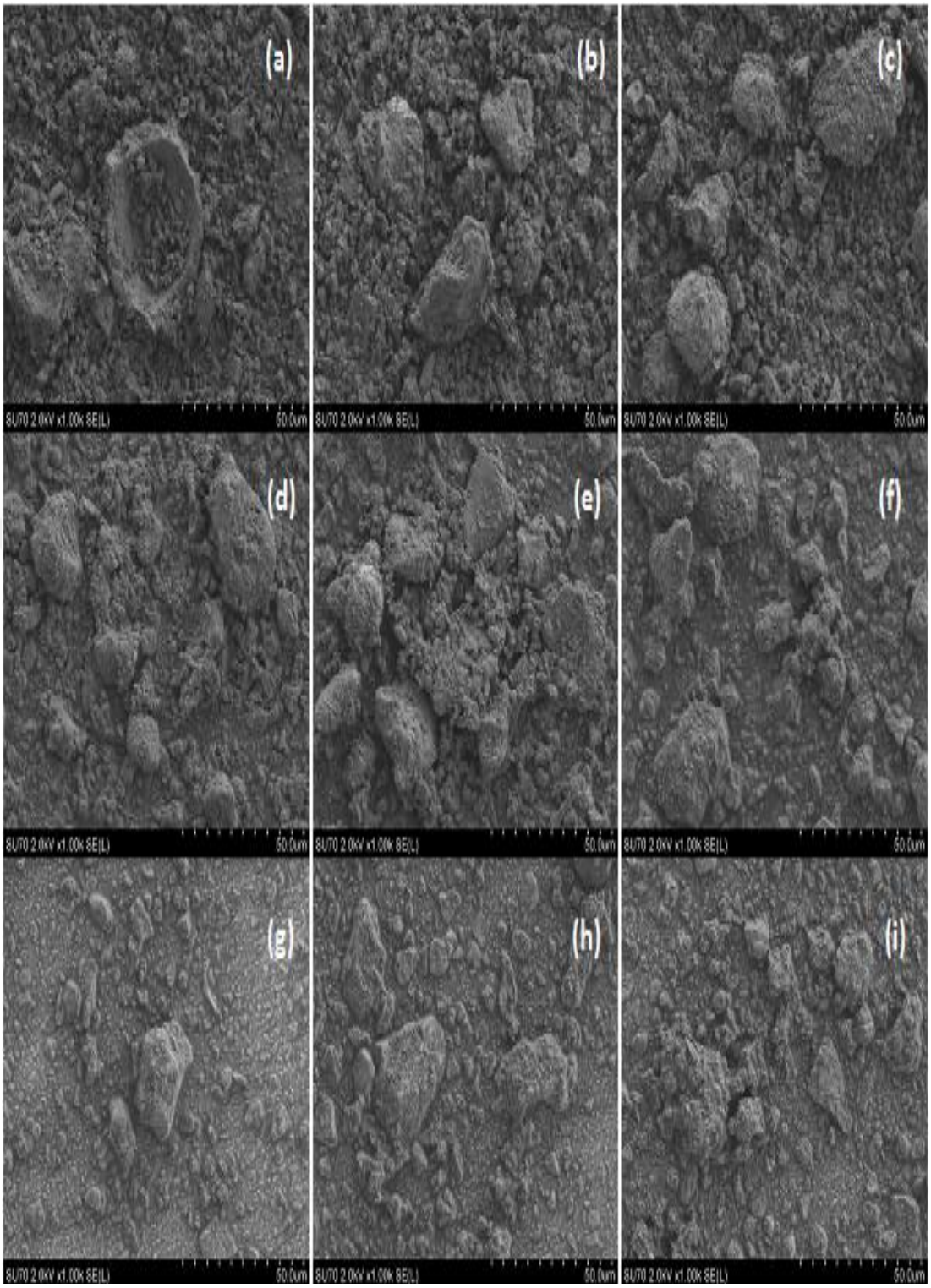

Figure 31. The SEM micrographs of Eu^{3+} doped $Ho_3Al_5O_{12}$ a), b) and c) 0.25 mol Eu d), e) and f) 0.75 mol Eu; g), h) and i) 1.00 mol Eu

4.2.2 The studies for $Dy_3Al_5O_{12}$ doped with Eu^{3+} (Eu:DAG)

4.2.2.1 The XRD studies of Eu:DAG

The XRD patterns of 5 different amount of Eu^{3+} doped $Dy_3Al_5O_{12}$ garnets are shown in figures from 32 to 36.

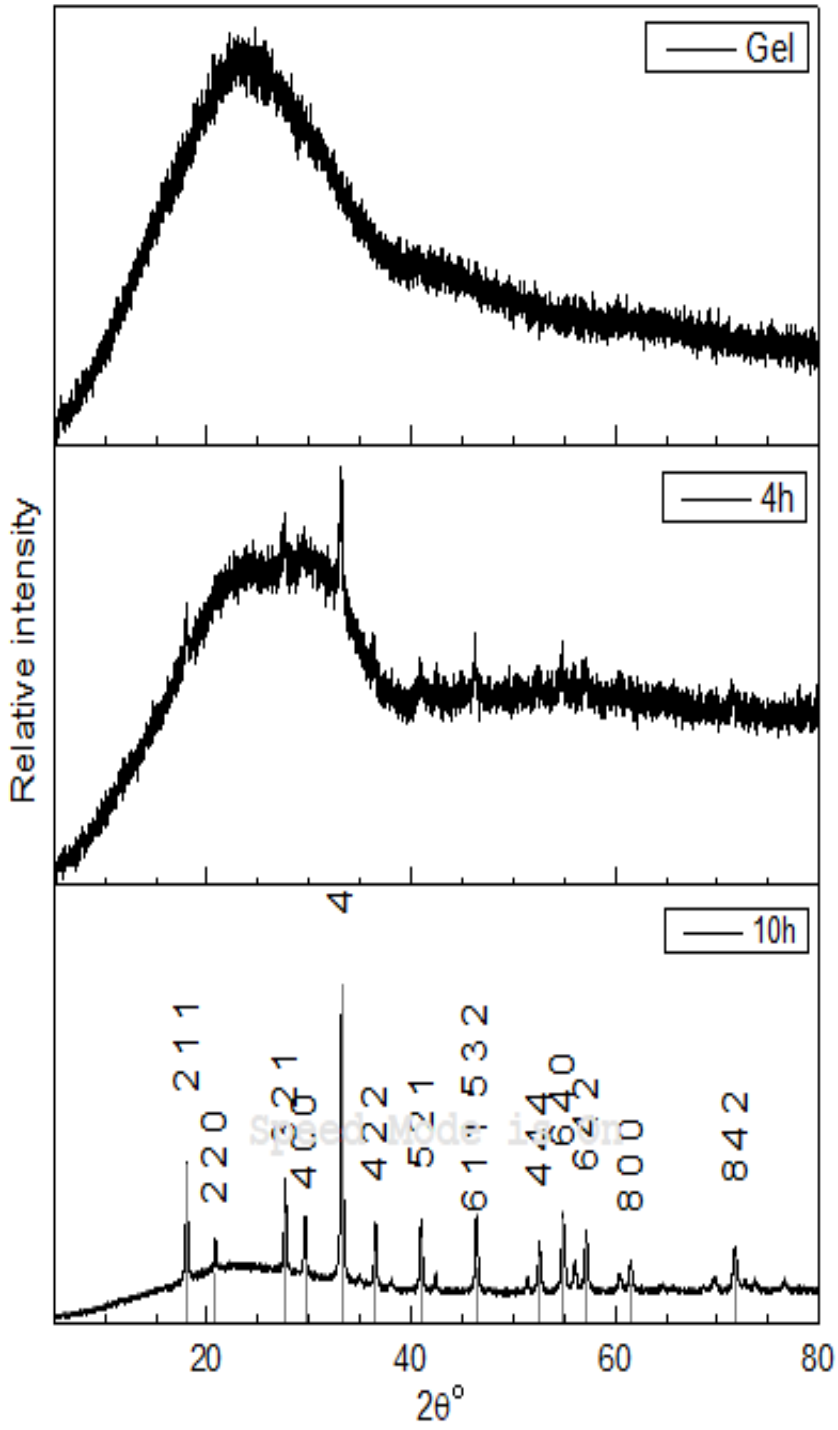

Figure 32. The XRD pattern of 0.10 mol Eu^{3+} doped $Dy_3Al_5O_{12}$

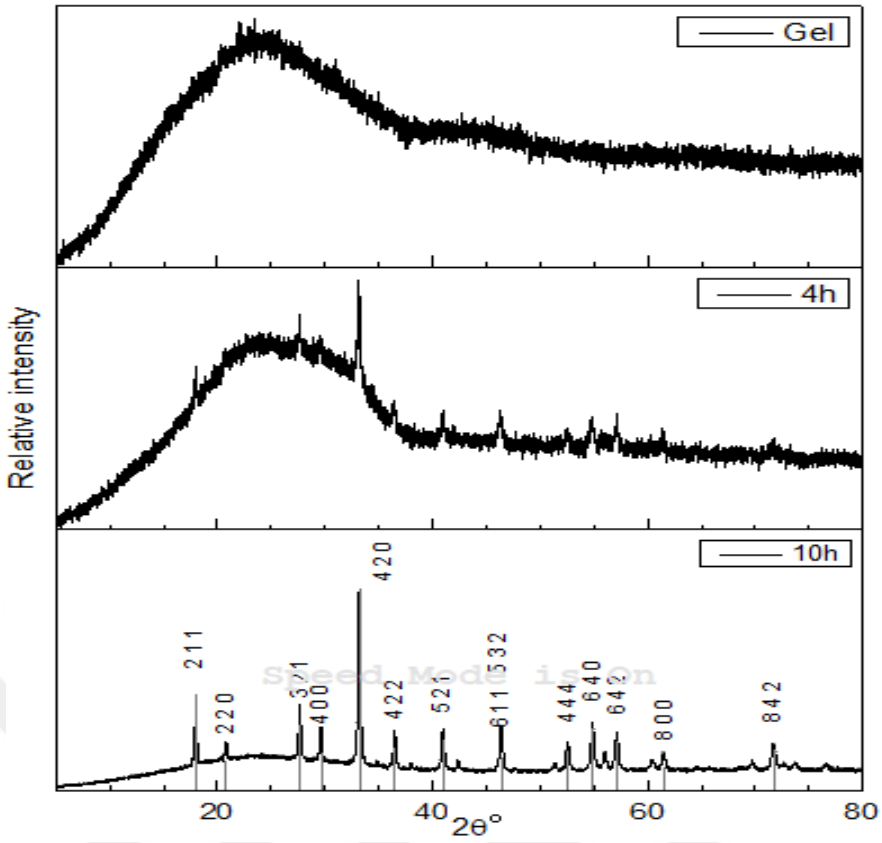

Figure 33. The XRD pattern of 0.25 mol Eu^{3+} doped $Dy_3Al_5O_{12}$

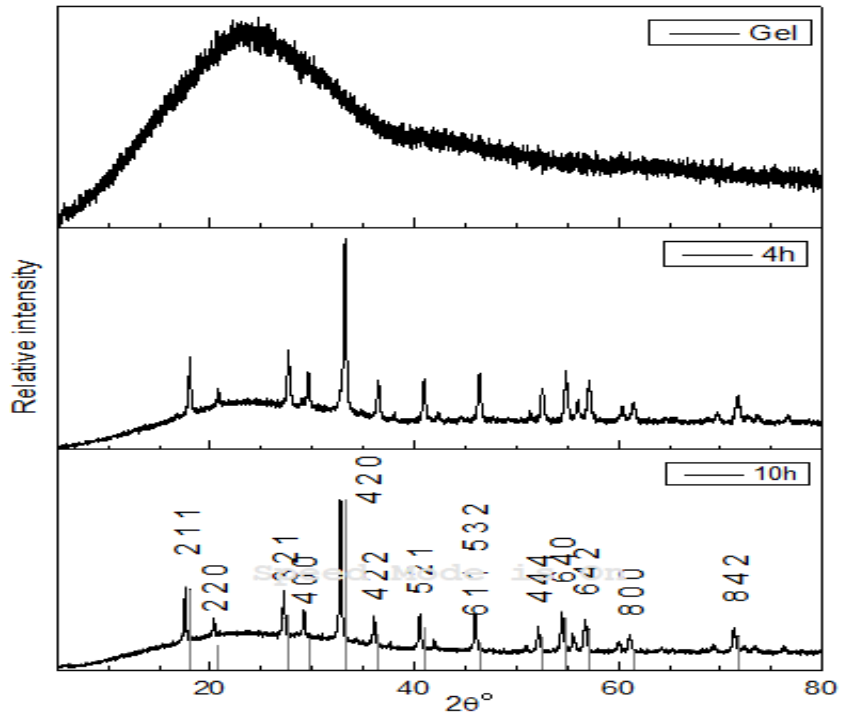

Figure 34. The XRD pattern of 0.50 mol Eu^{3+} doped $Ho_3Al_5O_{12}$

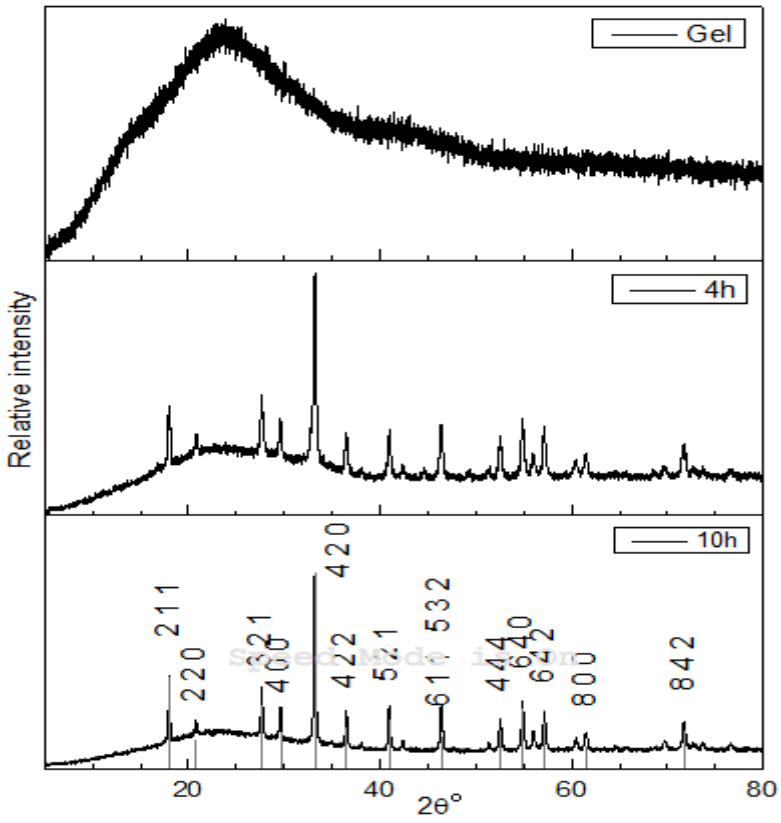

Figure 35. The XRD pattern of 0.75 mol Eu^{3+} doped $Dy_3Al_5O_{12}$

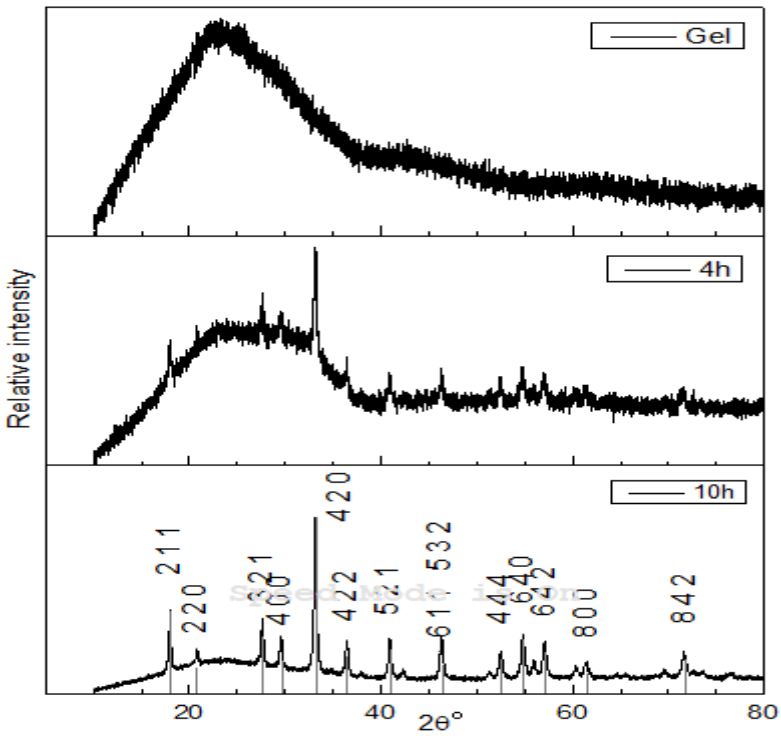

Figure 36. The XRD pattern of 1.00 mol Eu^{3+} doped $Dy_3Al_5O_{12}$

It should be noted that when Eu^{3+} doped into $Dy_3Al_5O_{12}$, is shown in the figure 32-36 is synthesized, there is no special condition or change. The lack of impurity peaks show us that the synthesized garnets doped with Eu^{3+} are pure and phase stable. The peak positions and relative intensity is also in agreement with the reference data for $Dy_3Al_5O_{12}$ (PDF [04-006-4053]).

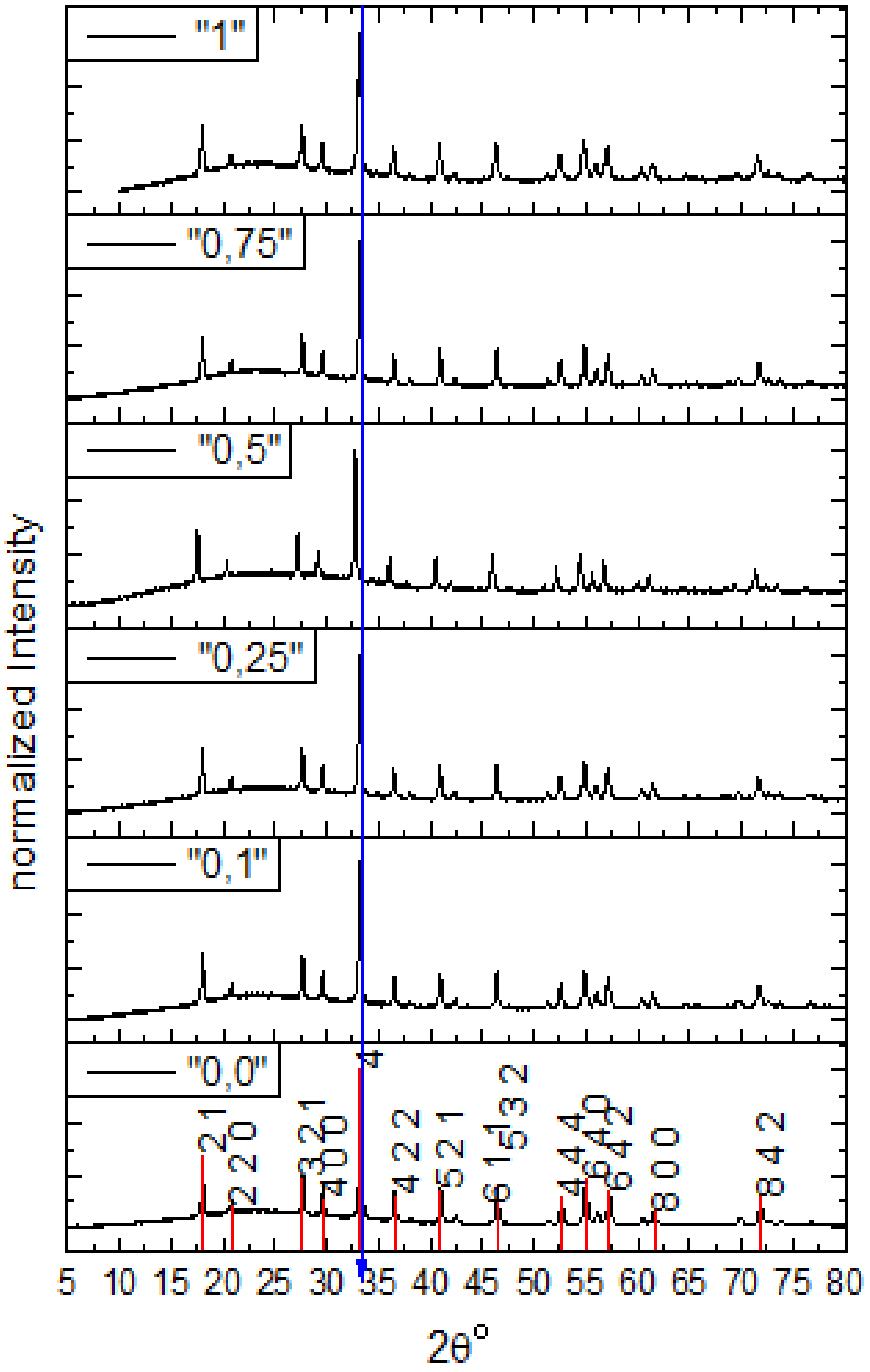

Figure 37. The XRD pattern of Eu^{3+} doped $Dy_3Al_5O_{12}$ after 10 hours

As can be seen from the XRD patterns, there is no structural change in the garnet after doping with Eu^{3+}. Thus we can understand this situation as it took place the formation of Eu^{3+} doped $Dy_3Al_5O_{12}$ garnets.

4.2.2.2 The FTIR spectroscopy studies of Eu:DAG

5 different concentrations of Eu^{3+} which were used to obtain Eu^{3+} doped $Dy_3Al_5O_{12}$ garnets then 5 different amounts of Eu^{3+} doped garnets are obtained. These amounts are 0.10, 0.25, 0.50, 0.75 and 1.00 mol Eu^{3+}. FTIR spectra of 0.10, 0.25, 0.50, 0.75 and 1.00 mol Eu^{3+} doped garnet can be seen in figures 38-42.

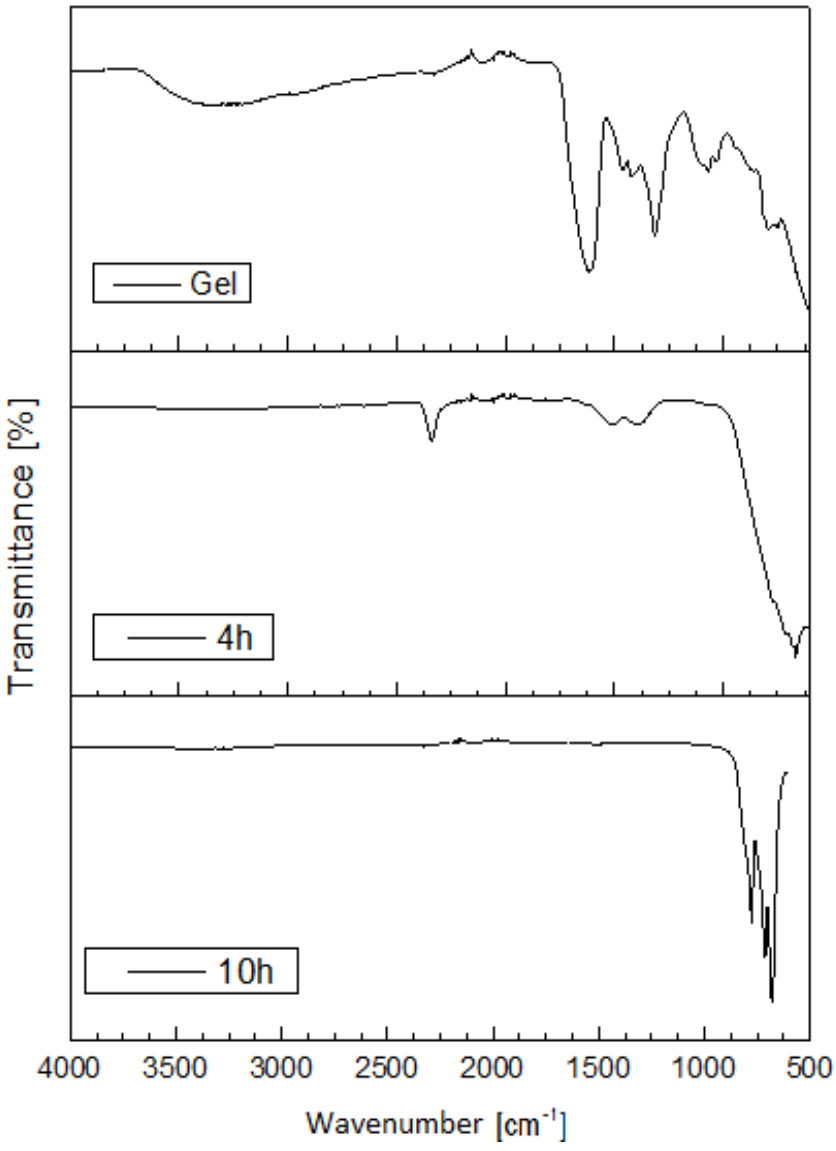

Figure 38. The FTIR spectroscopy of 0.10 mol Eu^{3+} doped $Dy_3Al_5O_{12}$

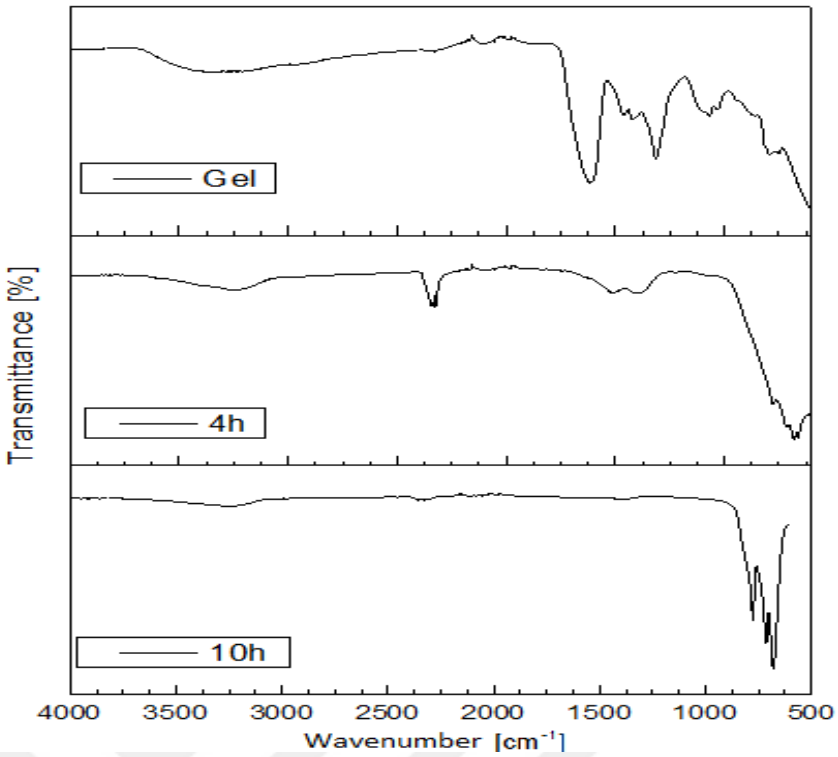

Figure 39. The FTIR spectroscopy of 0.25 mol Eu^{3+} doped $Dy_3Al_5O_{12}$

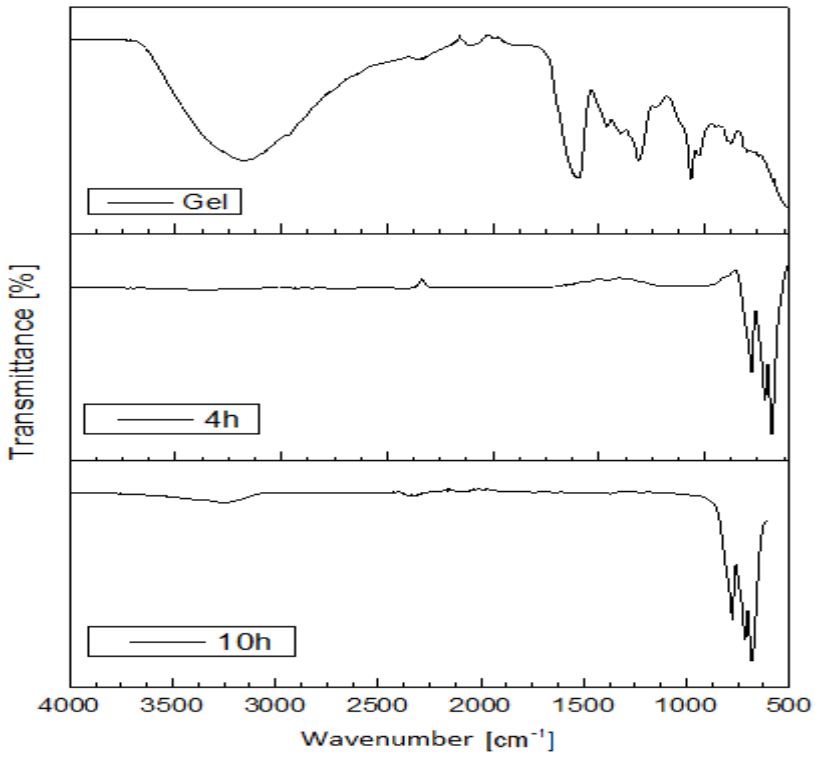

Figure 40. The FTIR spectroscopy of 0.50 mol Eu^{3+} doped $Dy_3Al_5O_{12}$

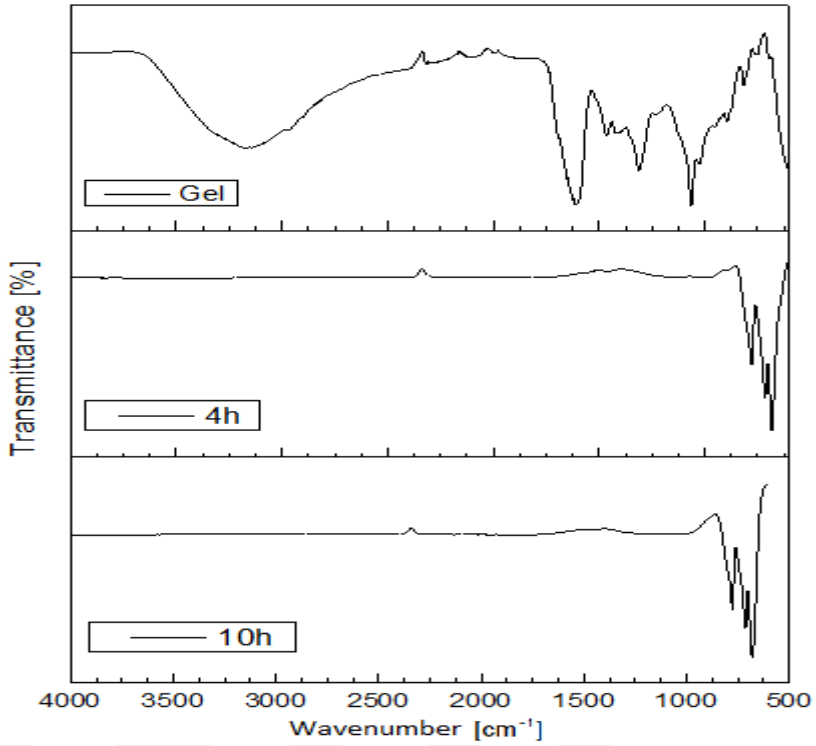

Figure 41. The FTIR spectroscopy of 0.75 mol Eu^{3+} doped $Dy_3Al_5O_{12}$

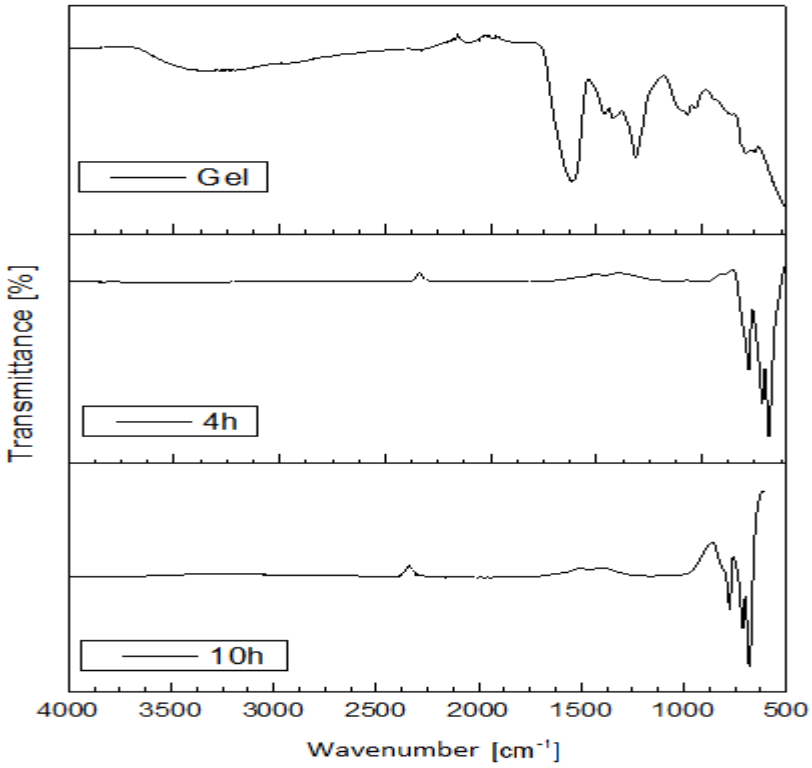

Figure 42. The FTIR spectroscopy of 1.00 mol Eu^{3+} doped $Dy_3Al_5O_{12}$

The FTIR spectra of $Dy_3Al_5O_{12}$ garnets with europium that shown in Figure 38-42 were very similar to those shown in Figure 11. The most important feature is that intensive bands are not changed under 1000 cm^{-1} after being doped Eu^{3+} in 5 different ratio. The structure of $Dy_3Al_5O_{12}$ is not changing after the dopant Eu^{3+}. So the metal-oxygen (M-O) bonds in the $Dy_3Al_5O_{12}$ are protected and do not change. Furthermore after the crystallization there is no organic matter in the structure.

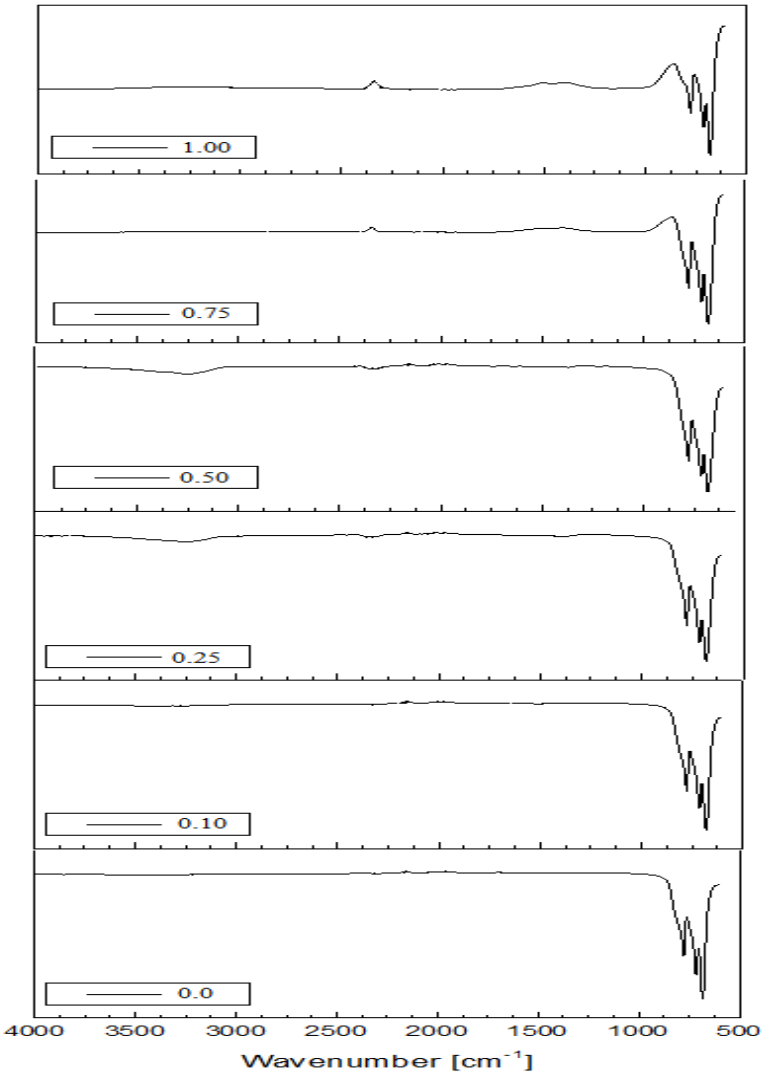

Figure 43. The FTIR spectroscopy results comparisons for Eu^{3+} doped $Dy_3Al_5O_{12}$ (all after 10 hours heating)

As can be seen from the infrared spectra in figure 43, there is no structural change or shift in the garnet after doping with Eu^{3+}. Thus we can understand this situation as it took place the formation of Eu^{3+} doped $Dy_3Al_5O_{12}$ garnets.

4.2.2.3 Thermal studies (TG/DTA) of Eu:DAG

The TG/DTA curves of the 0.10 mol Eu^{3+} doped $Dy_3Al_5O_{12}$ with Eu^{3+} for both gel form and after heated form are shown in figure 44 a), b) and c) respectively. The heating was in temperature range from room temperature to 1000^{o}C as like in the dysprosium garnet without Eu. There the peaks are replaced at 400 ^{o}C and 800 ˚C. Therefore, the curves indicate that this 0.10 mol Eu^{3+} doped $Dy_3Al_5O_{12}$ crystal is also thermodynamically stable upon 900˚C and there are very small amount of weight loss after 900˚C and the calcination would have been done at 1000 ˚C.

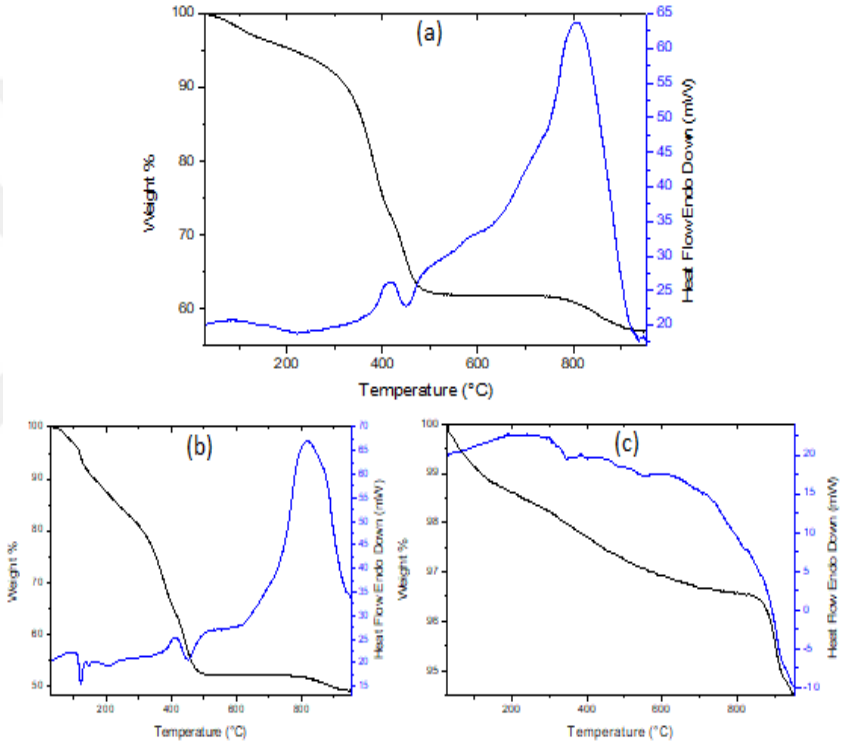

Figure 44. The TG/DTA curves of the $Dy_3Al_5O_{12}$ a) gel form of DAG, b) 0.10 mol Eu doped gel form of Eu:DAG, c) 0.10 mol Eu^{3+} doped after 4h heated

4.2.2.4 The UV-vis/DRS studies of Eu:DAG

The absorbance and reflectance spectra of Eu^{3+} doped $Dy_3Al_5O_{12}$ garnets are shown in figures 45 and 46 respectively. As can be seen from figures all investigated Eu^{3+} doped Dy-Al-O garnet structure compounds show no change after doping. There are groups of absorption peaks around 450 nm, 750 nm, 800 nm, 890 nm and also a few clear peaks in UV region. However, there are peaks at UV-invisible region

arounds of 800 and 900 nm, as well. The spectrum of all samples shows the same peaks with different absorption amounts. The highest absorption is detected with 1.00 mol Eu^{3+} doped sample. The garnet structures are stable after doping Eu^{3+}. Blue-shift is observable with increasing Eu^{3+} molar amount until 0.75 mol Eu^{3+}. This conclusion is compatible with the results those are obtained from FTIR, XRD, SEM and EDX studies.

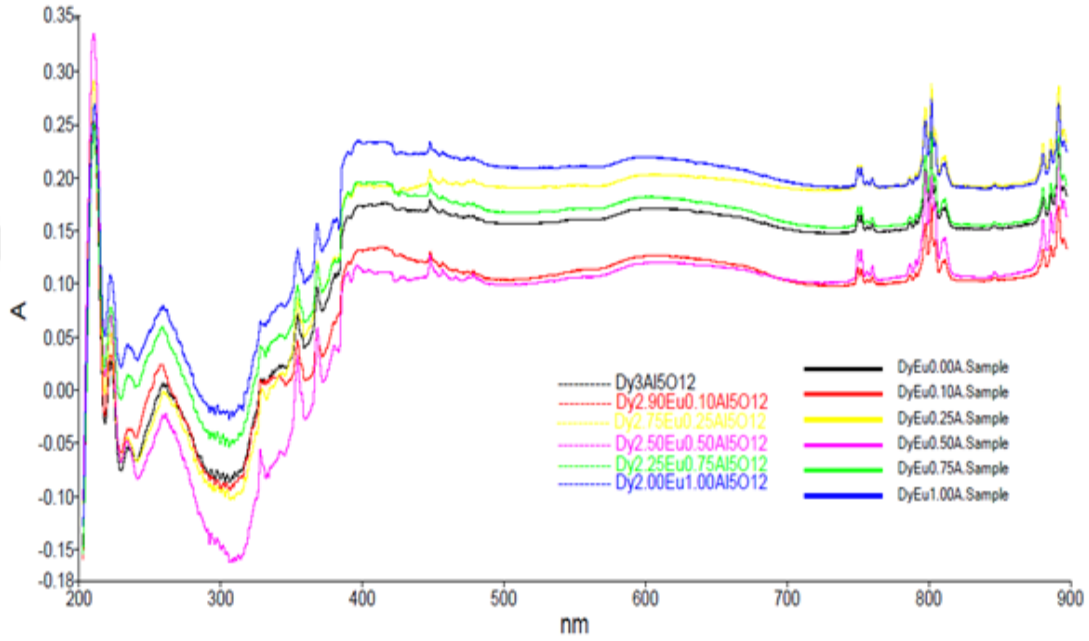

Figure 45. The UV-vis/DRS absorption spectra of Eu^{3+} doped $Dy_3Al_5O_{12}$

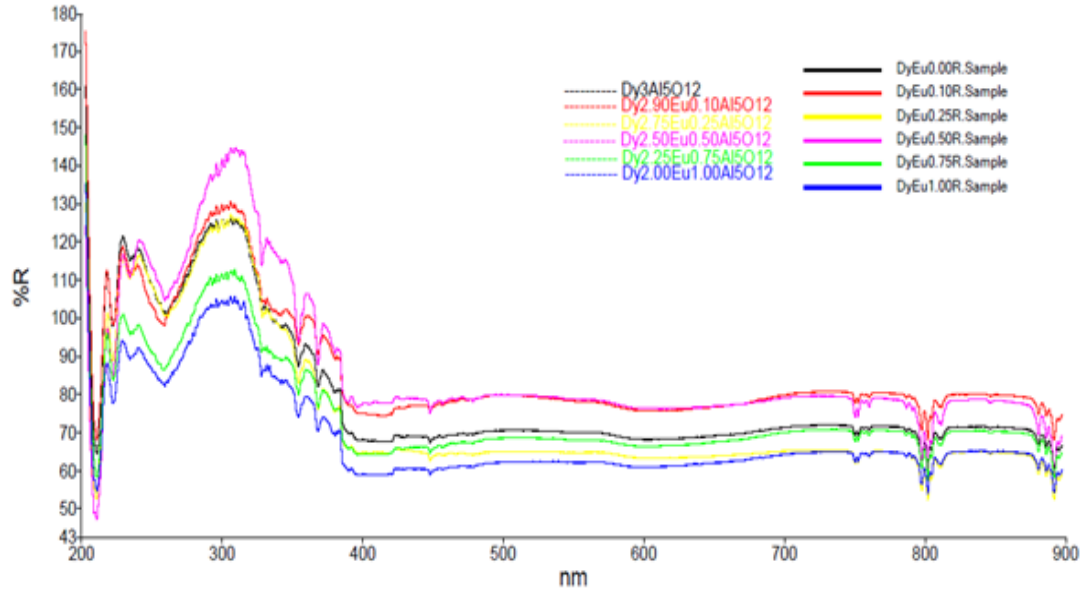

Figure 46. The UV-vis/DRS reflaction pectra of Eu^{3+} doped $Dy_3Al_5O_{12}$

4.2.2.5 The SEM studies of Eu:DAG

SEM and EDX results showed that the host crystal structures were protected prediction with smooth surfaces on micrographs and it is predicted that the doping the metal atoms is successful. In these images, the small grains onto the large-grains can be observe, easily.

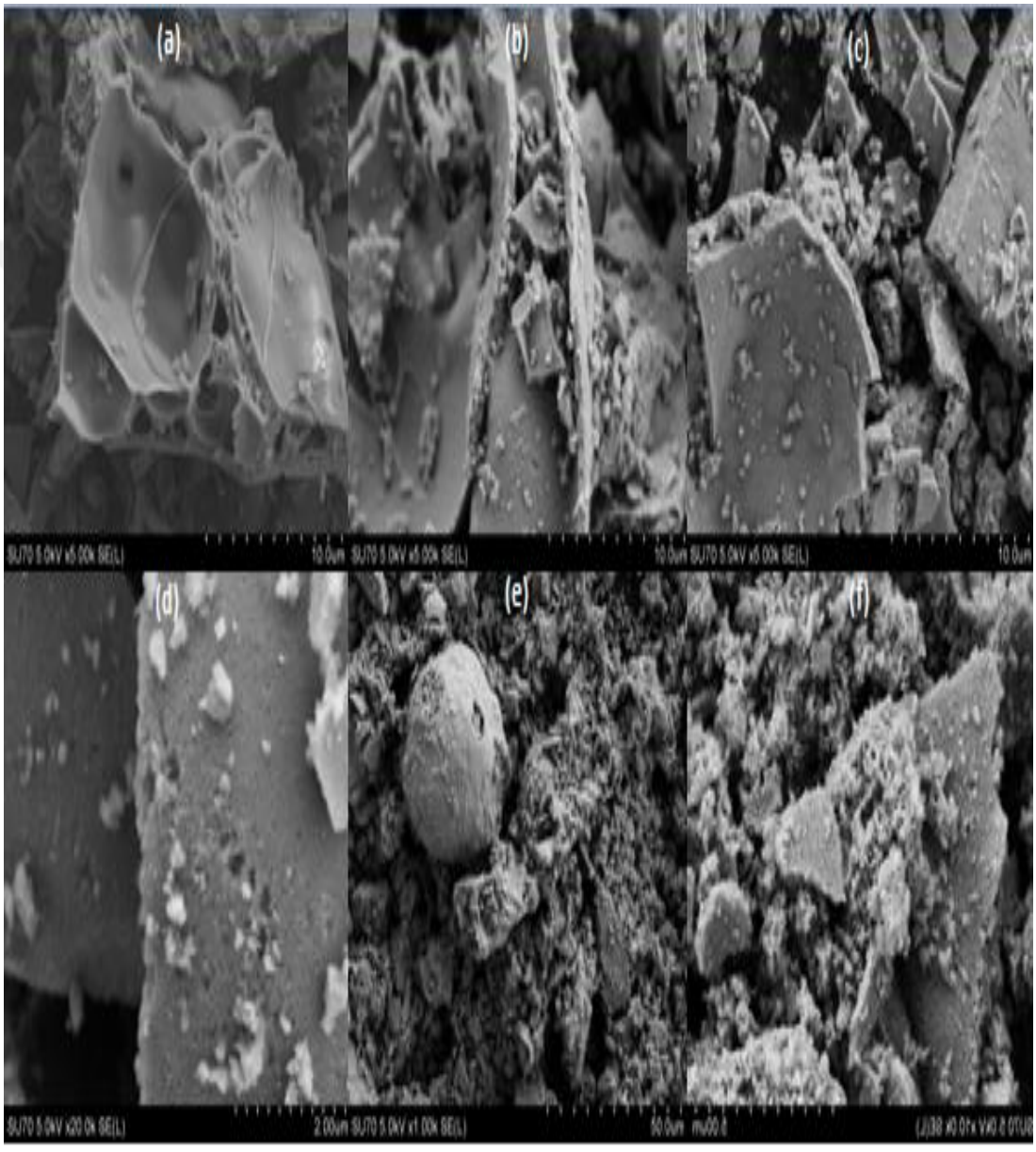

Figure 47. The SEM micrographs of $Dy_3Al_5O_{12}$ a) unheated gel form of 0.10 mol Eu doped DAG; b), c) and d) 0.10 mol Eu^{3+} doped after 4 hours heating at 800˚C; e), f) 0.10 mol Eu^{3+} doped after 10 hours at 1000˚C.

4.2.3 The studies for $Tb_3Al_5O_{12}$ doped with Eu^{3+} (Eu:TAG)

4.2.3.1 The XRD studies of Eu:TAG

The XRD patterns of 5 different amount of Eu^{3+} doped $Tb_3Al_5O_{12}$ garnets are shown in figures from 48 to 52.

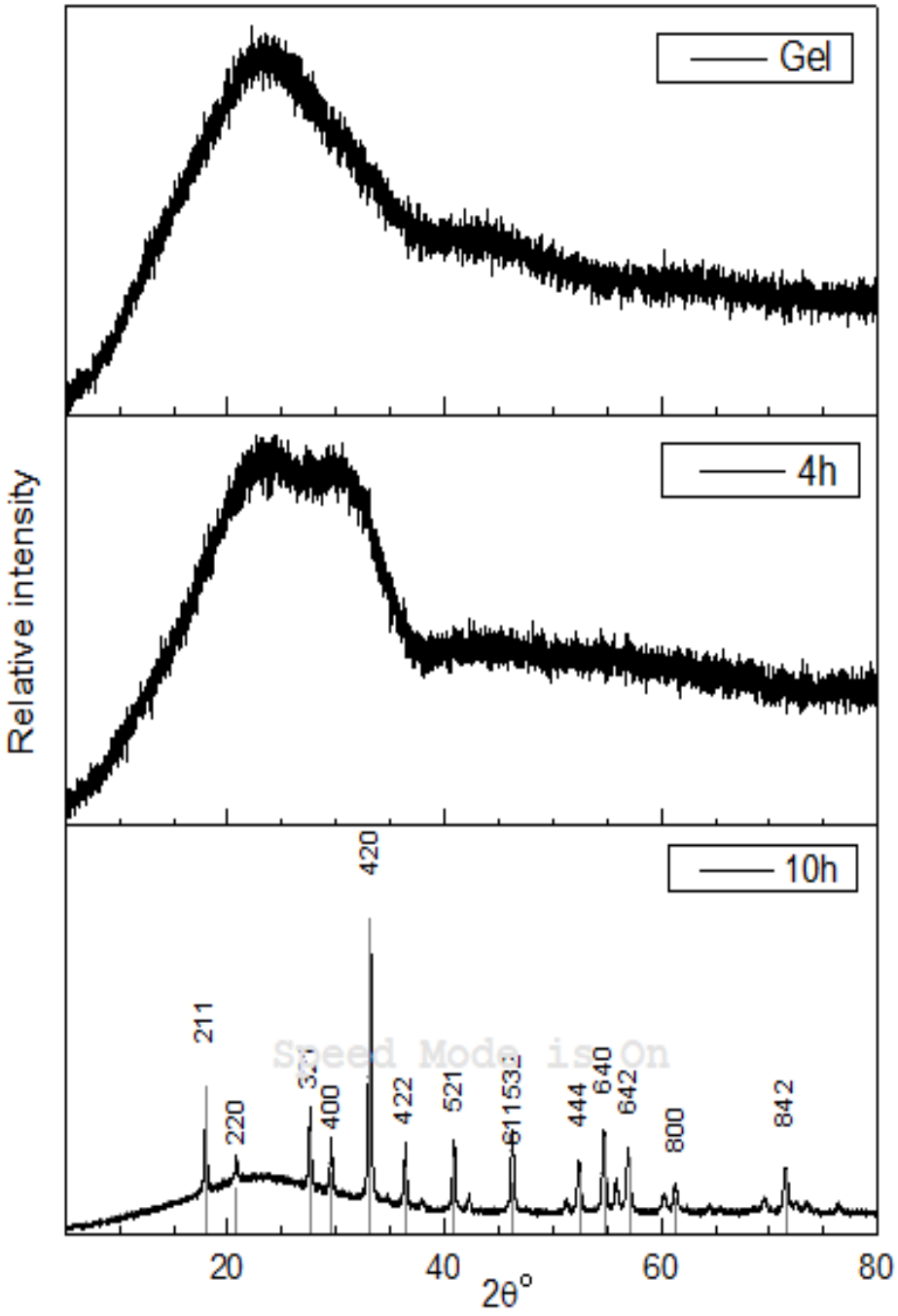

Figure 48. The XRD pattern of 0.10 mol Eu^{3+} doped $Tb_3Al_5O_{12}$

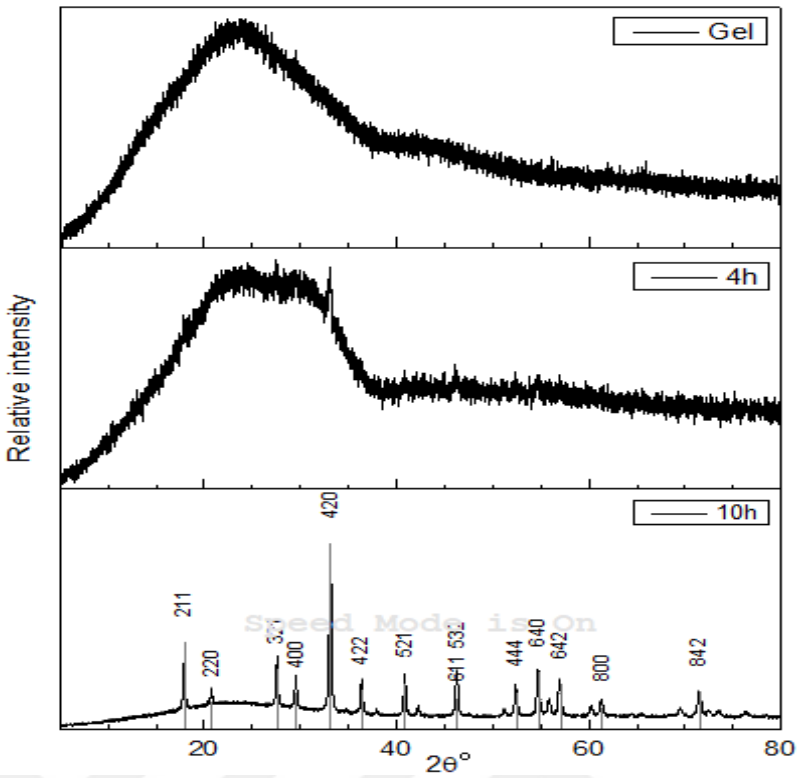

Figure 49. The XRD pattern of 0.25 mol Eu^{3+} doped $Tb_3Al_5O_{12}$

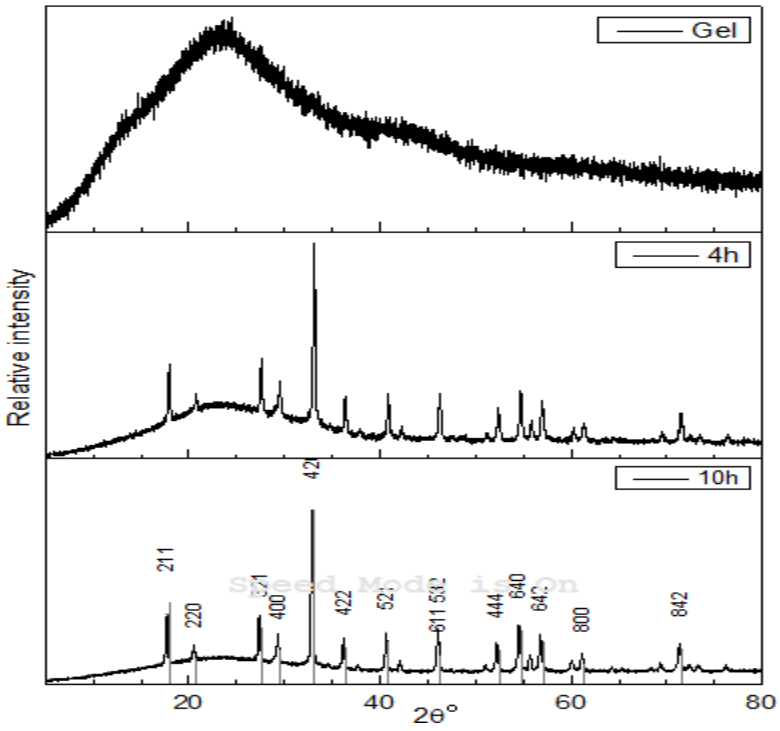

Figure 50. The XRD pattern of 0.50 mol Eu^{3+} doped $Tb_3Al_5O_{12}$

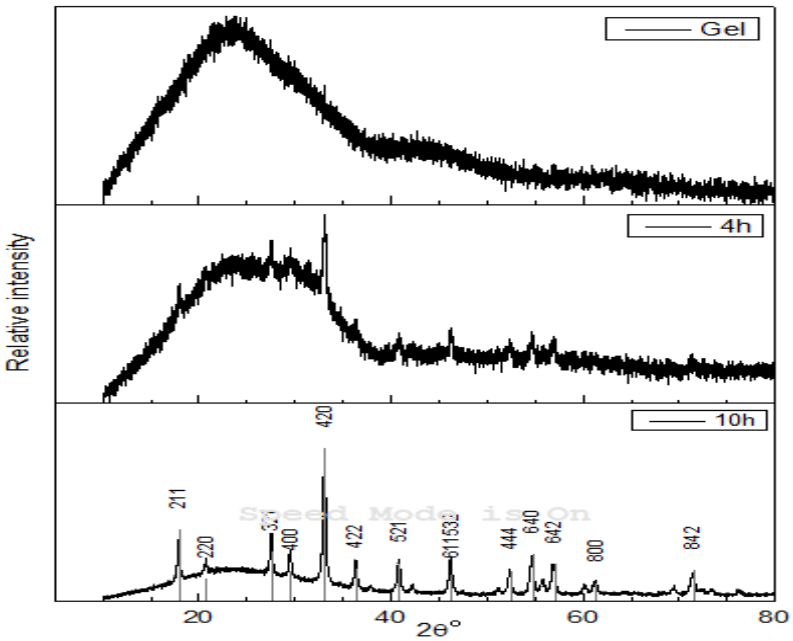

Figure 51. The XRD pattern of 0.75 mol Eu^{3+} doped $Tb_3Al_5O_{12}$

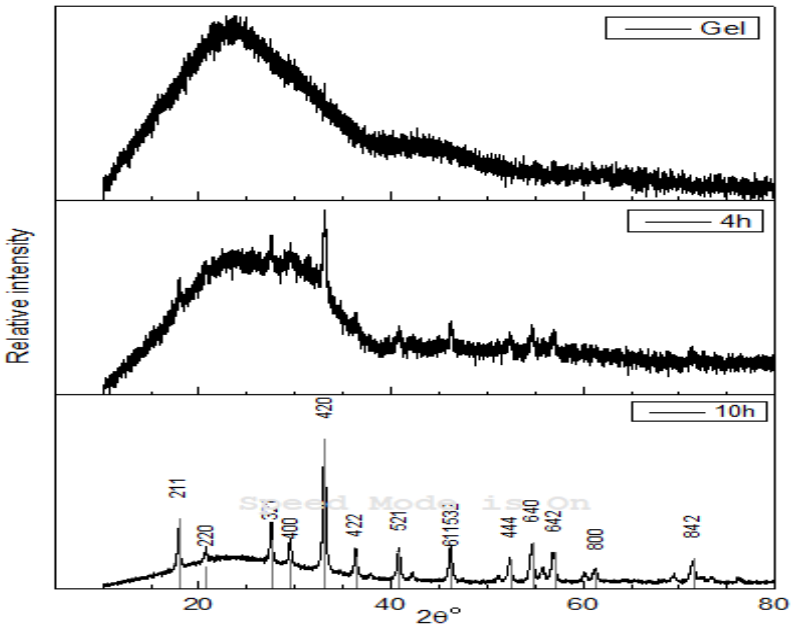

Figure 52. The XRD pattern of 1.00 mol Eu^{3+} doped $Tb_3Al_5O_{12}$

It should be noted that when Eu^{3+} doped into$Tb_3Al_5O_{12}$, is shown in the figure 48-52 is synthesized, there is no special condition or change. The lack of impurity peaks show us that the synthesized garnets doped with Eu^{3+} are pure and phase stable. The peak positions and relative intensity is also in agreement with the reference data for $Tb_3Al_5O_{12}$ (PDF [04-006-4054]).

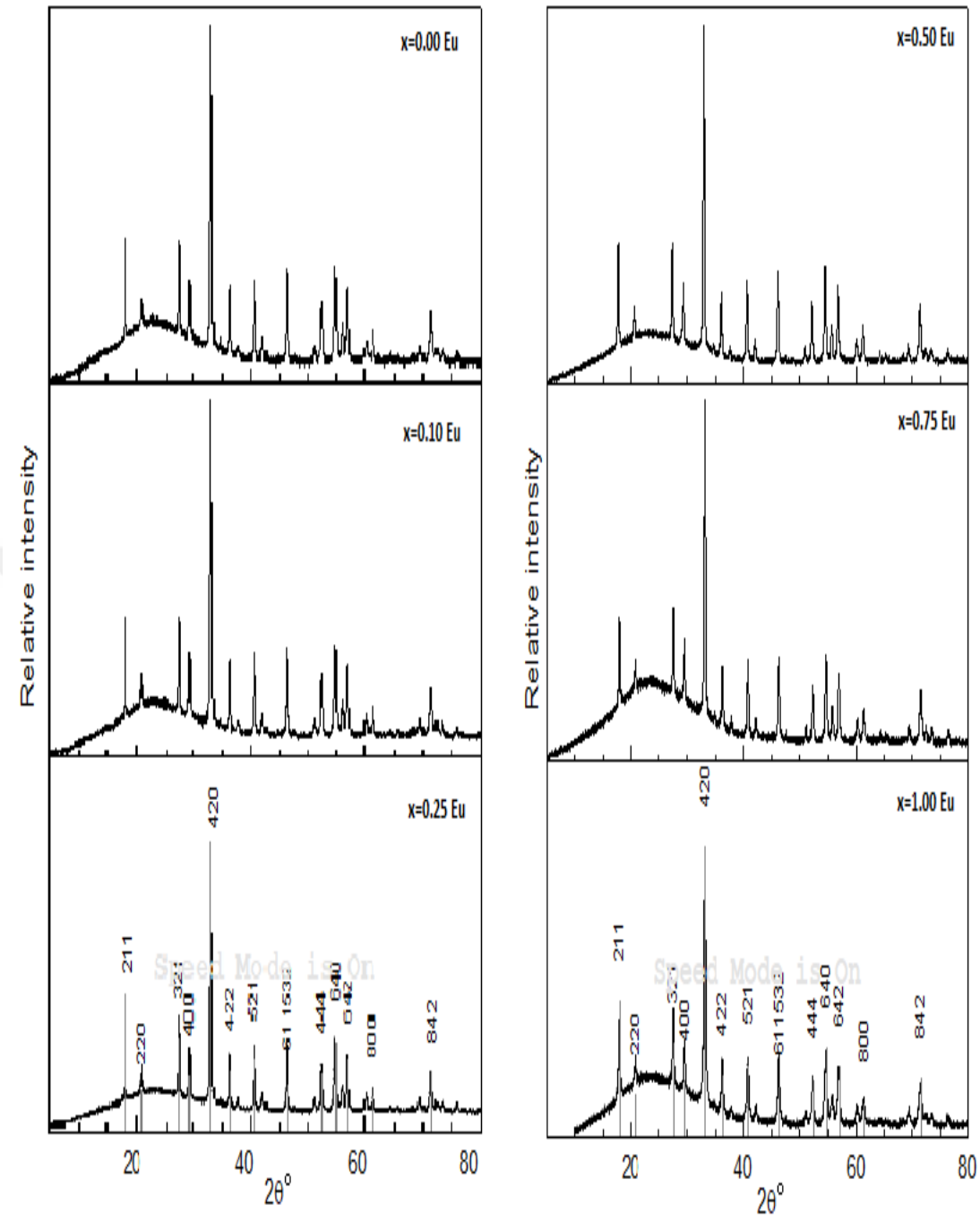

Figure 53. The XRD pattern of Eu^{3+} doped $Tb_3Al_5O_{12}$ after 10 hours

As can be seen from the XRD patterns, there is no structural change in the garnet after doping with Eu^{3+}. Thus we can understand this situation as it took place the formation of Eu^{3+} doped $Tb_3Al_5O_{12}$ garnets.

4.2.3.2 The FTIR spectroscopy studies of Eu:TAG

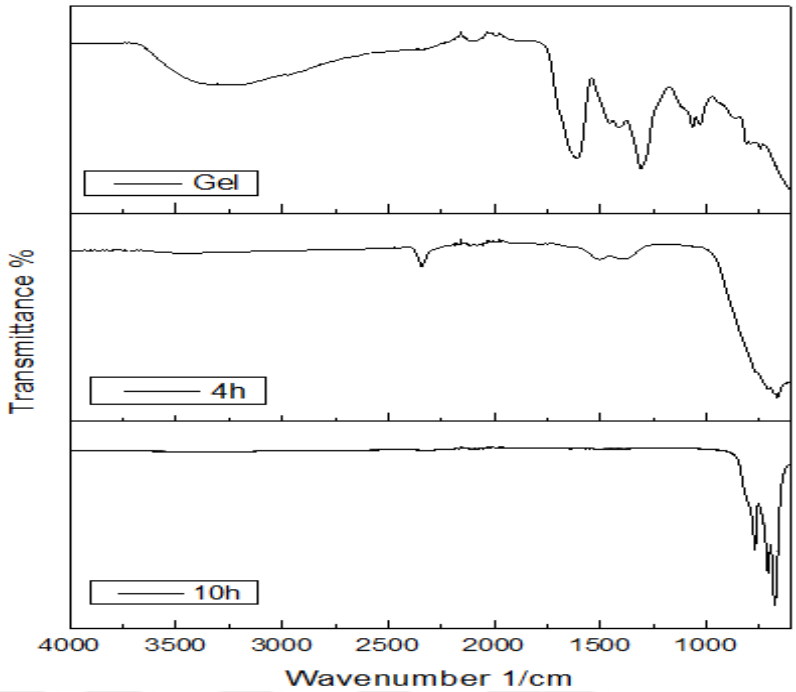

Figure 54. The FTIR spectroscopy of 0.10 mol Eu^{3+} doped $Tb_3Al_5O_{12}$

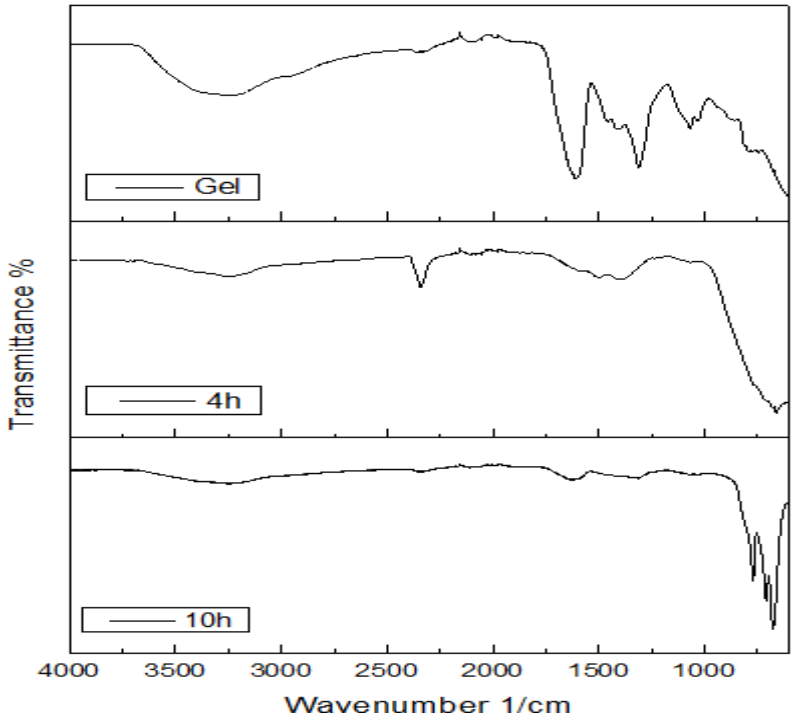

Figure 55. The FTIR spectroscopy of 0.25 mol Eu^{3+} doped $Tb_3Al_5O_{12}$

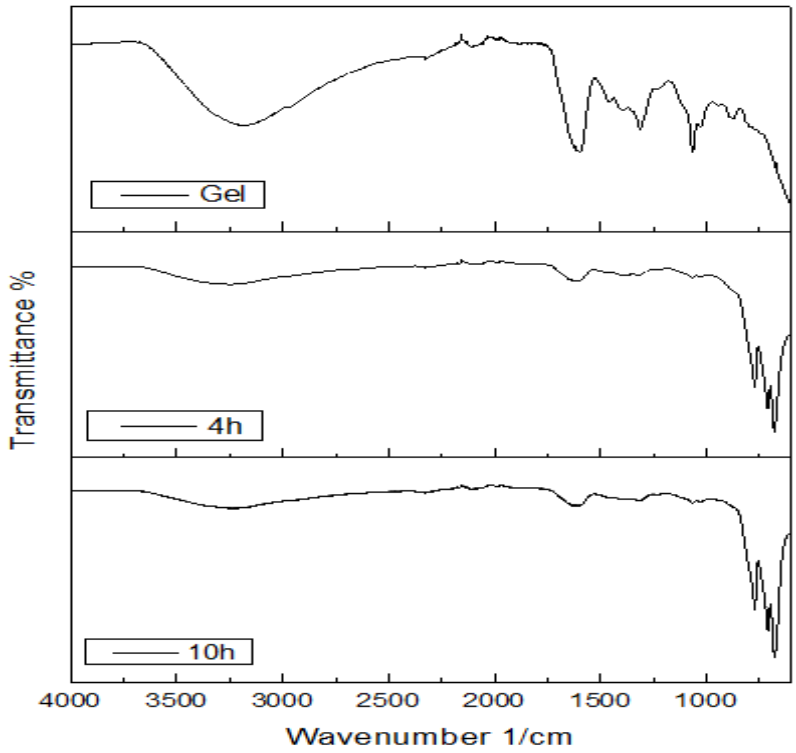

Figure 56. The FTIR spectroscopy of 0.50 mol Eu^{3+} doped $Tb_3Al_5O_{12}$

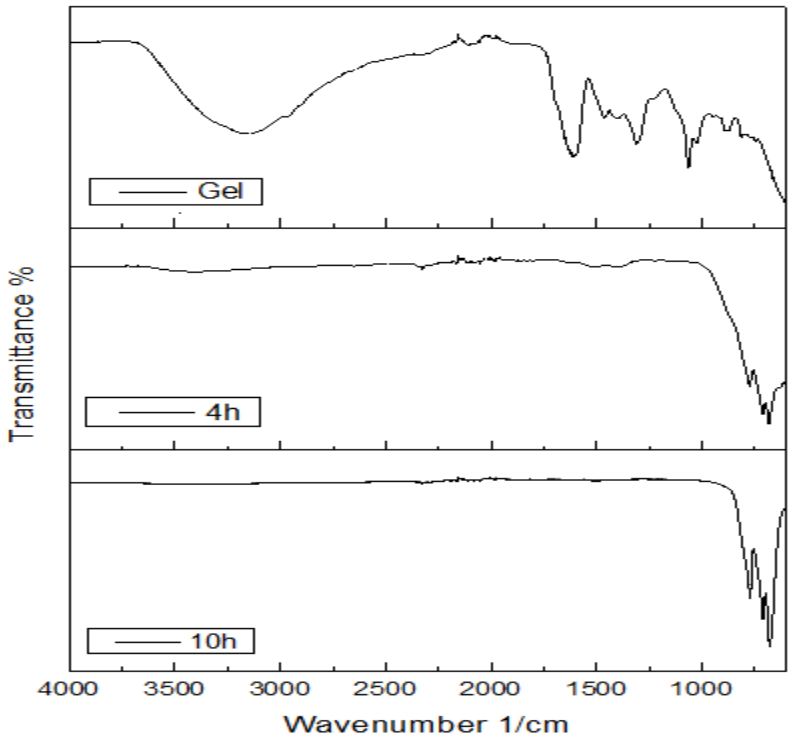

Figure 57. The FTIR spectroscopy of 0.75 mol Eu^{3+} doped $Tb_3Al_5O_{12}$

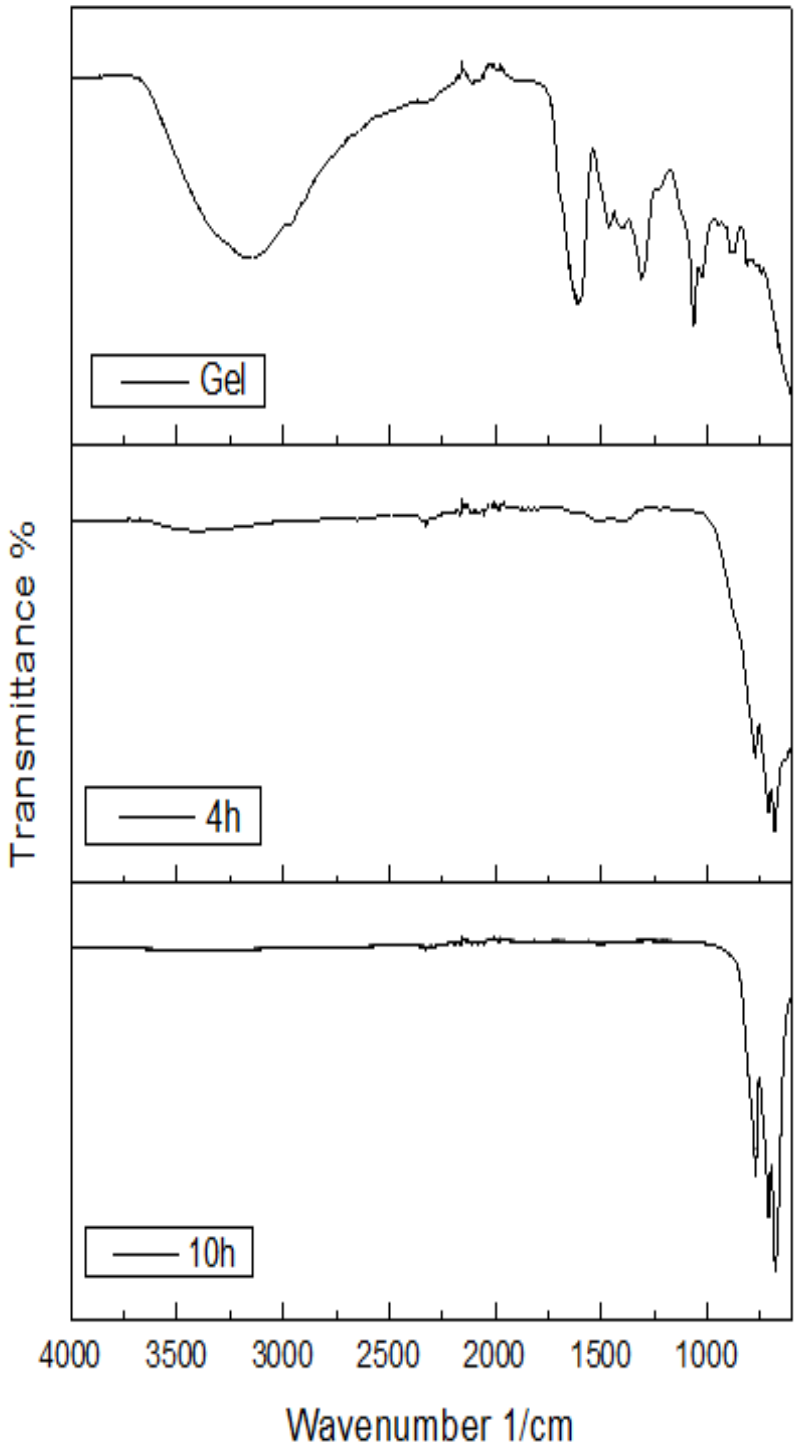

Figure 58. The FTIR spectroscopy of 1.00 mol Eu^{3+} doped $Tb_3Al_5O_{12}$

As can be seen , The $Tb_3Al_5O_{12}$ shows the same ordinary garnet Al-O peaks with $Ho_3Al_5O_{12}$ and $Dy_3Al_5O_{12}$. After 10 hour heat treatment, the all samples are took place as single $Tb_3Al_5O_{12}$ without any impurities or organic matters (Veith M. et al., 1999).

4.2.3.3 Thermal Studies (TG/DTA) of Eu:TAG

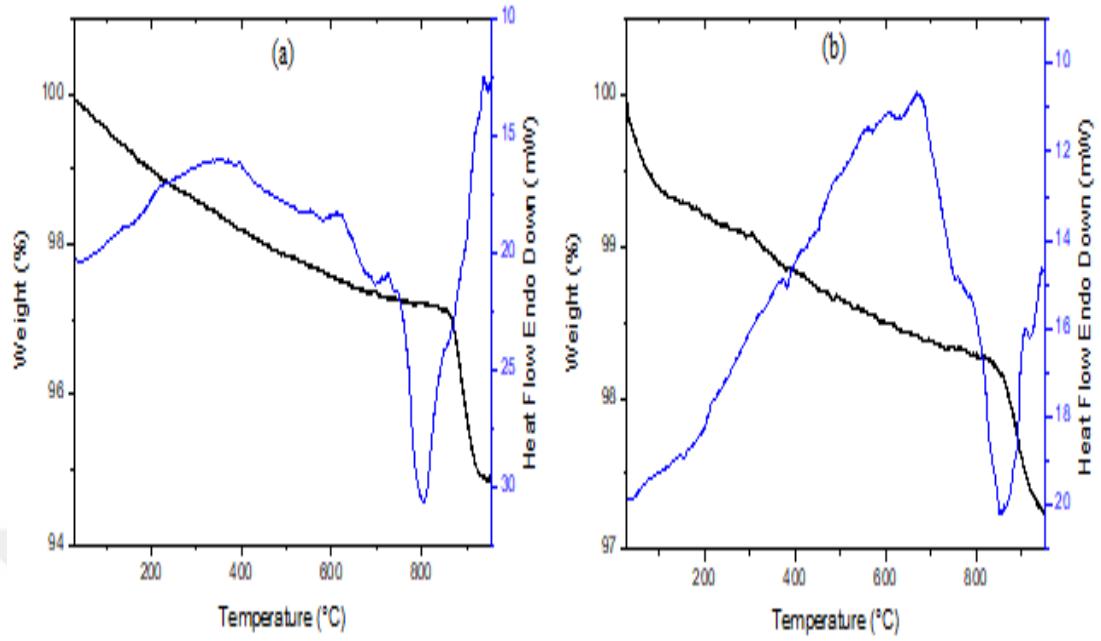

Figure 59. The TG/DTA curves of the $Tb_3Al_5O_{12}$ a) 0.25 mol Eu^{3+} doped TAG after 4 hours heating, b) 0.75 mol Eu^{3+} doped TAG after 4 hours heating

The thermal decomposition of 4 hour heated sample of $Tb_3A_5O_{12}$ is also similarly the same as 4 hour heated $Ho_3A_5O_{12}$ and $Dy_3A_5O_{12}$ by occuring a peak at 800˚C and continuing with immensely sharp losing of weight.

4.2.3.4 The UV-vis/DRS studies of Eu:TAG

The absorbance and reflectance spectra of Eu^{3+} doped $Tb_3Al_5O_{12}$ garnets are shown in figures 60 and 61 respectively. However, there is 2 major peaks between 200 and 300 nm, there cannot be seen any peaks in UV-visible spectral ranges that are 400 and 900 nm. Besides, doping of europium is caused a decrease on the absorptivity as its molar level increasing, interestingly. This result indicates that the europium acted like as donor depends on distortion caused by grain sizes. Also, 0.50 Eu^{3+} doped sample showed high absorption result. The blue-shift can be observe by increasing amount of Eu^{3+} in the sample. It indicates that the 0.50 Eu^{3+} doping is the best efficient way to obtain the most luminescent scintillator for Eu:TAG.

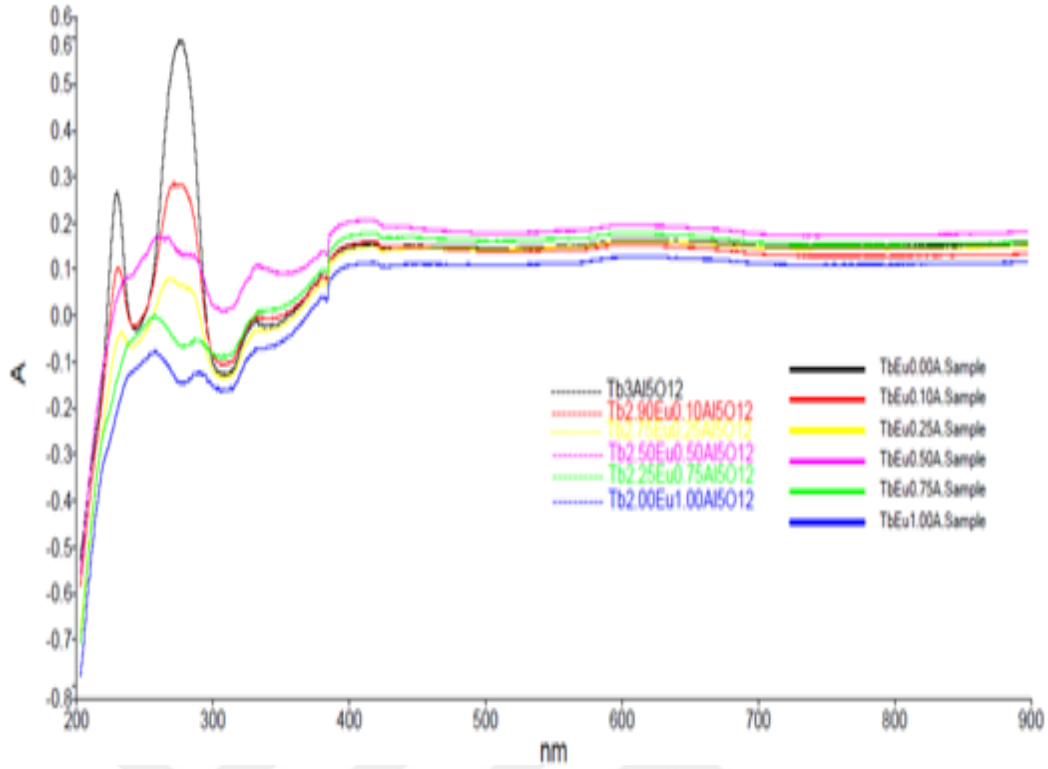

Figure 60. The UV-vis/DRS absorption Spectra of Eu^{3+} doped $Tb_3Al_5O_{12}$

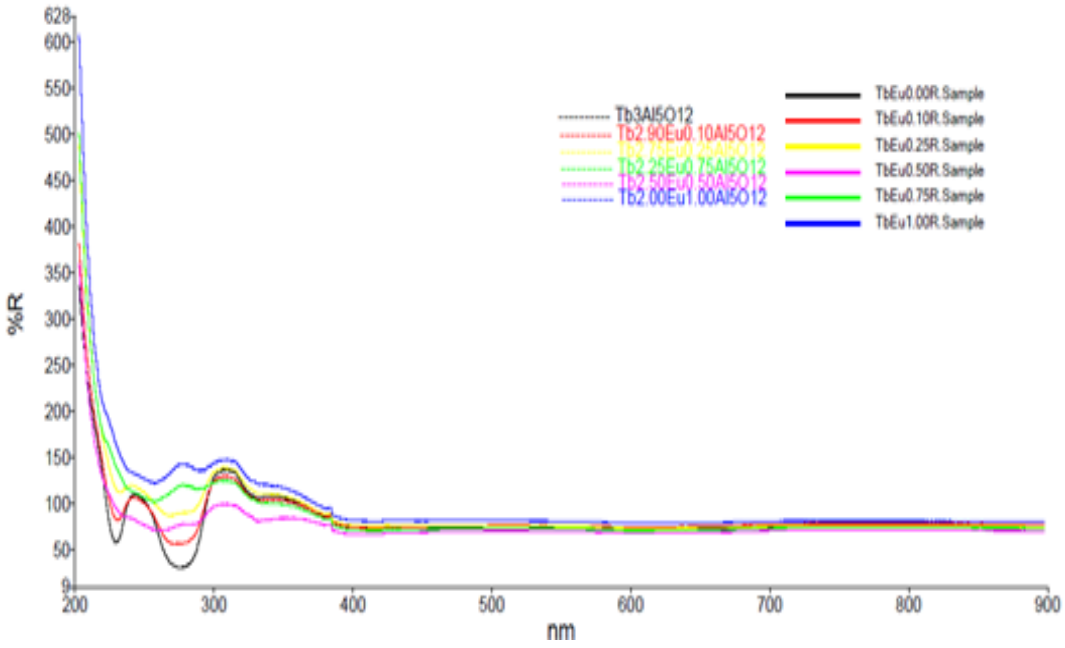

Figure 61. The UV-vis/DRS reflection spectra of Eu^{3+} doped $Tb_3Al_5O_{12}$

4.2.3.5 The SEM studies of Eu:TAG

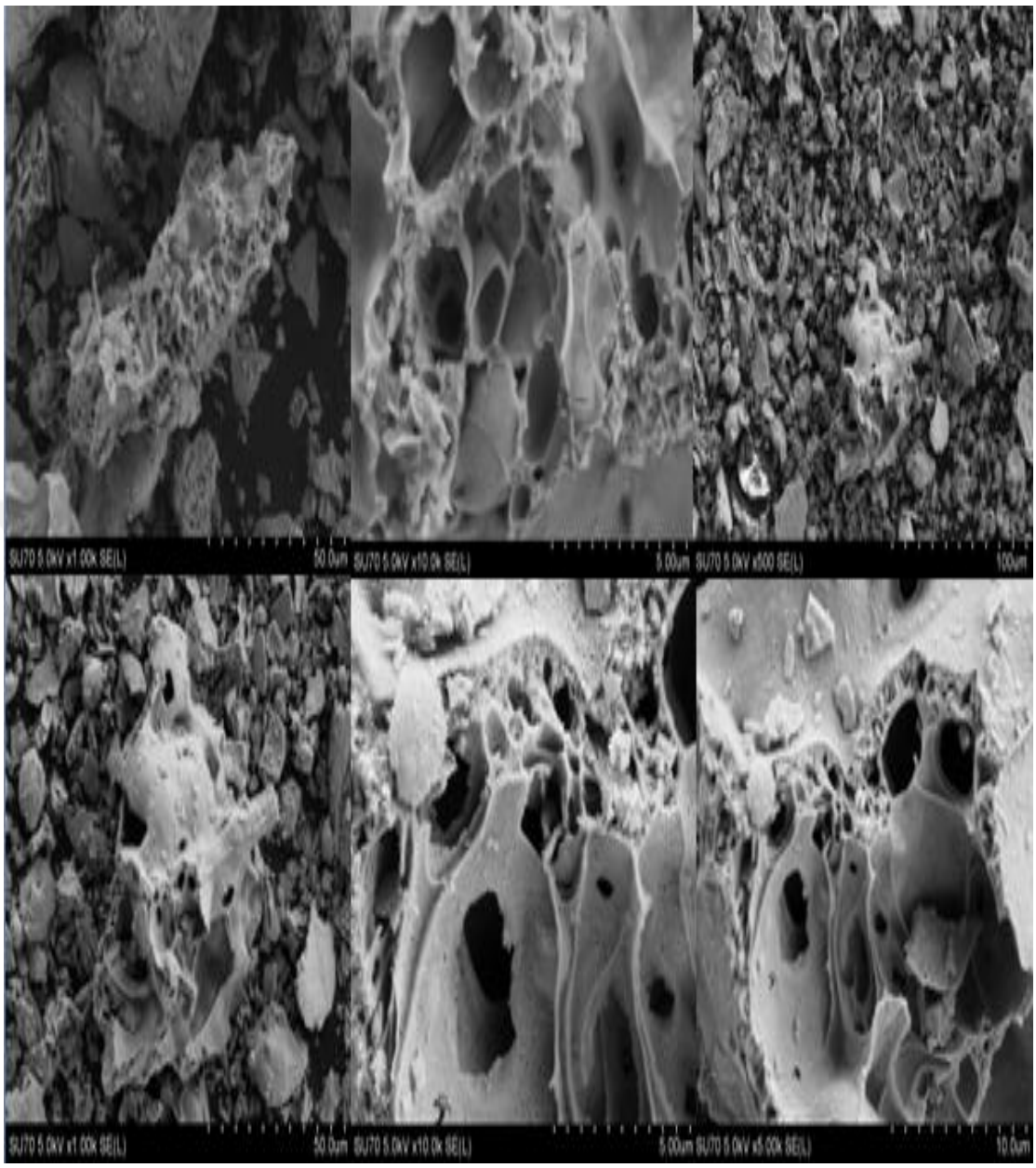

Figure 62. The SEM micrograph of Eu^{3+} doped $Tb_3Al_5O_{12}$

The porous images are taken places due to the gases out while the reaction occurs with metal-nitrate precursors. The nitrogen gases occurs while the sol is preparing and also the organic carbon presences, may comes from complexing agent of ethylene glycol at high temperatures, flies and goes as CO_2, as well.

4.2.4 The comparison of the XRD studies of 10 hours sintered HAG, DAG and TAG

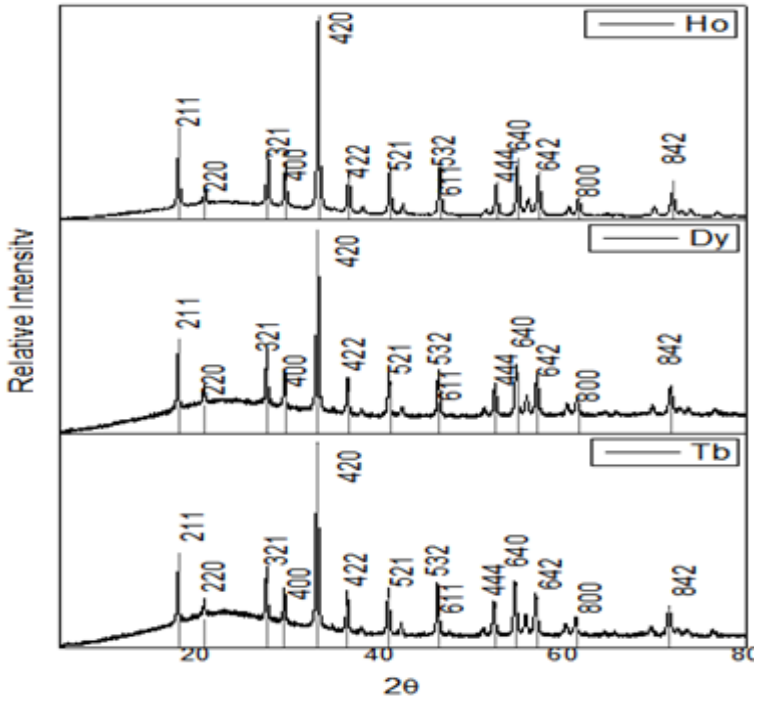

Figure 63. The XRD patterns of Ho-Al-O, Dy-Al-O and Tb-Al-O garnets

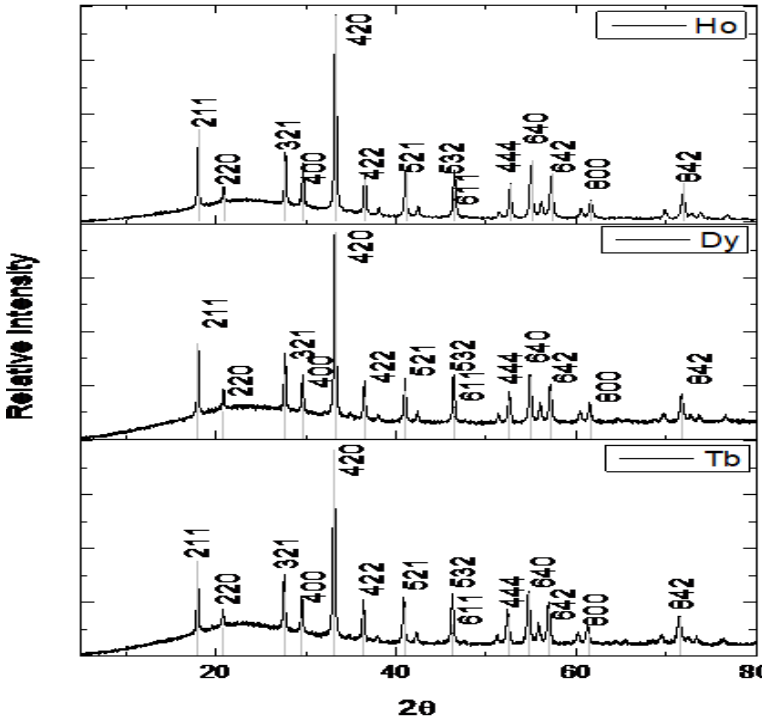

Figure 64. The XRD patterns of Ho-Al-O, Dy-Al-O and Tb-Al-O garnets those are doped with 0.10 mol Eu^{3+}

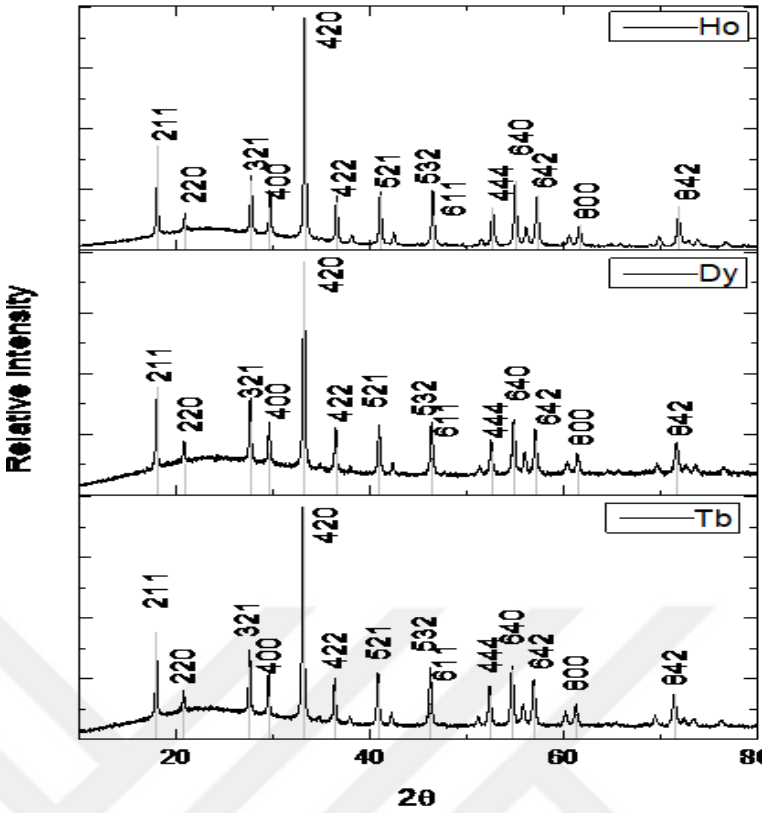

Figure 65. The XRD patterns of Ho-Al-O, Dy-Al-O and Tb-Al-O garnets those are doped with 0.25 mol Eu^{3+}

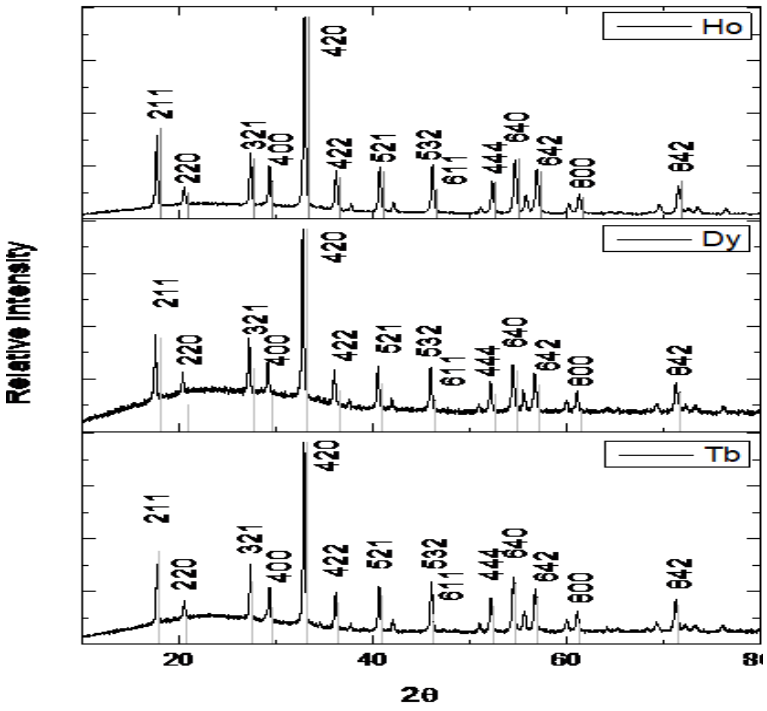

Figure 66. The XRD patterns of Ho-Al-O, Dy-Al-O and Tb-Al-O garnets those are doped with 0.50 mol Eu^{3+}

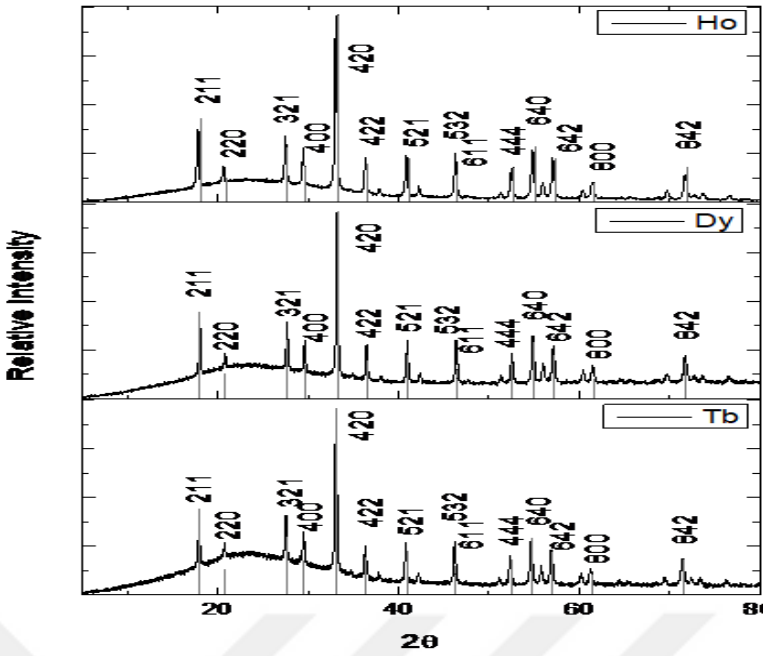

Figure 67. The XRD patterns of Ho-Al-O, Dy-Al-O and Tb-Al-O garnets those are doped with 0.75 mol Eu^{3+}

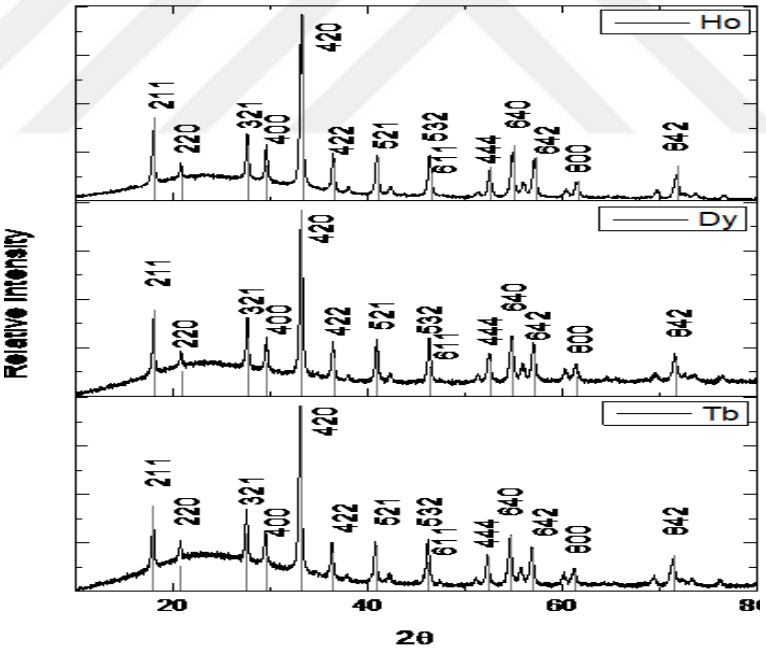

Figure 68. XRD patterns of Ho-Al-O, Dy-Al-O and Tb-Al-O garnets those are doped with 1.00 mol Eu^{3+}

As can be seen in figures 63-68, The XRD results of all synthetized crystals are demonstrated the same specific garnet XRD patterns with the same hkl values for Ho,Dy and Tb aluminum garnets, where the results also overlaps with their relative ICDD data indicated on previous studies.

4.3 Results and discussion of transition metals (Mn,Cr,Fe) doped in holmium aluminum garnets

4.3.1 The studies for Cr^{3+} doped HAG (Cr:HAG)

4.3.1.1 The XRD studies of Cr:HAG

The XRD was also used to analysis the different amount of Cr^{3+} doped holmium garnet, $Ho_3Al_5O_{12}$. Skaudzius, R.et al. (2012), synthetized of $Y_3Al_{5-x}Cr_xO_{12}$ by obtaining of Y-Al-Cr-O precursor gels at first by using nitrates as starting materials and indicated the typical XRD patterns. In this study, the XRD results are coincided with studies of Skaudzius, R. et al., (2012).

The figure 69 shows the XRD patterns of Cr^{3+} doped holmium garnets. All of the 0.10, 0.25, 0.50, 0.75 ve 1.00 mol Cr^{3+} doped $Ho_3Al_5O_{12}$ garnets are observed by XRD and the results are the same with the undoped garnet. So according to XRD analysis of Cr^{3+} doped $Ho_3Al_5O_{12}$ garnets there is no change in the structure of garnets as can be seen in figure 69.

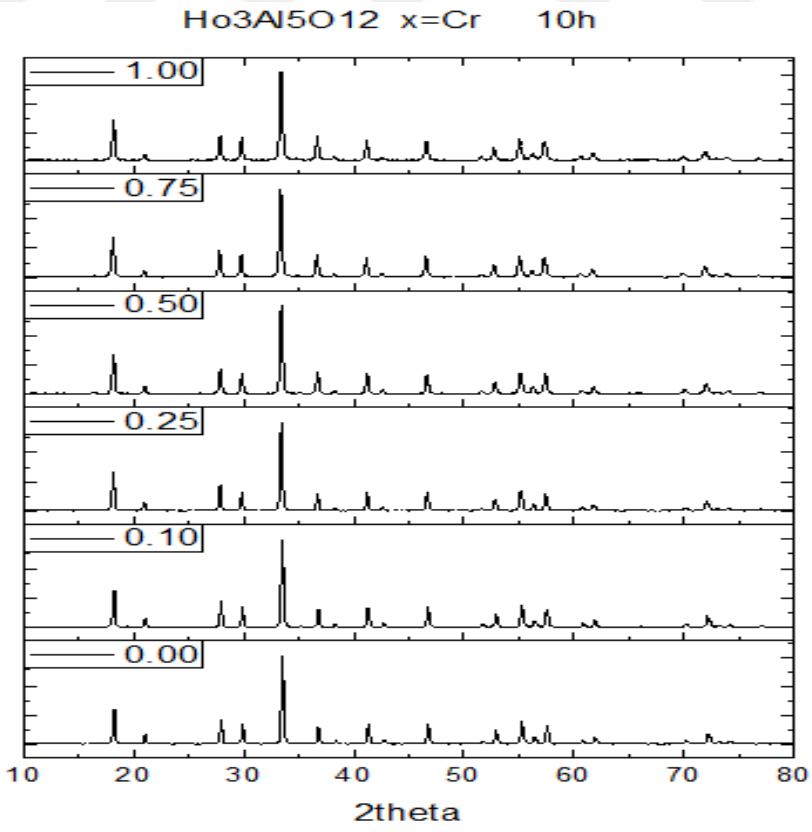

Figure 69. The XRD patterns of Cr^{3+} doped $Ho_3Al_5O_{12}$

4.3.1.2 The FTIR spectroscopy studies of Cr:HAG

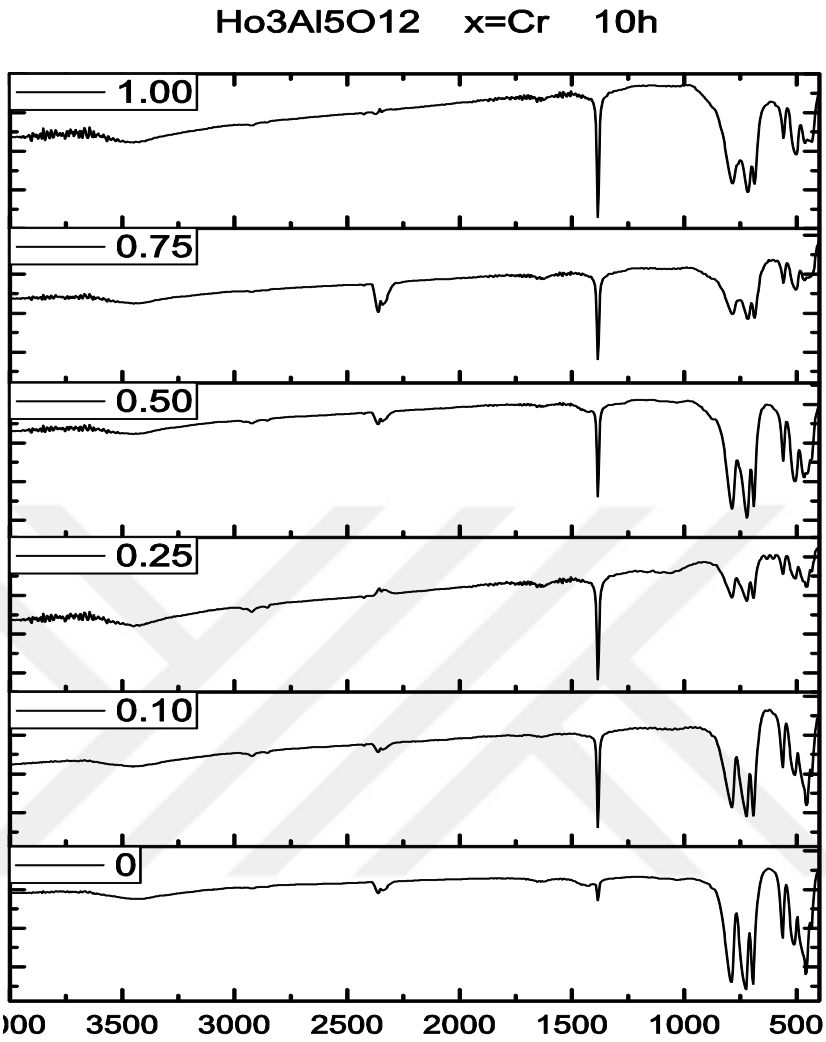

Figure 70. The FTIR spectroscopy of Cr^{3+} doped $Ho_3Al_5O_{12}$

The infrared peaks are demonstrated that the characteristic Cr-Al-O streching lines under 900 cm^{-1} (Skaudzius, R.et al., 2012).

4.3.1.3 The UV-vis/DRS studies of Cr:HAG

The absorbance and reflectance spectra of Cr^{3+} doped $Ho_3Al_5O_{12}$ garnets are shown in figures 71 and 72 respectively. There is no big change after Cr doping until 0.5% level. For this reason the maximum Cr^{3+} doping level can be taken as 0.5%. When the Cr^{3+} doping level is increased to 0.75% and 1% the absorbance level of the holmium aluminum garnet is increasing in all wavelengths. Then the absorbance peaks are starting to disappearing. But there is no new peak in spectrum. It can be

seen that all level Cr^{3+} doped $Ho_3Al_5O_{12}$ garnets are showing the same absorbance peaks. Blue-shift occurs, when the Cr^{3+} amount increases. This determination can be concluded as there is no structural change after the doping Cr^{3+} into the holmium aluminum garnet. This result is compatible with the results those are obtained from FTIR, XRD, SEM and EDX studies.

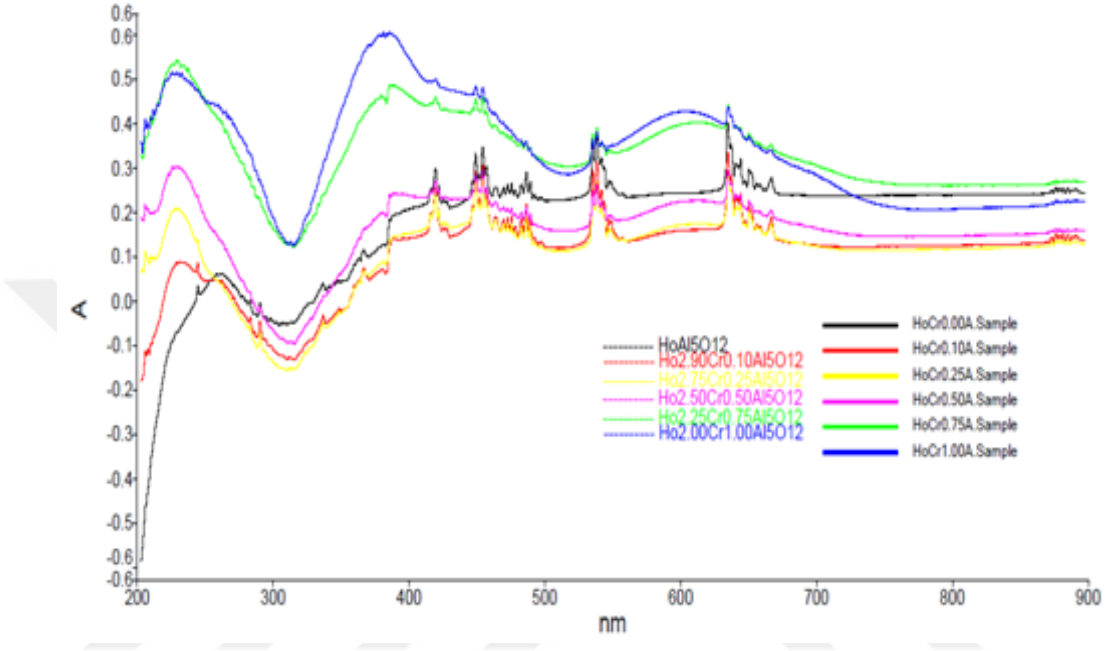

Figure 71. The UV-vis/DRS absorption spectra of Cr^{3+} doped $Ho_3Al_5O_{12}$

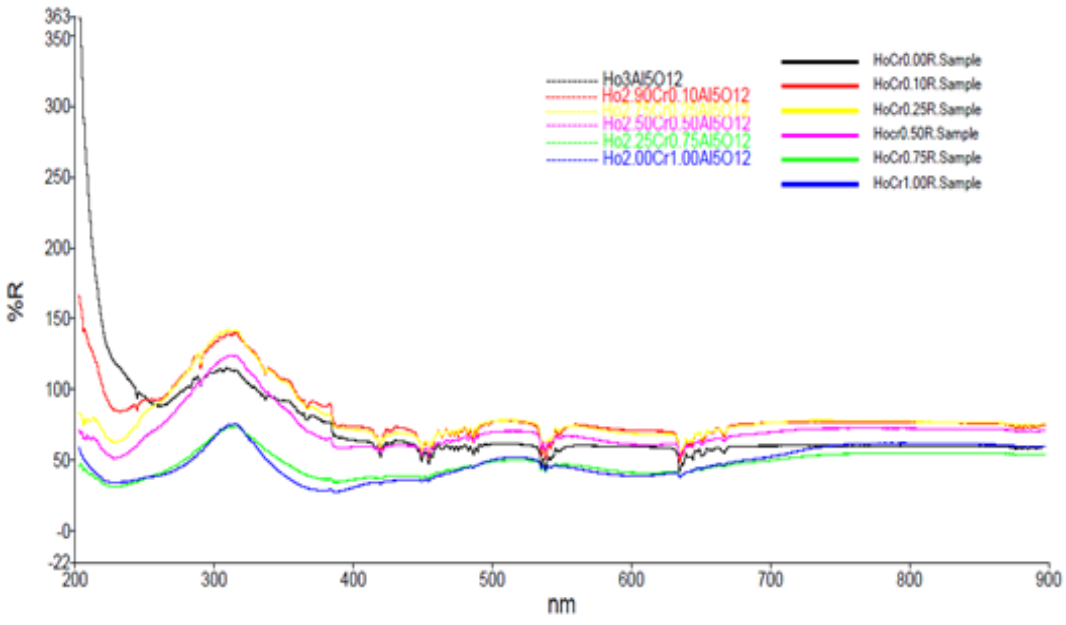

Figure 72. The UV-vis/DRS reflection spectra of Cr^{3+} doped $Ho_3Al_5O_{12}$

4.3.1.4 The SEM and EDX studies of Cr:HAG

The SEM images of 0.10 mol Cr^{3+} doped $Ho_3Al_5O_{12}$ can be seen in figure 73. It can be seen clearly from figure 73 that the doped Cr^{3+} is covered on the surface of the holmium garnet. The small grains show the tendency to form larger grains.

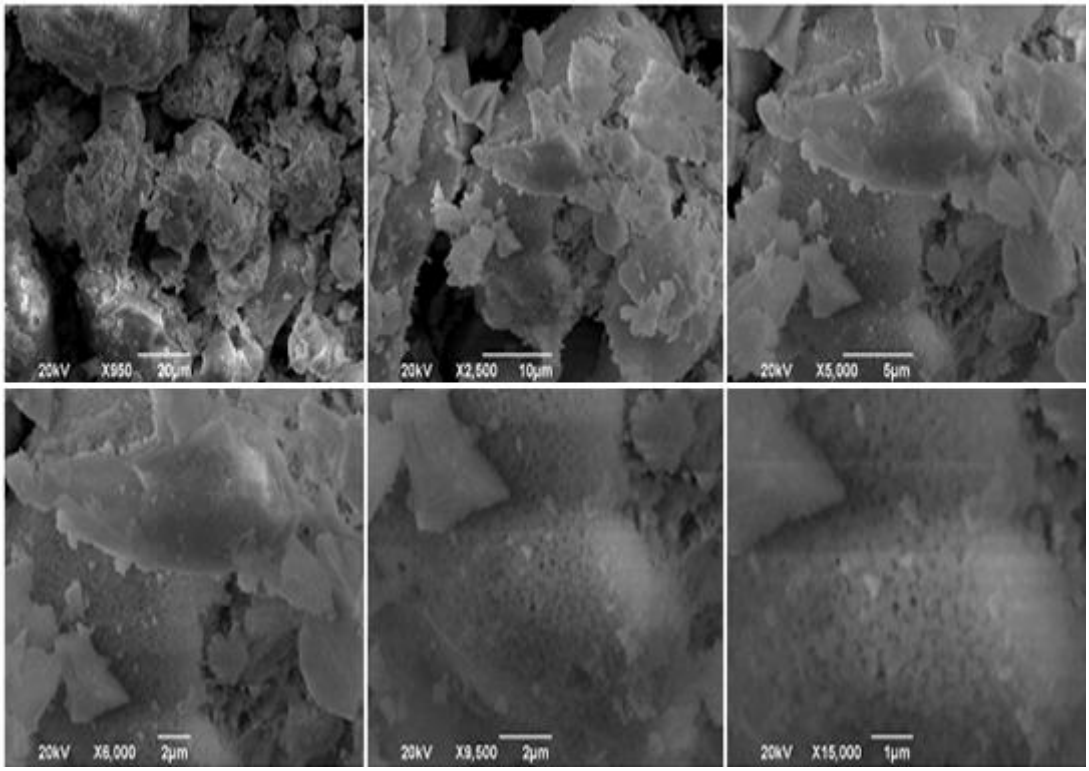

Figure 73. The SEM micrographs of 0.10 mol Cr^{3+} doped $Ho_3Al_5O_{12}$

Table 2. The EDX analysis of 0.10 mol Cr^{3+} doped $Ho_3Al_5O_{12}$

Elt.	Line	Intensity (c/s)	Error 2-sig	Conc	Units	
O	Ka	50.44	2.593	22.595	wt.%	
Al	Ka	119.35	3.989	16.396	wt.%	
Cr	Ka	4.29	0.757	0.551	wt.%	
Ho	La	76.45	3.193	60.458	wt.%	
				100.000	wt.%	Total

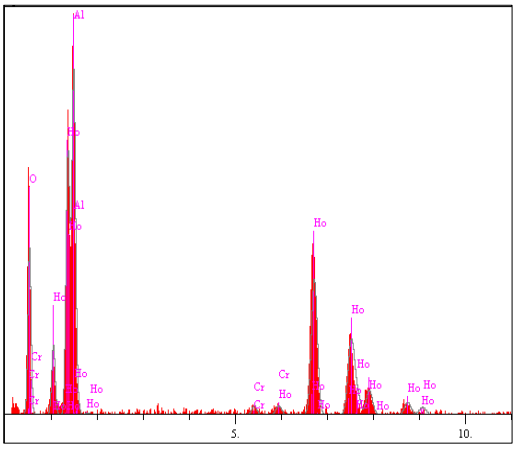

Figure 74. The EDX analysis of 0.10 mol Cr^{3+} doped $Ho_3Al_5O_{12}$

The EDX analysis shown in figure 74 and table 2 determined that the peak intensities of the 0.10 mol Cr^{3+} doped $Ho_3Al_5O_{12}$.

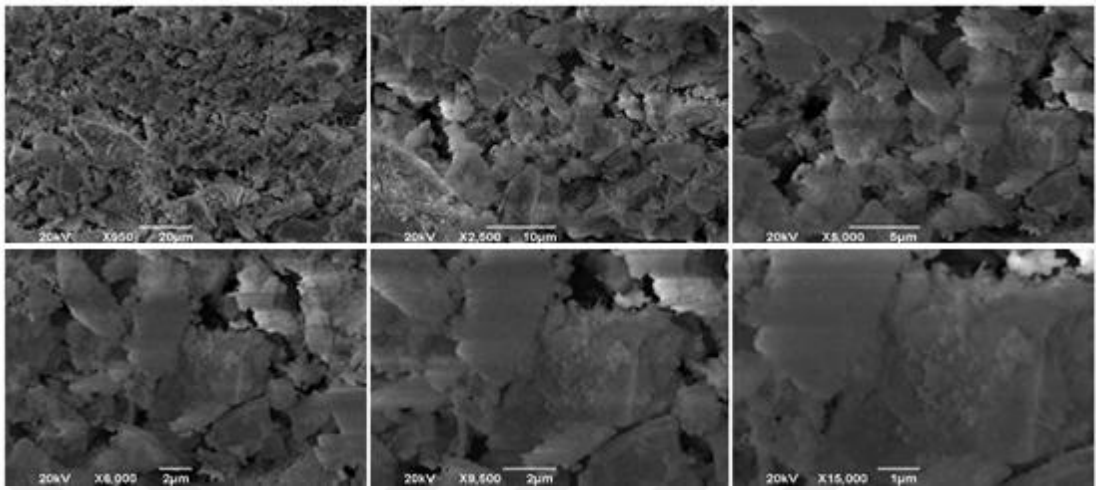

Figure 75. The SEM micrographs of 0.25 mol Cr^{3+} doped $Ho_3Al_5O_{12}$

The SEM images of 0.25 mol Cr^{3+} doped $Ho_3Al_5O_{12}$ can be seen in figure 75. It can be seen clearly from the figure, the doped Cr^{3+} is covered on the surface of the holmium garnet. The smooth-surfaced small particles viewed superimposed.

The EDX analysis shown in Figure 76 and Table 3 determined that the peak intensities of the 0.25 mol Cr^{3+} doped $Ho_3Al_5O_{12}$ as expected as like in the 0.10 mol Cr^{3+} doped holmium garnet.

Table 3. The EDX analysis of 0.25 mol Cr^{3+} doped $Ho_3Al_5O_{12}$

Elt.	Line	Intensity (c/s)	Error 2-sig	Conc	Units	
O	Ka	42.96	2.393	20.251	wt.%	
Al	Ka	95.49	3.568	14.017	wt.%	
Cr	Ka	9.83	1.145	1.308	wt.%	
Ho	La	78.69	3.239	64.423	wt.%	
				100.000	wt.%	Total

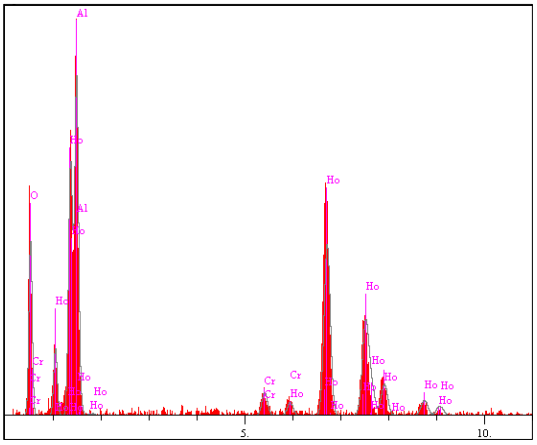

Figure 76. The EDX analysis of 0.25 mol Cr^{3+} doped $Ho_3Al_5O_{12}$

The SEM images of 0.50 mol Cr^{3+} doped $Ho_3Al_5O_{12}$ can be seen in figure 77. It can be seen clearly from the figure that the doped Cr^{3+} is covered on the surface of the holmium garnet as like in the 0.10 mol and 0.25 mol Cr^{3+} doped holmium garnets. The small grains seems like branched-shape and show a tendency to form large grains.

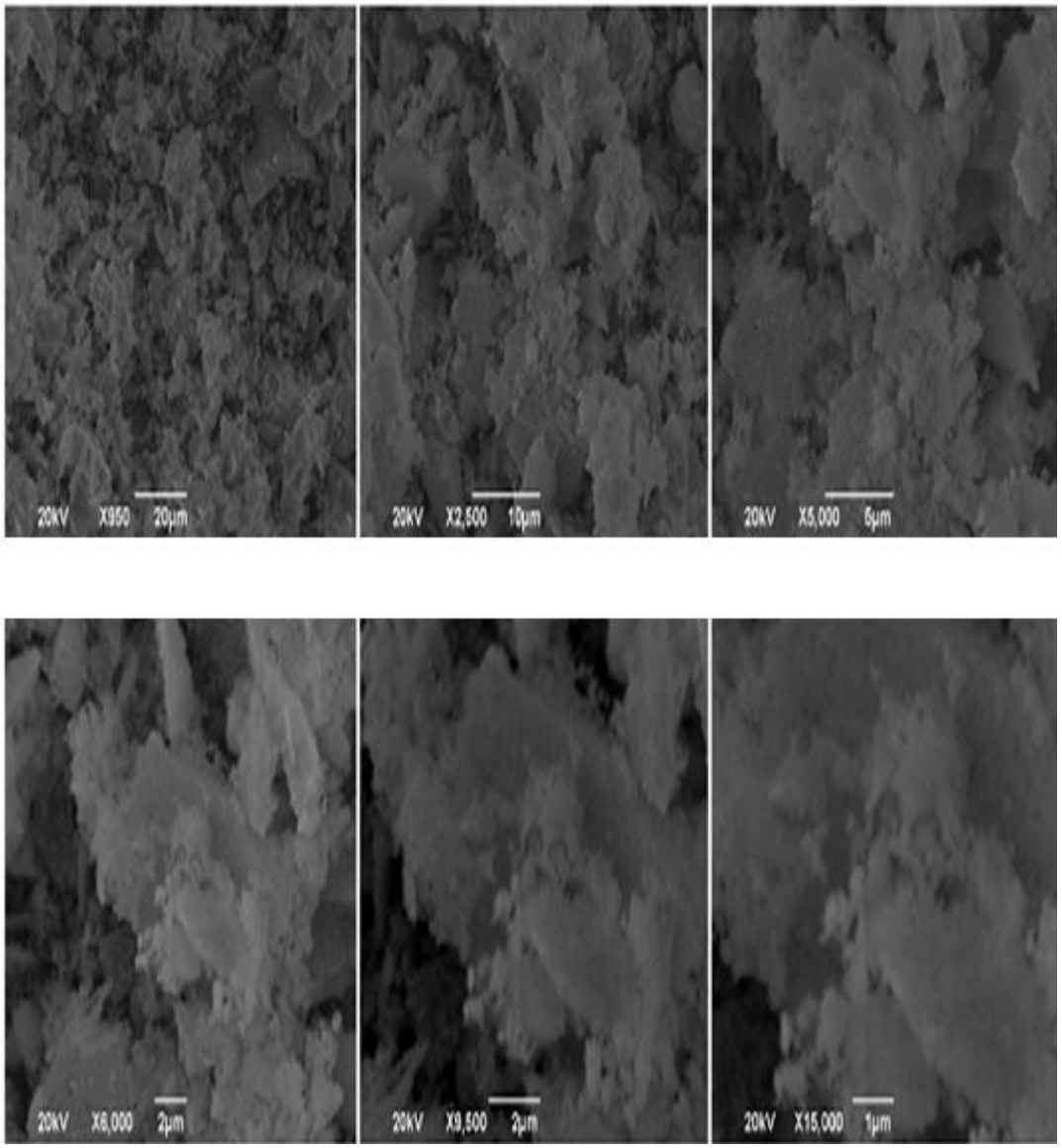

Figure 77. The SEM micrographs of 0.50 mol Cr^{3+} doped $Ho_3Al_5O_{12}$

The EDX analysis shown in Figure 78 and Table 4 determined that the peak intensities of the 0.50 mol Cr doped $Ho_3Al_5O_{12}$ as expected as like in the 0.10 mol and 0.25 mol Cr^{3+} doped holmium garnets.

Table 4. The EDX analysis of 0.50 mol Cr^{3+} doped $Ho_3Al_5O_{12}$

Elt.	Line	Intensity (c/s)	Error 2-sig	Conc	Units	
O	Ka	50.04	2.583	21.273	wt.%	
Al	Ka	110.56	3.839	14.647	wt.%	
Cr	Ka	23.38	1.766	2.852	wt.%	
Ho	La	81.26	3.291	61.229	wt.%	
				100.000	wt.%	Total

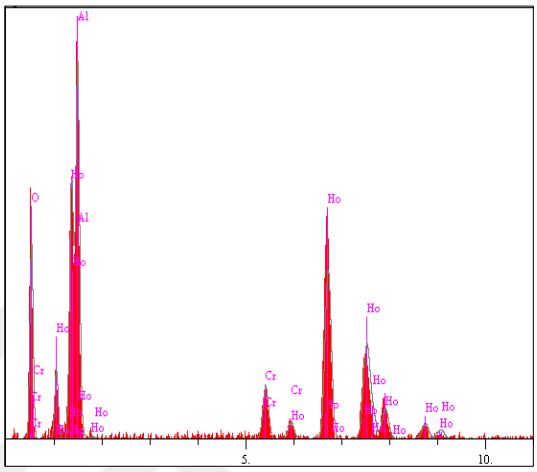

Figure 78. The EDX analysis of 0.50 mol Cr^{3+} doped $Ho_3Al_5O_{12}$

The SEM images of 0.75 mol Cr^{3+} doped $Ho_3Al_5O_{12}$ can be seen in Figure 79. It can be seen clearly from figure that the doped Cr^{3+} is covered on the surface of the holmium garnet as like in the 0.10 mol, 0.25 mol and 0.50 mol Cr^{3+} doped holmium garnets. The resolution of the adjacent pictures increases, gradually. There can be seen clearly the plate-like shape of 0.75 mol Cr doped $Ho_3Al_5O_{12}$. There are large-grained matrixes and several small grains on their surfaces. The smooth surfaces are seems longitudinal and stick-like. The results shows an extensive particle size distrubution of the small grains. In addition, according to the pictures, these small grains tends to become a huge matrix to form big grains. The particles adhered well to the large surface. There is no porous surface in all 6 images. This is kind a classic ceramic composition electron microscopy images.

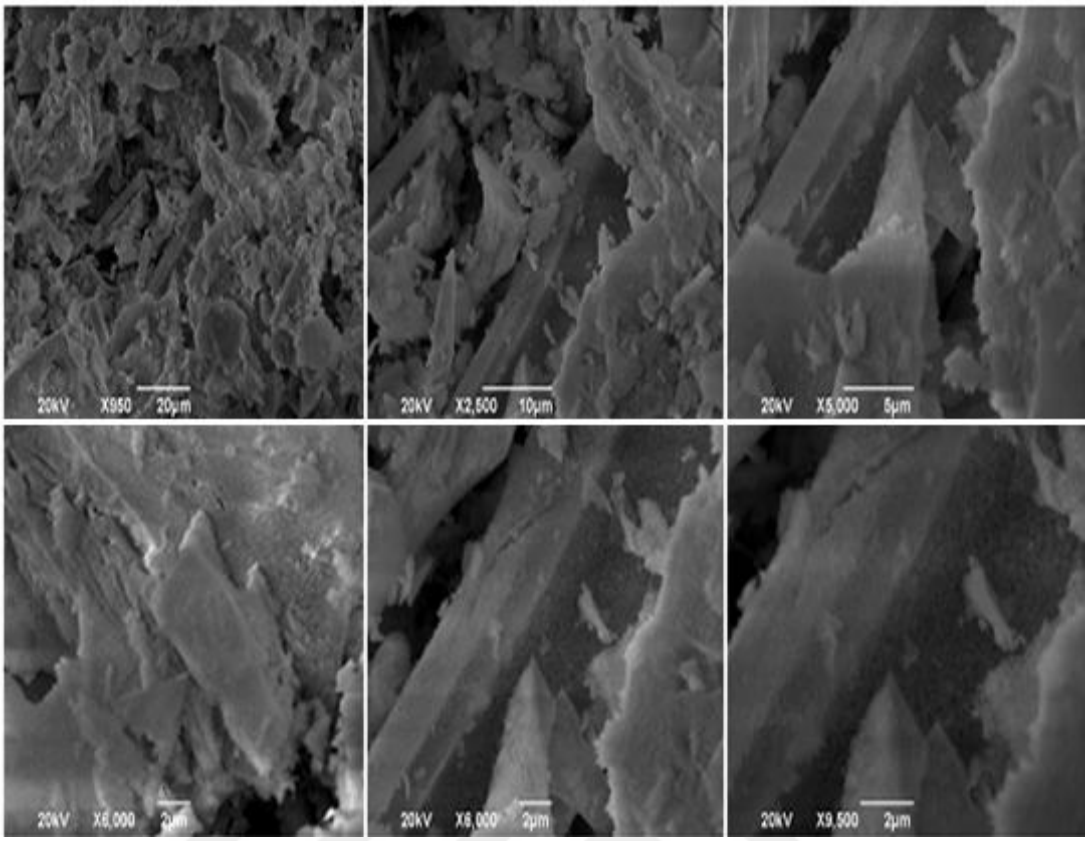

Figure 79. SEM micrographs of 0.75 mol Cr^{3+} doped $Ho_3Al_5O_{12}$

The EDX analysis shown in figure 80 and table 5 determined that the peak intensities of the 0.75 mol Cr^{3+} doped $Ho_3Al_5O_{12}$ as expected as like in the 0.10 mol, 0.25 mol, and 0.50 mol Cr^{3+} doped holmium garnets.

Table 5. The EDX analysis of 0.75 mol Cr^{3+} doped $Ho_3Al_5O_{12}$

Elt.	Line	Intensity (c/s)	Error 2-sig	Conc	Units	
O	Ka	61.24	2.857	25.237	wt.%	
Al	Ka	125.43	4.089	16.106	wt.%	
Cr	Ka	31.65	2.054	3.879	wt.%	
Ho	La	71.83	3.094	54.778	wt.%	
				100.000	wt.%	Total

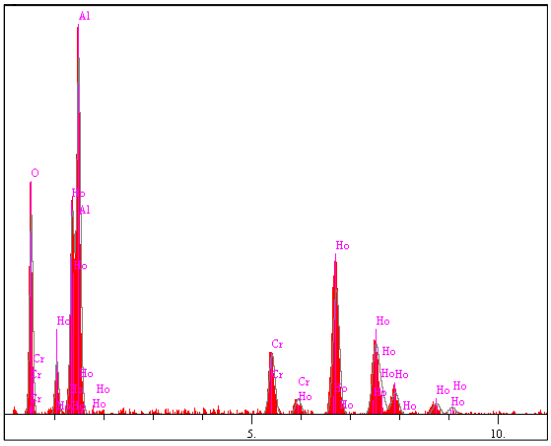

Figure 80. The EDX analysis of 0.75 mol Cr^{3+} doped $Ho_3Al_5O_{12}$

The SEM images of 1.00 mol Cr^{3+} doped $Ho_3Al_5O_{12}$ can be seen in figure 81. It can be seen clearly the small grains tend to form large grains as like in the 0.10 mol, 0.25 mol, 0.50 mol and 0.75 mol Cr^{3+} doped holmium garnets.

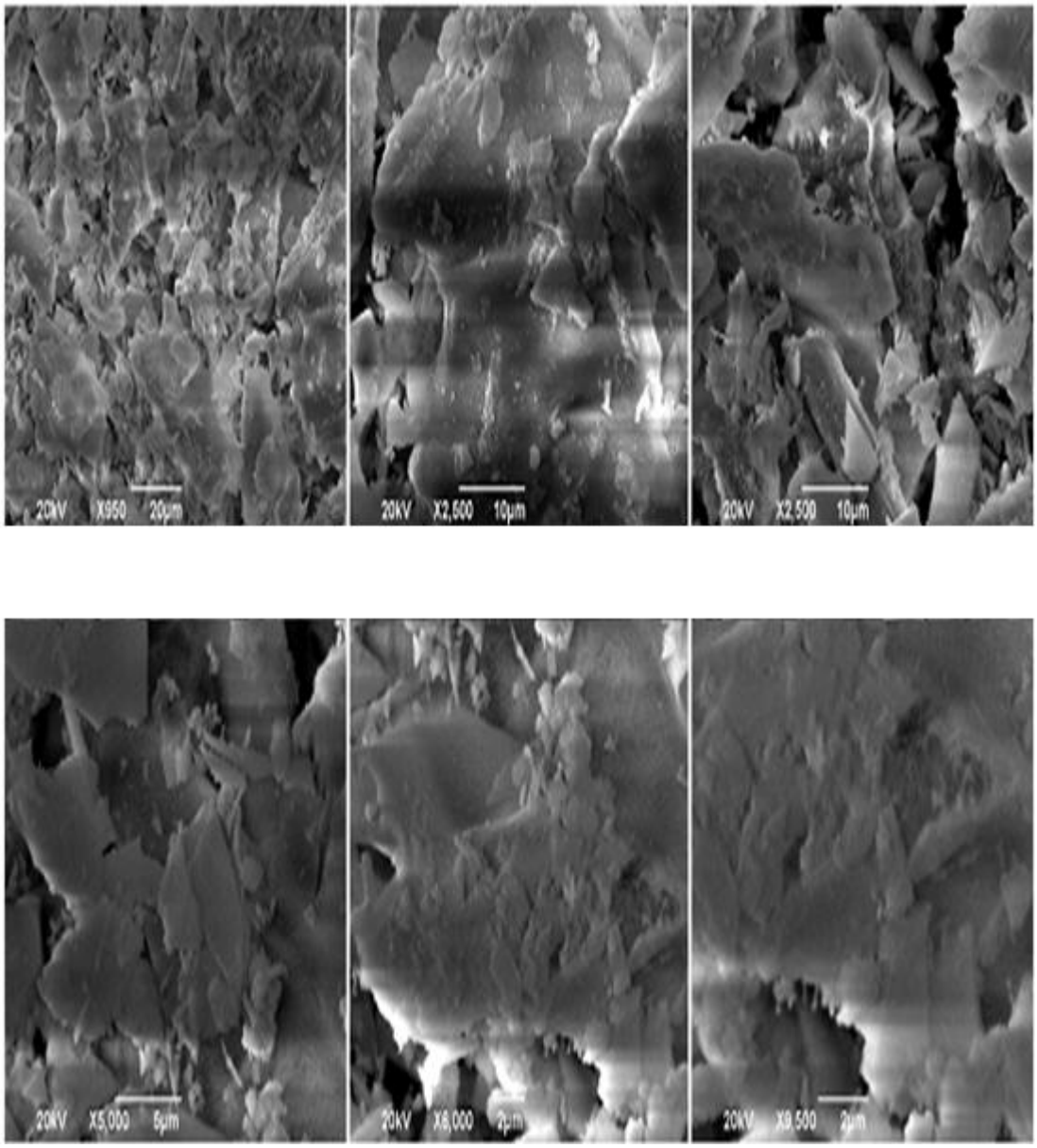

Figure 81. The SEM micrographs of 1.00 mol Cr^{3+} doped $Ho_3Al_5O_{12}$

The EDX analysis shown in figure 82 and table 6 determined that the peak intensities of the 1.00 mol Cr^{3+} doped $Ho_3Al_5O_{12}$ as expected as like in the 0.10 mol, 0.25 mol, 0.5 mol and 0.75 mol Cr^{3+} doped holmium garnets.

Table 6. The EDX analysis of 1.00 mol Cr^{3+} doped $Ho_3Al_5O_{12}$

Elt.	Line	Intensity (c/s)	Error 2-sig	Conc	Units	
O	Ka	57.79	2.776	22.784	wt.%	
Al	Ka	120.90	4.015	14.950	wt.%	
Cr	Ka	45.04	2.450	5.215	wt.%	
Ho	La	79.17	3.249	57.051	wt.%	
				100.000	wt.%	Total

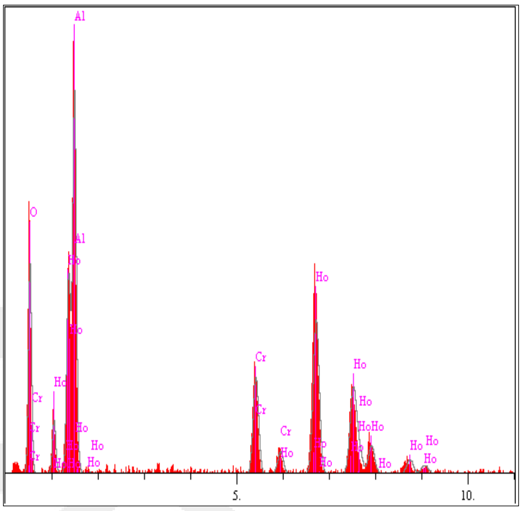

Figure 82. The EDX analysis of 1.00 mol Cr^{3+} doped $Ho_3Al_5O_{12}$

4.3.2 The studies for Mn^{3+} doped HAG (Mn:HAG)

4.3.2.1 The XRD studies of Mn:HAG

The XRD was also used to analysis the different amount of Mn^{3+} doped holmium garnet, structured molecular formula in $Ho_3Al_5O_{12}$. Skaudzius, R.et al., (2012), synthetized of $Y_3Al_{5-x}Mn_xO_{12}$ by obtaining of Y-Al-Mn-O precursor gels at first by using nitrates as starting materials and indicated the typical XRD patterns. In this study, the XRD results are coincided with studies of Skaudzius, R.et al., (2012).

The figure 83 shows the XRD patterns of Mn doped holmium garnets. All of the 0.10, 0.25, 0.50, 0.75 ve 1.00 mol Mn^{3+} doped $Ho_3Al_5O_{12}$ garnets are observed by XRD and the results are the same with the undoped garnet. So according to XRD analysis of Mn^{3+} doped $Ho_3Al_5O_{12}$ garnets there is no change in the structure of garnets as can be seen from figure 83.

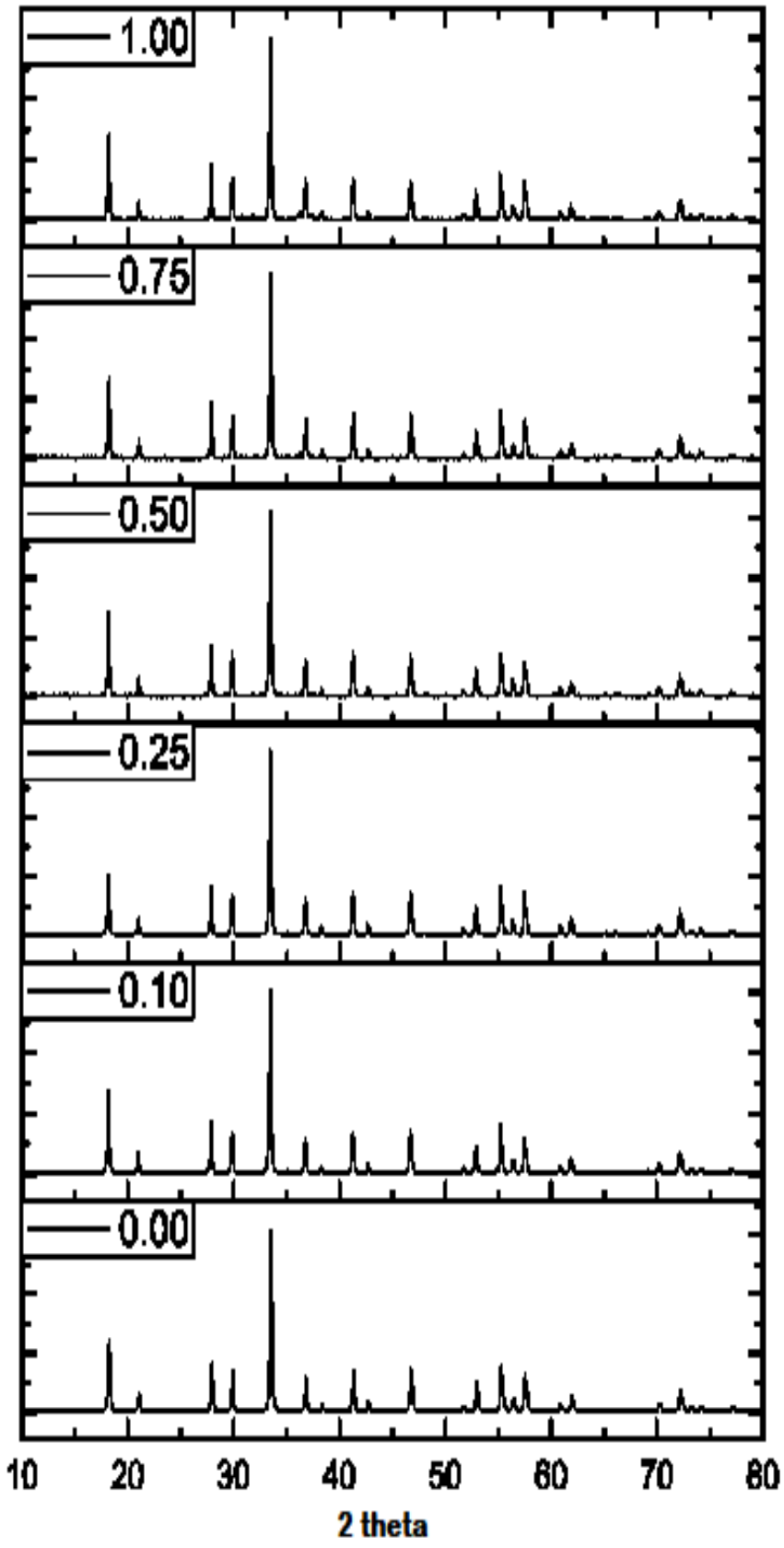

Figure 83. The XRD patterns of Mn^{3+} doped $Ho_3Al_5O_{12}$

4.3.2.2 The FTIR spectroscopy studies of Mn:HAG

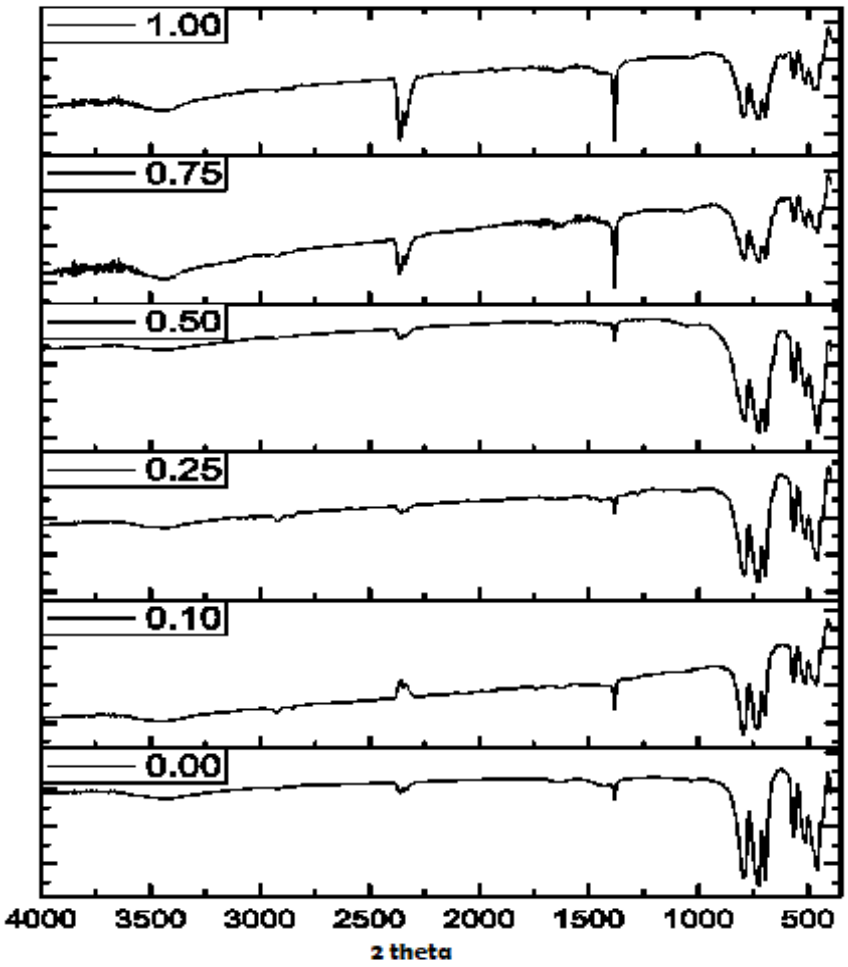

Figure 84. The FTIR spectroscopy of Mn^{3+} doped $Ho_3Al_5O_{12}$

The infrared peaks are demonstrated that the characteristic Mn-Al-O streching lines under 900 cm^{-1} (Skaudzius, R.et al., 2012).

4.3.2.3 The UV-vis/DRS studies of Mn:HAG

The absorbance and reflectance spectra of Mn^{3+} doped $Ho_3Al_5O_{12}$ garnets are shown in figures 85 and 86 respectively. There is no big change in peak points after Mn^{3+} doping. When doping level is increased more then 0.10% the absorbance of UV region of spectra is increasing. So the peak around 420 nm disappears. After the 0.25% level of Mn^{3+} doping the other peaks are also disappearing gradually but not completely. When the Mn^{3+} doping level is increased the absorbance level of the holmium aluminum garnet is increasing in all wavelengths. It should also be

indicated that all level Mn^{3+} doped $Ho_3Al_5O_{12}$ garnets are showing the same absorbance spectra. Blue-shift is observable with increasing Mn molar amount until 0.75 mol Mn^{3+}. This situation can be concluded as there is no structural change after the doping Mn^{3+} into the holmium aluminum garnet. This result is compatible with the results those are obtained from FTIR, XRD, SEM and EDX studies.

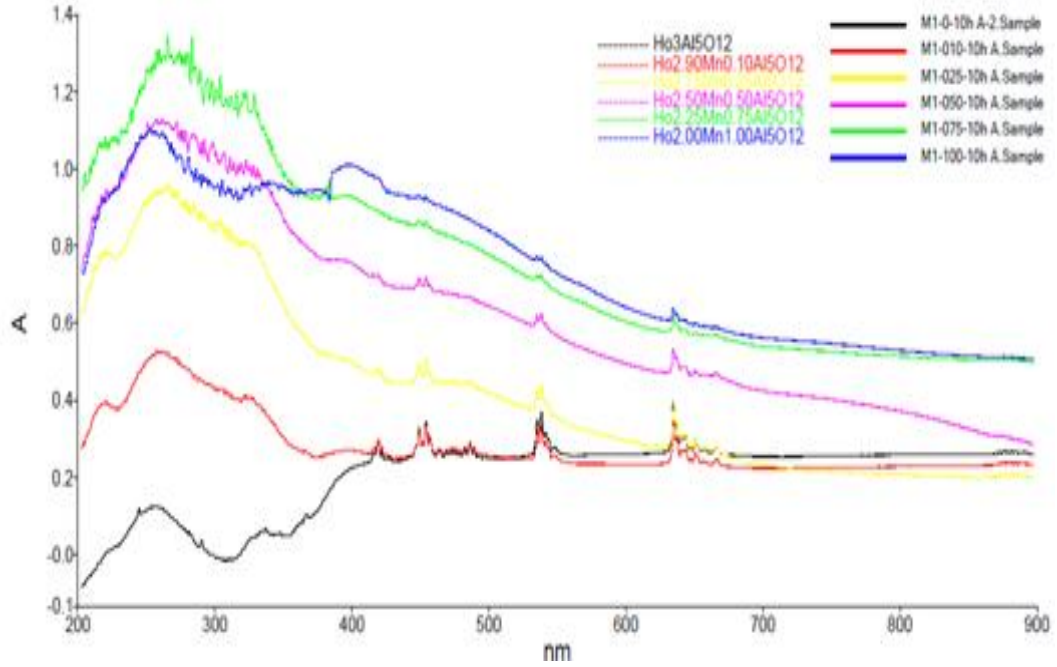

Figure 85. The UV-vis/DRS absorption spectra of Mn^{3+} doped $Ho_3Al_5O_{12}$

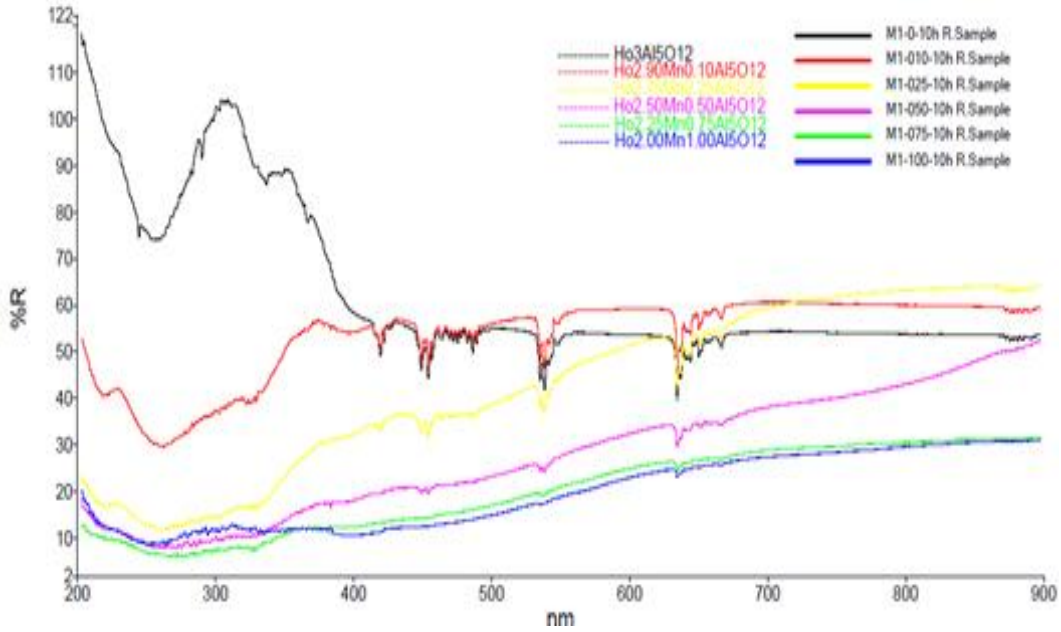

Figure 86. The UV-vis/DRS reflection spectra of Mn^{3+} doped $Ho_3Al_5O_{12}$

4.3.2.4 The SEM and EDX studies of Mn:HAG

The SEM images of 0.10 mol Mn^{3+} doped $Ho_3Al_5O_{12}$ can be seen in figure 87. The doped Mn^{3+} is covered on the surface of the holmium garnet.

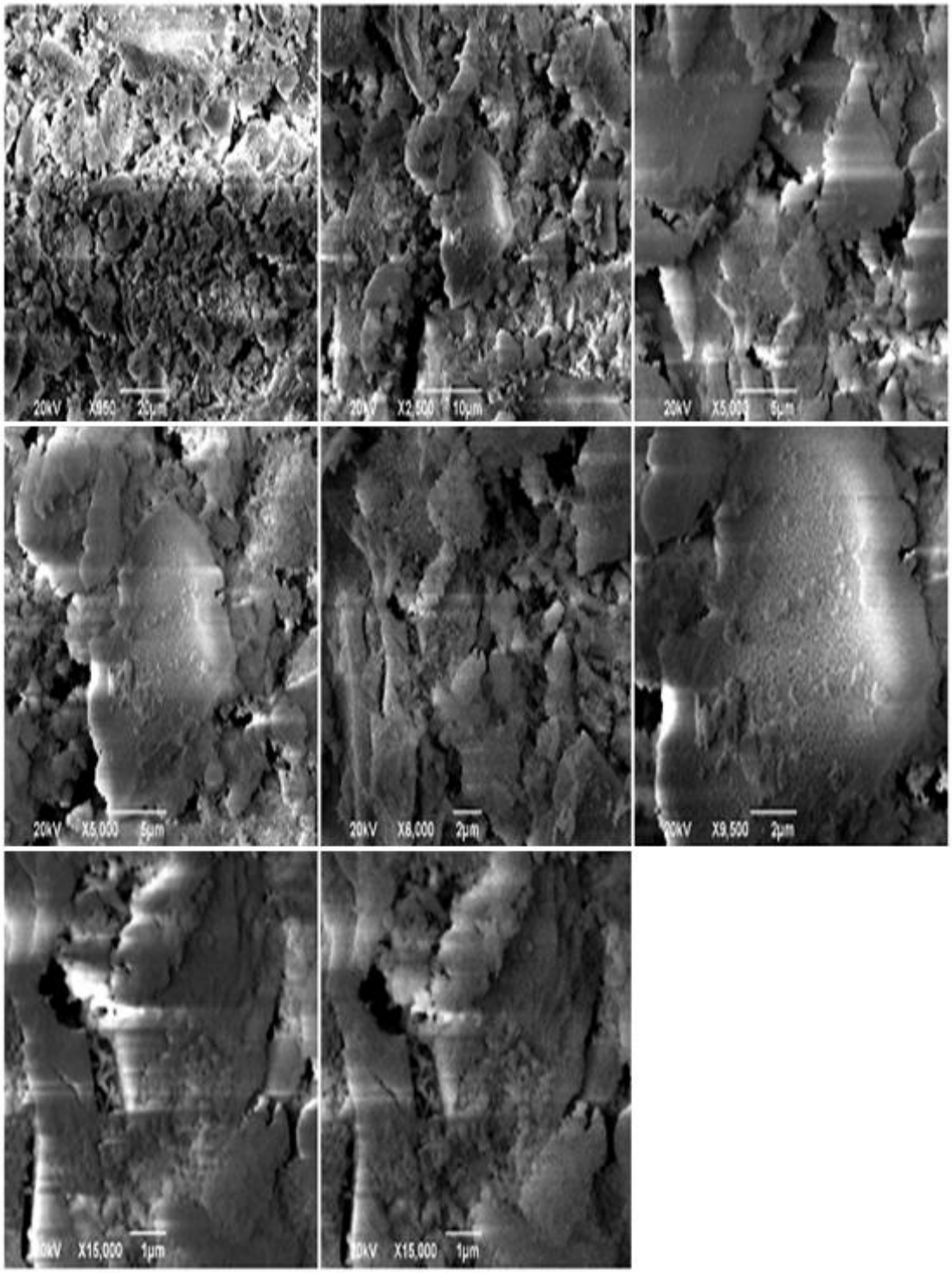

Figure 87. The SEM micrographs of 0.10 mol Mn^{3+} doped $Ho_3Al_5O_{12}$

The EDX analysis shown in figure 88 and table 7 determined that the peak intensities of the 0.10 mol Mn^{3+} doped $Ho_3Al_5O_{12}$ as expected. In the figure 88, the percentages of each element in the crystal surface is graphed as it is measured. In addition, the quantity of the percentage amounts of the elements is indicated on the table 7.

Table 7. The EDX Analysis of 0.10 mol Mn^{3+} doped $Ho_3Al_5O_{12}$

Elt.	Line	Intensity (c/s)	Error 2-sig	Conc	Units	
O	Ka	38.86	2.276	18.090	wt.%	
Al	Ka	95.37	3.566	13.763	wt.%	
Mn	Ka	2.87	0.619	0.414	wt.%	
o	La	85.83	3.383	67.733	wt.%	
				100.000	wt.%	Total

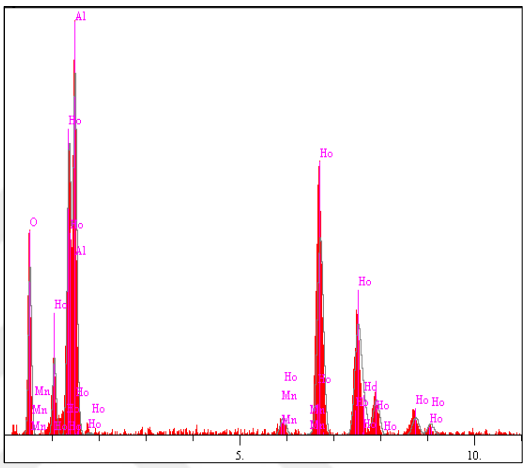

Figure 88. The EDX analysis of 0.10 mol Mn^{3+} doped $Ho_3Al_5O_{12}$

The SEM images of 0.25 mol Mn^{3+} doped $Ho_3Al_5O_{12}$ can be seen in figure 89. The doped Mn^{3+} is covered on the surface of the holmium garnet as like in the 0.10 mol Mn^{3+} doped holmium garnets. The resolution of the adjacent pictures increases, gradually. There can be seen clearly the plate-like shape of 0.25 mol Mn^{3+} doped $Ho_3Al_5O_{12}$. There are large-grained matrixes and several small granuls on their surfaces. The results shows an extensive particle size dispersion of the small grains. In addition, according to the pictures, these small grains tends to become a huge matrix to form large grains. The particles adhered well to the large surface. There is no big pores on the surface in all images. This is such a kind of an electron microscopy images for any classic ceramic compounds.

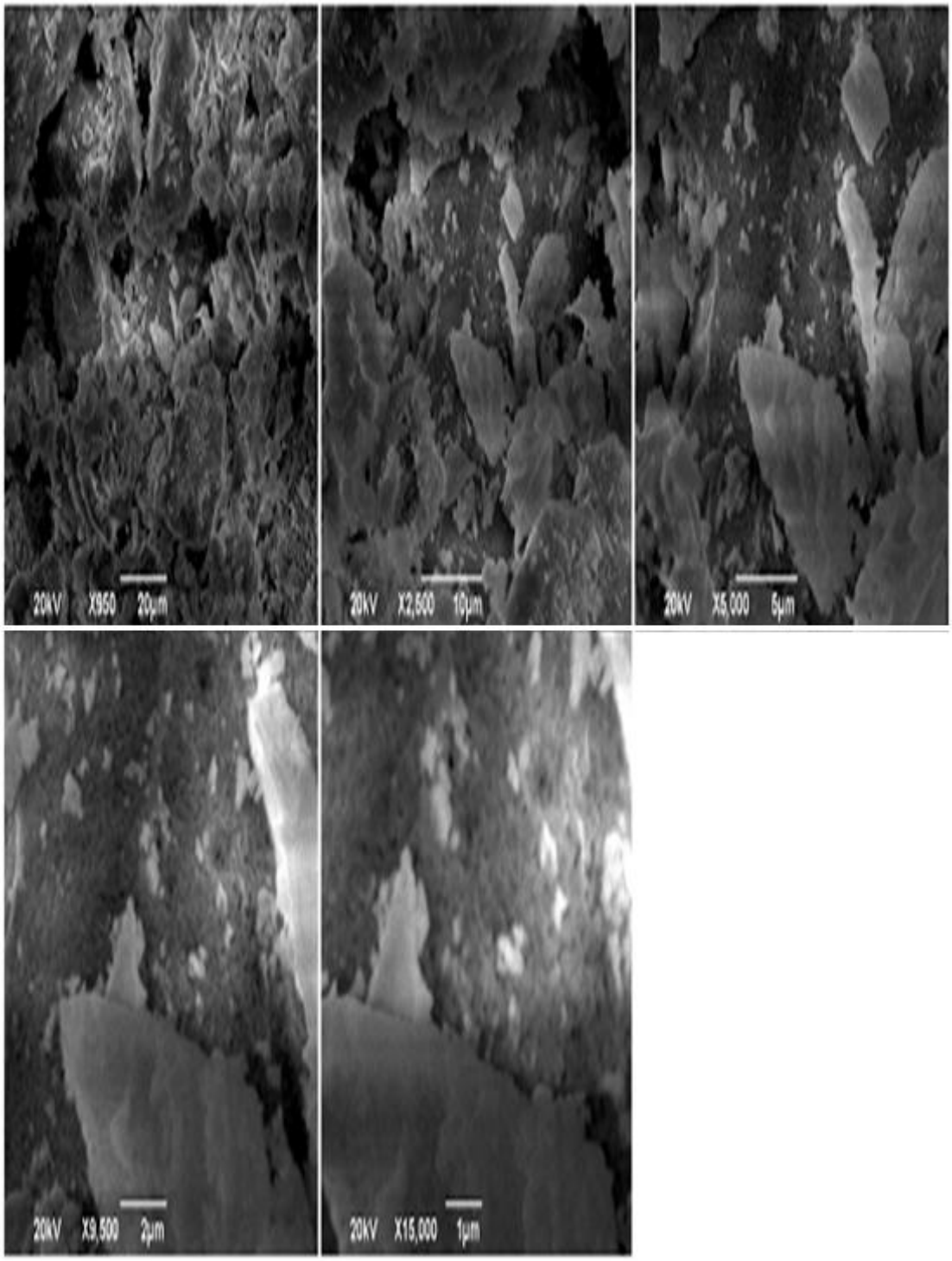

Figure 89. The SEM micrographs of 0.25 mol Mn^{3+} doped $Ho_3Al_5O_{12}$

The EDX analysis shown in figure 90 and table 8 determined that the peak intensities of the 0.25 mol Mn^{3+} doped $Ho_3Al_5O_{12}$ as expected as like in the 0.10 mol Mn^{3+} doped holmium garnets.

Table 8. The EDX analysis of 0.25 mol Mn^{3+} doped $Ho_3Al_5O_{12}$

Elt.	Line	Intensity (c/s)	Error 2-sig	Conc	Units	
O	Ka	42.95	2.393	19.520	wt.%	
Al	Ka	97.88	3.612	13.856	wt.%	
Mn	Ka	10.21	1.167	1.458	wt.%	
Ho	La	83.01	3.326	65.167	wt.%	
				100.000	wt.%	Total

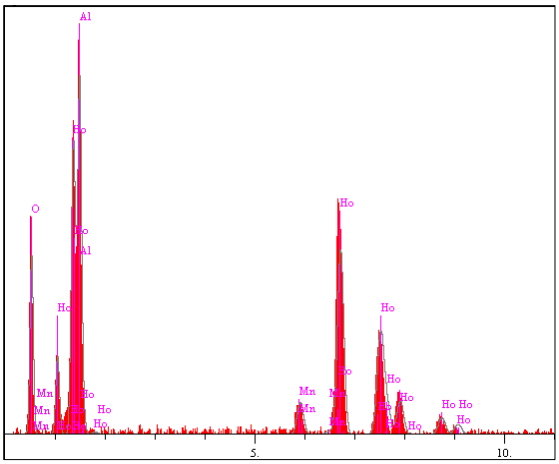

Figure 90. The EDX analysis of 0.25 mol Mn^{3+} doped $Ho_3Al_5O_{12}$

The SEM images of 0.50 mol Mn^{3+} doped $Ho_3Al_5O_{12}$ can be seen in figure 91. The doped Mn^{3+} is covered on the surface of the holmium garnet as like in the 0.10 mol Mn^{3+} doped and 0.25 mol Mn doped holmium garnets.

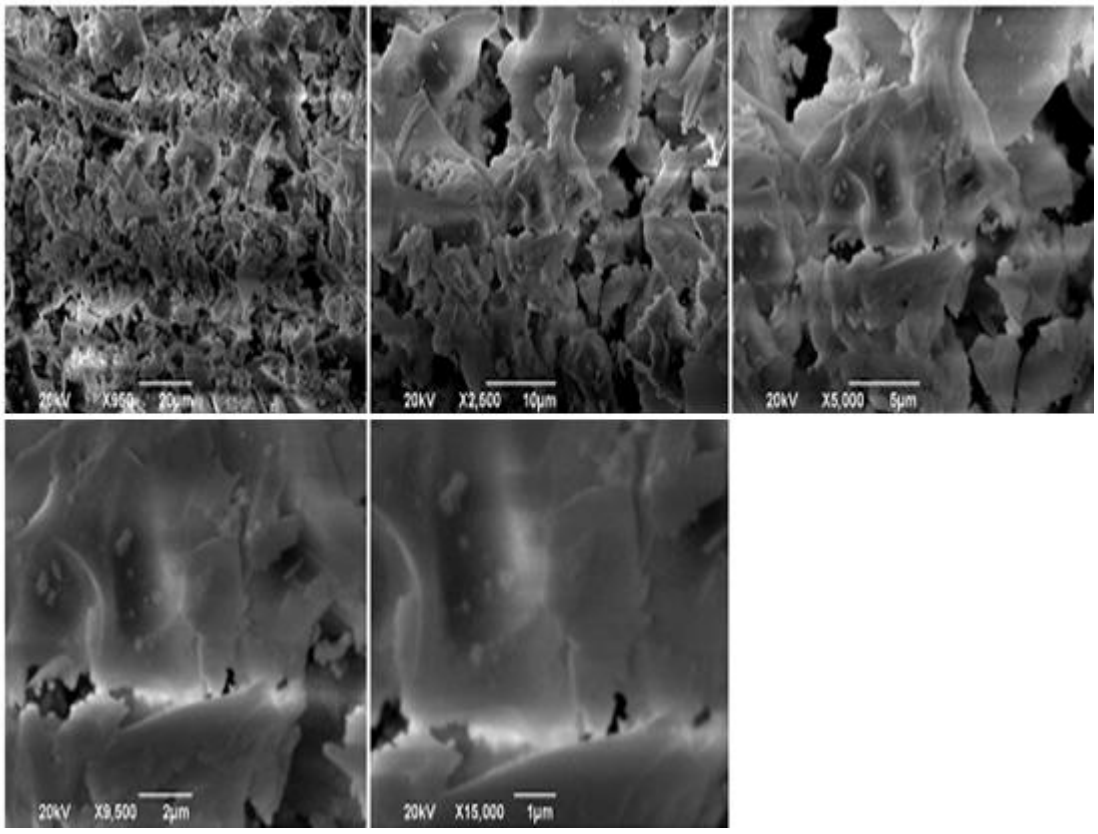

Figure 91. The SEM micrographs of 0.50 mol Mn^{3+} doped $Ho_3Al_5O_{12}$

The EDX analysis shown in figure 92 and table 9 determined that the peak intensities of the 0.50 mol Mn^{3+} doped $Ho_3Al_5O_{12}$ as expected as like in the 0.10 and 0.25 mol Mn^{3+} doped holmium garnets.

Table 9. The EDX analysis of 0.50 mol Mn^{3+} doped $Ho_3Al_5O_{12}$

Elt.	Line	Intensity (c/s)	Error 2-sig	Conc	Units	
O	Ka	47.11	2.506	20.685	wt.%	
Al	Ka	108.37	3.801	14.805	wt.%	
Mn	Ka	22.06	1.715	3.095	wt.%	
Ho	La	79.22	3.250	61.415	wt.%	
				100.000	wt.%	Total

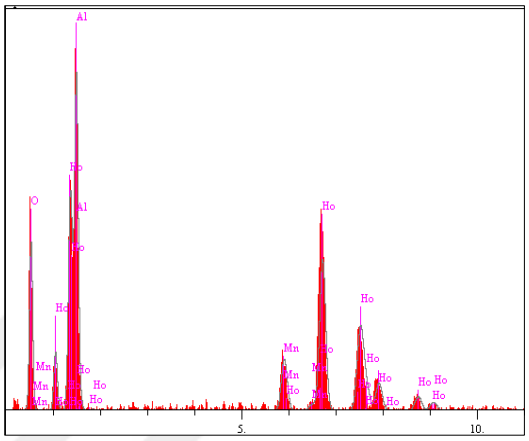

Figure 92. The EDX analysis of 0.50 mol Mn^{3+} doped $Ho_3Al_5O_{12}$

The SEM images of 0.75 mol Mn^{3+} doped $Ho_3Al_5O_{12}$ can be seen in figure 93. The craky plate-like pieces can be observe in these images, easily.

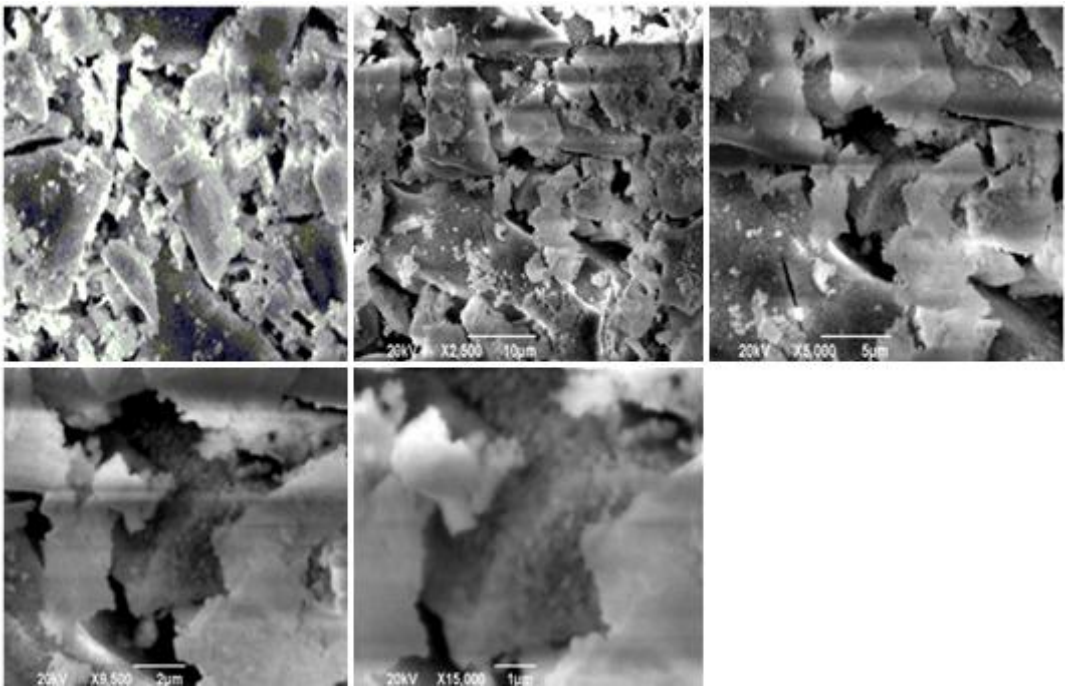

Figure 93. The SEM micrographs of 0.75 mol Mn^{3+} doped $Ho_3Al_5O_{12}$

The EDX analysis shown in figure 94 and table 10 determined that the peak intensities of the 0.75 mol Mn^{3+} doped $Ho_3Al_5O_{12}$ as expected as like in the 0.10, 0.25 and 0.75 mol Mn^{3+} doped holmium garnets.

Table 10. The EDX analysis of 0.75 mol Mn^{3+} doped $Ho_3Al_5O_{12}$

Elt.	Line	Intensity (c/s)	Error 2-sig	Conc	Units	
O	Ka	51.40	2.618	22.991	wt.%	
Al	Ka	117.65	3.960	16.346	wt.%	
Mn	Ka	35.07	2.162	5.162	wt.%	
Ho	La	67.79	3.006	55.502	wt.%	
				100.000	wt.%	Total

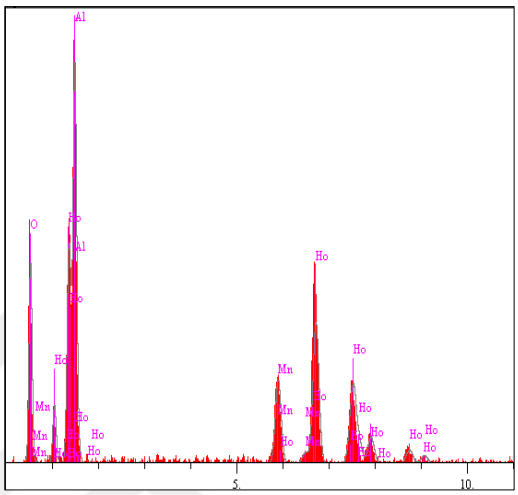

Figure 94. The EDX analysis of 0.75 mol Mn^{3+} doped $Ho_3Al_5O_{12}$

4.3.3 The studies for Fe^{3+} doped HAG (Fe:HAG)

4.3.3.1 The XRD studies of Fe:HAG

The XRD was also used to analysis the different amount of Fe^{3+} doped holmium garnet, structured molecular formula in $Ho_3Al_5O_{12}$. Skaudzius, R.et al., (2012), synthetized vary of $Y_3Al_{5-x}M_xO_{12}$ by obtaining of Y-Al-M-O (M=transition metals) precursor gels at first by using nitrates as starting materials and indicated the typical XRD patterns. In this study, the XRD results are coincided with studies of Skaudzius, R.et al., (2012) and Garskaite, E. et al., (2006).

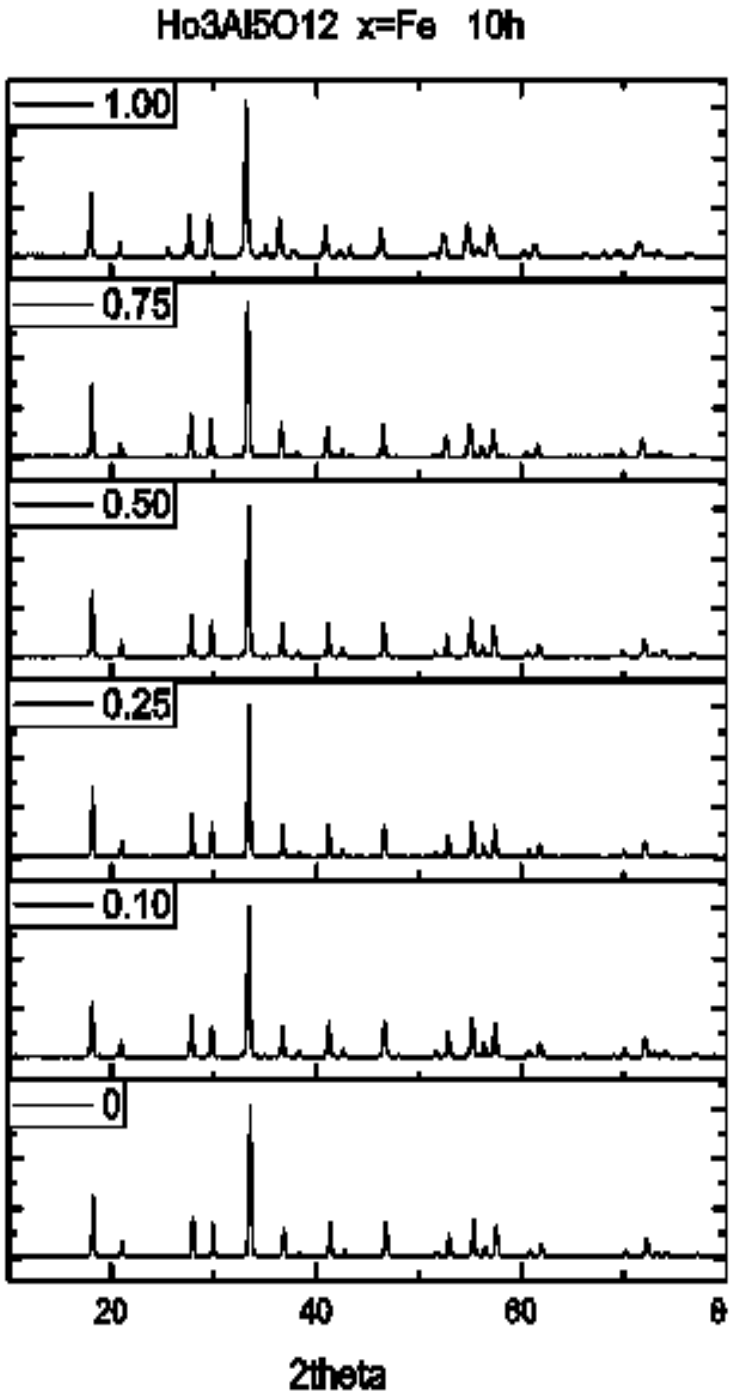

Figure 95. The XRD patterns of Fe^{3+} doped $Ho_3Al_5O_{12}$

The Figure 95 shows the XRD patterns of Fe^{3+} doped holmium garnets. All of the 0.10, 0.25, 0.50, 0.75 ve 1.00 mol Fe^{3+} doped $Ho_3Al_5O_{12}$ garnets are observed by XRD and the results are the same with the undoped garnet. So according to XRD analysis of Fe^{3+} doped $Ho_3Al_5O_{12}$ garnets there is no change in the structure of garnets as can be seen from figure 95.

4.3.3.2 The FTIR spectroscopy studies of Fe:HAG

The infrared peaks are demonstrated that the characteristic Fe-Al-O streching lines under 900 cm^{-1} (Garskaite, E. et al., 2006).

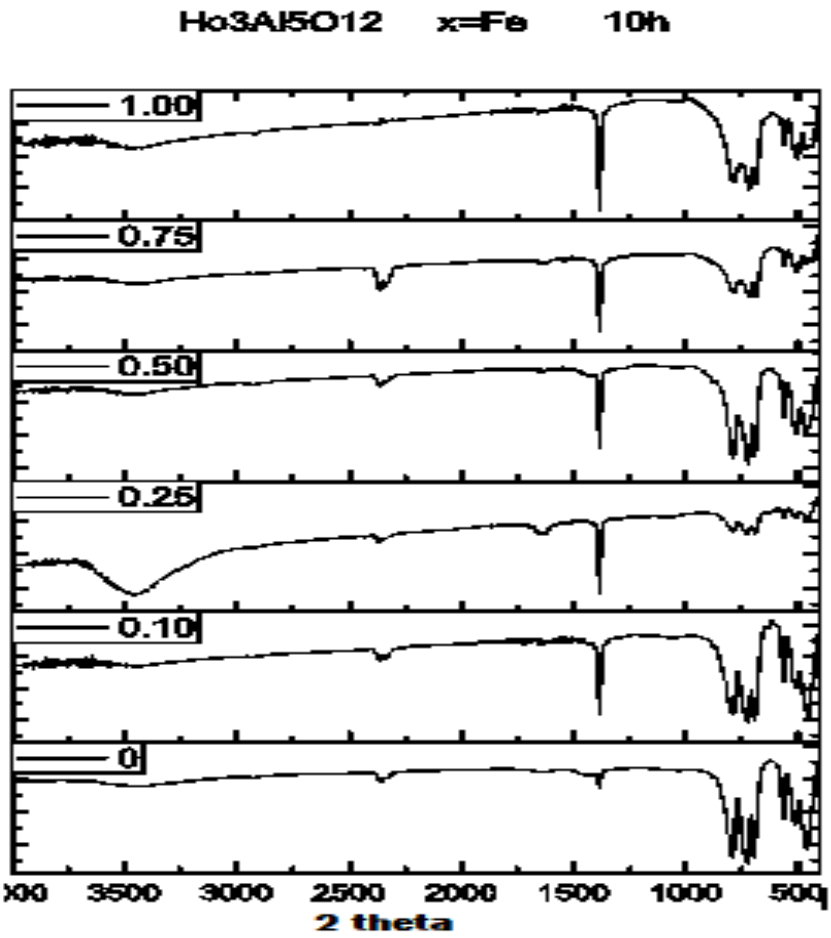

Figure 96. The FTIR spectroscopy of Fe^{3+} doped $Ho_3Al_5O_{12}$

4.3.3.3 The UV-vis/DRS studies of Fe:HAG

The absorbance and reflectance spectra of Fe^{3+} doped $Ho_3Al_5O_{12}$ garnets are shown in figures 97 and 98 respectively. There is a change in line extension and small peak shifts after Fe^{3+} doping may since comes from magnetic dipole moment presents of iron. When doping level is increased more then 0.10% the absorbance of UV region of spectra is increasing, as well. So the peak around 420 nm disappears. After the 0.25% level of Fe^{3+} doping the other peaks are also disappearing gradually but not completely. When the Fe^{3+} doping level is increased the absorbance level of the holmium aluminum garnet is increasing in all wavelengths. It should also be

indicated that all level Fe^{3+} doped $Ho_3Al_5O_{12}$ garnets are showing the same absorbance spectra. Red-shift is observed by increasing Fe^{3+} molar amount in the sample. This situation can be concluded as there is no structural change after the doping Fe^{3+} into the holmium aluminum garnet. This result is compatible with the results those are obtained from FTIR, XRD, SEM and EDX studies.

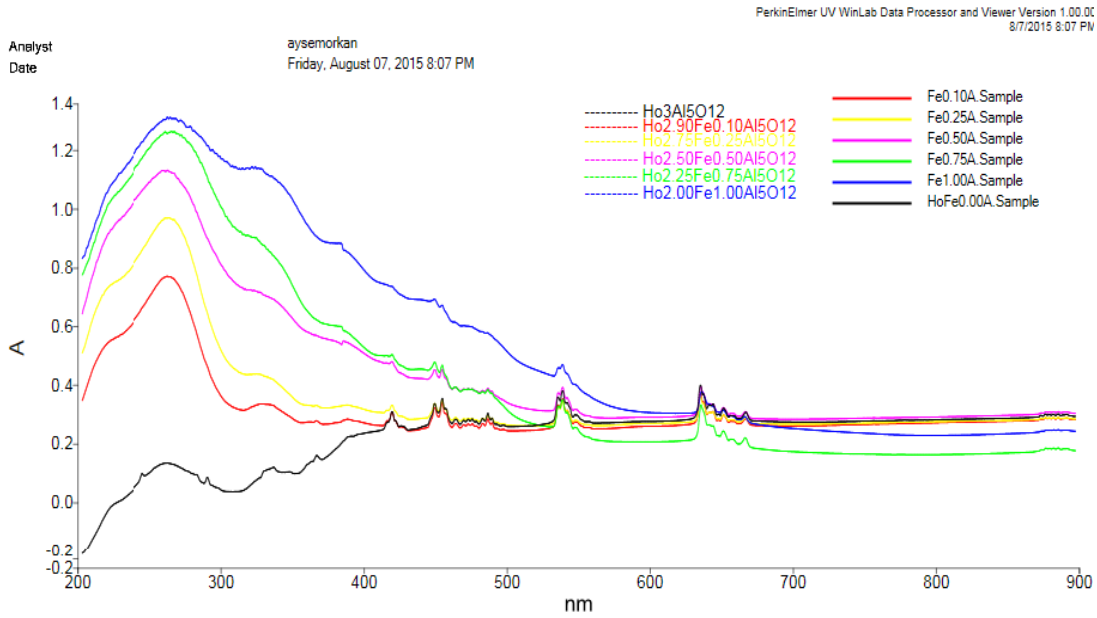

Figure 97. The UV-vis/DRS absorption spectra of Fe^{3+} doped $Ho_3Al_5O_{12}$

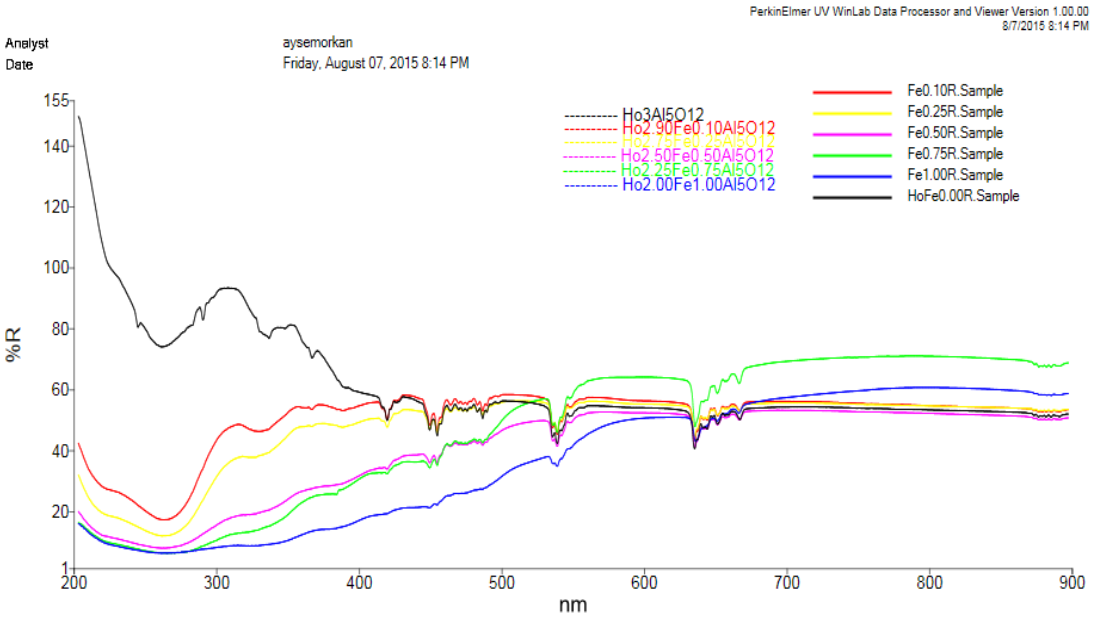

Figure 98. The UV-vis/DRS reflection spectra of Fe^{3+} doped $Ho_3Al_5O_{12}$

4.3.3.4 The SEM and EDX studies of Fe:HAG

The SEM images of 0.10 mol Fe^{3+} doped $Ho_3Al_5O_{12}$ can be seen in figure 99. It can be seen clearly from figure that the doped Fe^{3+} is covered on the surface of the holmium garnet. The large-grains can be observe with small pieces onto them.

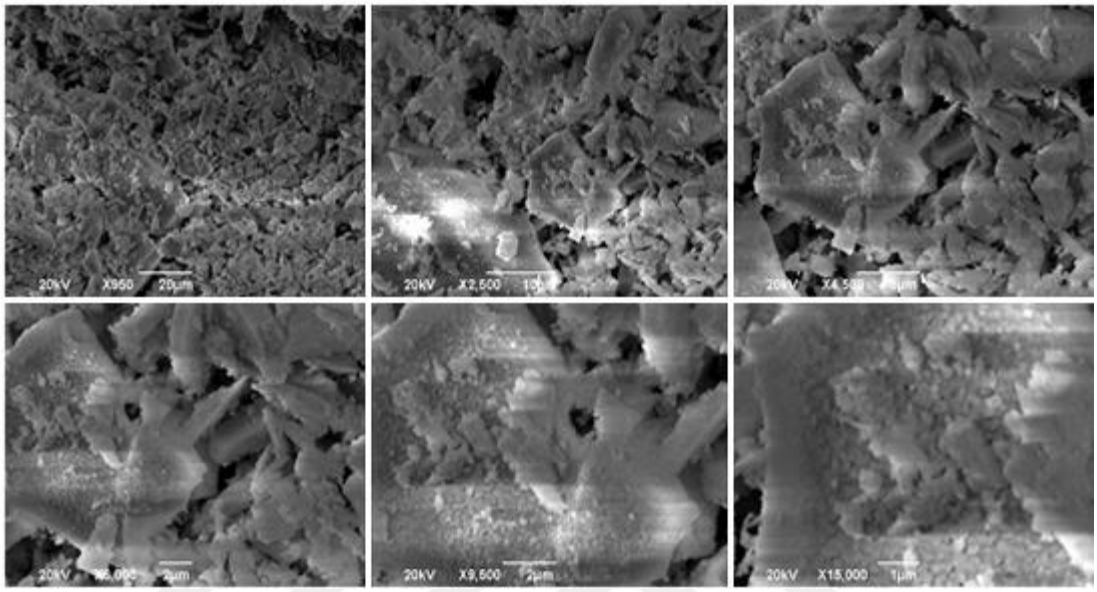

Figure 99. The SEM micrographs of 0.10 mol Fe^{3+} doped $Ho_3Al_5O_{12}$

The EDX analysis shown in figure 100 and table 11 determined that the peak intensities of the 0.10 mol Fe^{3+} doped $Ho_3Al_5O_{12}$.

Table 11. The EDX analysis of 0.10 mol Fe^{3+} doped $Ho_3Al_5O_{12}$

Elt.	Line	Intensity (c/s)	Error 2-sig	Conc	Units	
O	Ka	41.67	2.357	19.658	wt.%	
Al	Ka	99.53	3.642	14.526	wt.%	
Fe	Ka	3.41	0.674	0.552	wt.%	
Ho	La	80.55	3.277	65.263	wt.%	
				100.000	wt.%	Total

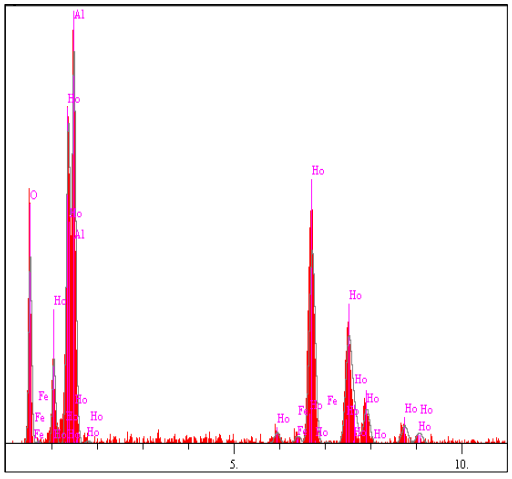

Figure 100. The EDX analysis of 0.10 mol Fe^{3+} doped $Ho_3Al_5O_{12}$

The SEM images of 0.25 mol Fe^{3+} doped $Ho_3Al_5O_{12}$ can be seen in figure 101. It can be seen clearly from figure that the doped Fe^{3+} is covered on the surface of the holmium garnet. The plate-like large-grains can be observe with small pieces onto them.

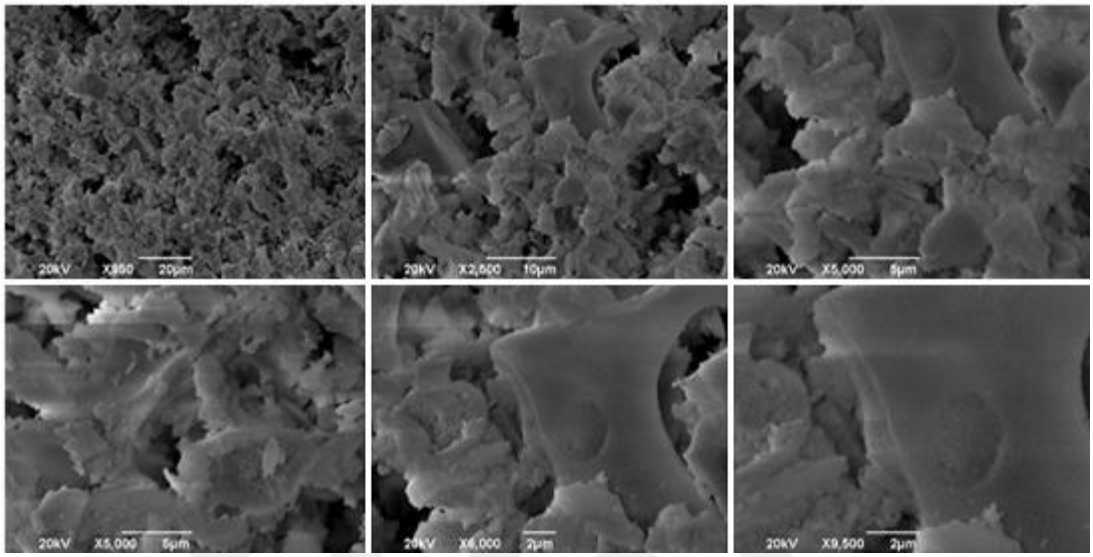

Figure 101. The SEM micrographs of 0.25 mol Fe^{3+} doped $Ho_3Al_5O_{12}$

The EDX analysis shown in figure 102 and table 12 determined that the peak intensities of the 0.10 mol Fe^{3+} doped $Ho_3Al_5O_{12}$ as expected as like in the 0.10 mol Fe^{3+} doped holmium garnets.

Table 12. The EDX analysis of 0.25 mol Fe^{3+} doped $Ho_3Al_5O_{12}$

Elt.	Line	Intensity (c/s)	Error 2-sig	Conc	Units	
O	Ka	39.75	2.302	18.039	wt.%	
Al	Ka	94.15	3.543	13.326	wt.%	
Fe	Ka	9.41	1.120	1.451	wt.%	
Ho	La	87.08	3.407	67.184	wt.%	
				100.000	wt.%	Total

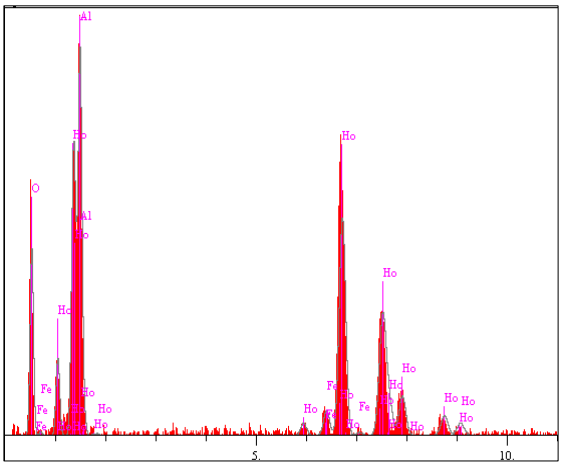

Figure 102. The EDX analysis of 0.25 mol Fe^{3+} doped $Ho_3Al_5O_{12}$

The SEM images of 0.50 mol Fe^{3+} doped $Ho_3Al_5O_{12}$ can be seen in figure 103. It can be seen clearly from figure that the doped Fe^{3+} is covered on the surface of the holmium garnet as like in the 0.10 mol and 0.25 mol Fe^{3+} doped holmium garnets.

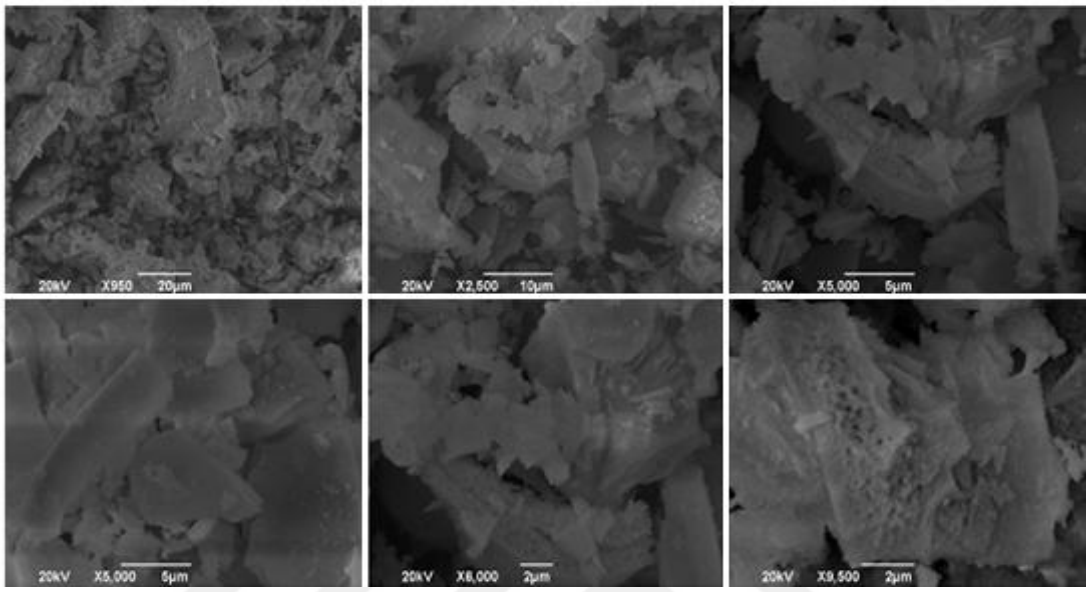

Figure 103. The SEM micrographs of 0.50 mol Fe^{3+} doped $Ho_3Al_5O_{12}$

The EDX analysis shown in figure 104 and table 13 determined that the peak intensities of the 0.10 mol Fe^{3+} doped $Ho_3Al_5O_{12}$ as expected as like in the 0.10 mol and 0.25 mol Fe^{3+} doped holmium garnets.

Table 13. The EDX analysis of 0.50 mol Fe^{3+} doped $Ho_3Al_5O_{12}$

Elt.	Line	Intensity (c/s)	Error 2-sig	Conc	Units	
O	Ka	38.49	2.265	17.053	wt.%	
Al	Ka	97.97	3.614	13.548	wt.%	
Fe	Ka	21.16	1.679	3.185	wt.%	
Ho	La	87.90	3.423	66.214	wt.%	
				100.000	wt.%	Total

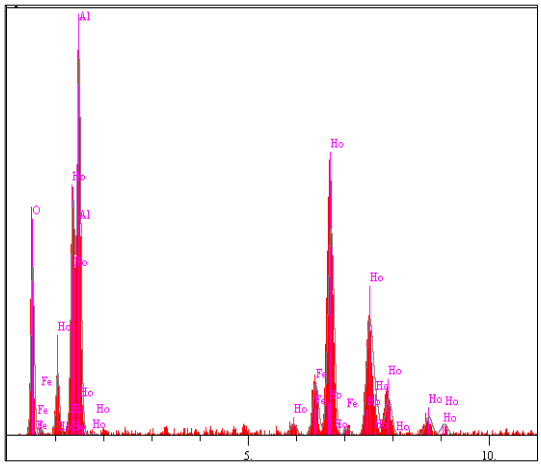

Figure 104. The EDX analysis of 0.50 mol Fe^{3+} doped $Ho_3Al_5O_{12}$

The SEM images of 0.75 mol Fe^{3+} doped $Ho_3Al_5O_{12}$ can be seen in figure 105. It can be seen clearly from figure that the doped Fe^{3+} is covered on the surface of the holmium garnet as like in the 0.10 mol, 0.25 mol and 0.50 mol Fe^{3+} doped holmium garnets.

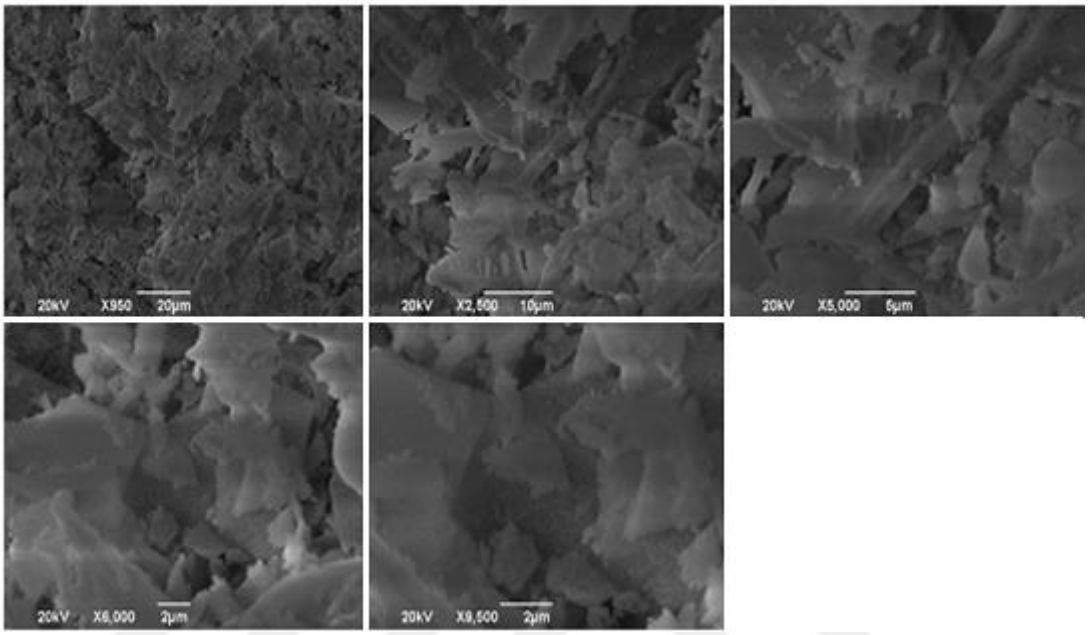

Figure 105. The SEM micrographs of 0.75 mol Fe^{3+} doped $Ho_3Al_5O_{12}$

The EDX analysis shown in Figure 106 and Table 14 determined that the peak intensities of the 0.75 mol Fe^{3+} doped $Ho_3Al_5O_{12}$ as expected as like in the 0.10 mol, 0.25 mol, and 0.50 mol Fe^{3+} doped holmium garnets.

Table 14. The EDX analysis of 0.75 mol Fe^{3+} doped $Ho_3Al_5O_{12}$

Elt.	Line	Intensity (c/s)	Error 2-sig	Conc	Units	
O	Ka	38.52	2.266	16.465	wt.%	
Al	Ka	88.19	3.429	11.937	wt.%	
Fe	Ka	31.78	2.058	4.618	wt.%	
Ho	La	92.16	3.505	66.980	wt.%	
				100.000	wt.%	Total

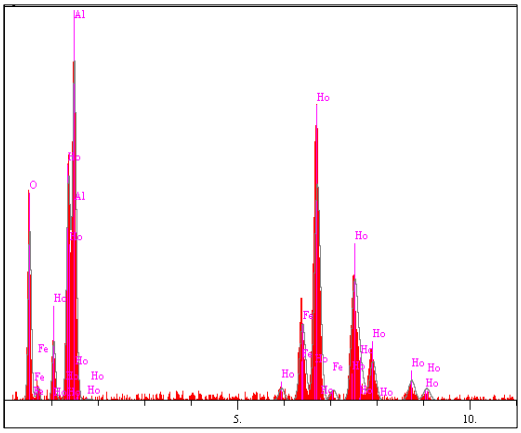

Figure 106. The EDX analysis of 0.75 mol Fe^{3+} doped $Ho_3Al_5O_{12}$

The SEM images of 1.00 mol Fe^{3+} doped $Ho_3Al_5O_{12}$ can be seen in figure 107. It can be seen clearly from figure that the doped Fe^{3+} is covered on the surface of the holmium garnet as like in the 0.10 mol, 0.25 mol, 0.50 mol and 0.75 mol Fe doped holmium garnets.

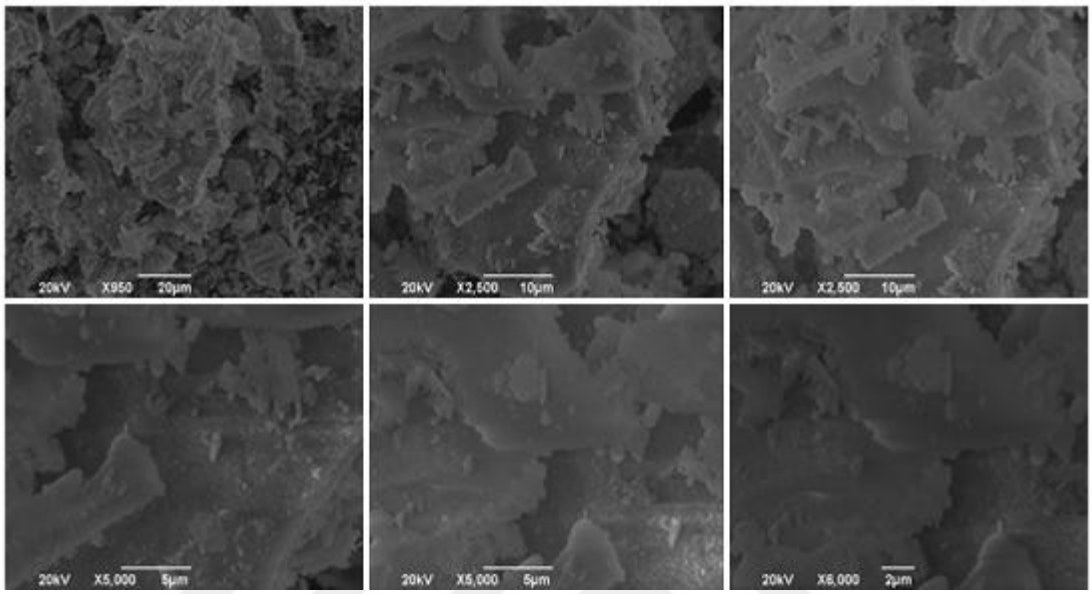

Figure 107. The SEM micrographs of 1.00 mol Fe^{3+} doped $Ho_3Al_5O_{12}$

The EDX analysis shown in Figure 108 and Table 15 determined that the peak intensities of the 1.00 mol Fe^{3+} doped $Ho_3Al_5O_{12}$ as expected as like in the 0.10 mol, 0.25 mol, 0.5 mol and 0.75 mol Fe^{3+} doped holmium garnets.

Table 15. The EDX analysis of 1.00 mol Fe^{3+} doped $Ho_3Al_5O_{12}$

Elt.	Line	Intensity (c/s)	Error 2-sig	Conc	Units	
O	Ka	39.02	2.281	19.405	wt.%	
Al	Ka	106.42	3.767	16.416	wt.%	
Fe	Ka	41.14	2.342	7.228	wt.%	
Ho	La	64.65	2.936	56.951	wt.%	
				100.000	wt.%	Total

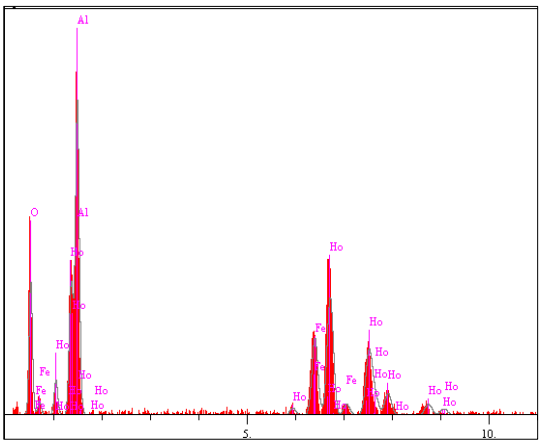

Figure 108. The EDX analysis of 1.00 mol Fe^{3+} doped $Ho_3Al_5O_{12}$

5. CONCLUSION

In the first part of the study; the precursor gels were prepared to synthesize of Eu^{3+} doped to holmium aluminum garnet ($Ho_{3-x}Eu_xAl_5O_{12}$) dysprosium aluminum garnet ($Dy_{3-x}Eu_xAl_5O_{12}$) and terbium aluminum garnet ($Tb_{3-x}Eu_xAl_5O_{12}$), in molar ratios of 0.10, 0.25, 0.50, 0.75 and 1.00 by using aqueous sol-gel technique.

In the second part; Cr^{3+} , Mn^{3+} and Fe^{3+} were used as doping agents separetely into holmium aluminum garnets ($Ho_{3-x}Cr_xAl_5O_{12}$, $Ho_{3-x}Mn_xAl_5O_{12}$, $Ho_{3-x}Fe_xAl_5O_{12}$), with the same molar ratios of 0.10, 0.25, 0.50, 0.75, 1.00 to synthesize with aqueous sol-gel method.

The gelation processes for all products were succesfully done at low temperature ($\sim 100^oC$). The gel products were heated to obtain crystalline garnets at $1000\ ^oC$.

According to the FTIR studies, the organic residues have flown after 10 hours for all products. The vibrational bands of M-O bonds have been seen under $1000cm^{-1}$ like that of typical garnet crystals.

All XRD patterns showed the same hkl values. It indicated that the all metal doping processes have been done succesfully without any change in the crystal structure of the monophasic host garnet materials.

The curves observed in the thermal analysis through TG/DTA indicated that all prepared garnets were thermodynamically stable upon 900^oC since the very small amount of weight loss was observed after 900^oC.

The SEM studies showed that the lanthanide aluminum garnets were in the same plate-like shape, independently the nature of the lanthanides or doping agents of Eu^{3+}, Cr^{3+}, Mn^{3+}, Fe^{3+}.

The EDX studies showed, the intensities of the lanthanide (Ho, Dy or Tb) decreased, while the intensities of the doping agents (Eu^{3+}, Cr^{3+}, Mn^{3+}, Fe^{3+}) increased depending on the increasing amount of the doping agents.

The UV-vis/DRS studies demonstrated that the minimum and maximum values of absorption and reflection for all garnets prepared in this work. The results can be assessable to have good absorbent materials. In addition, red-shifts and blue shifts were detected depending on the increasing or decreasing amounts of doping agents.

According to the UV-vis/DRS studies:

- $Ho_{3-x}Al_xO_{12}:Eu^{3+}$ showed red-shift, while the Eu^{3+} concentration increased, regularly.

- $Dy_{3-x}Al_xO_{12}:Eu^{3+}$ showed blue-shift by increasing Eu^{3+} concentration up to x=0.75 mol of Eu^{3+} while the red-shift was observed after 0.75.

- $Tb_{3-x}Al_xO_{12}:Eu^{3+}$ showed blue-shift, while the Eu^{3+} concentration increased, regularly.

- $Ho_{3-x}Al_xO_{12}:Cr^{3+}$ showed blue-shift, by increasing the concentration of the Cr^{3+}, regularly.

- $Ho_{3-x}Al_xO_{12}:Mn^{3+}$ showed blue-shift by increasing Mn^{3+} concentration, up to x=0.75 mol of Mn^{3+} while the red-shift was observed after 0.75.

- $Ho_{3-x}Al_xO_{12}:Fe^{3+}$ showed red-shift by increasing the concentration of the Fe^{3+} , regularly.

6. REFERENCES

Anh T, Benalloul P, Barthou C, Giang LT, Vu N, & Minh L (2007). Luminescence, energy transfer, and upconversion mechanisms of Y_2O_3 nanomaterials doped with Eu^{3+}, Tb^{3+}, Tm^{3+}, Er^{3+}, and Yb^{3+} ions. Journal of Nanomaterials, 2007 (1), 4.

Armbruster T, Geiger CA, Lager GA (1992) "Single-crystal X-ray structure study of synthetic pyrope almandine garnets at 100 and 293 K." American Mineralogist, 77(5-6), 512-521.

Badar N, Kamarulzaman N, Rusdi R, Aziz ND A, & Fun HK (2014). Increased conductivities of Cr doped $Al_{2-x}Cr_xO_3$ powders due to band gap narrowing. Physica B: Condensed Matter, 437, 32-35.

Berezovskaya IV, Khomenko OV, Poletaev NI, Khlebnikova ME, Stoyanova IV, Efryushina, NP, & Dotsenko VP (2018). Oxidation states and microstructure of manganese impurity centers in nanosized Al_2O_3 obtained by combustion method. Functional materials.

Bishop A, Woolley A, & Hamilton W (1999) Cambridge guide to minerals, rocks and fossils. 2nd edition. Cambridge University Press, Cambridge.

Blosi M, Albonetti S, Dondi M, Costa AL, Ardit M, & Cruciani G (2009). Sol–gel combustion synthesis of chromium doped yttrium aluminum perovskites. Journal of sol-gel science and technology, 50(3), 449-455.

Boyer JC (2006) Synthesis and spectroscopy of upconverting lanthanide-doped nanocrystals (Doctoral dissertation, Concordia University), Montreal, Quebee.

Burshtein Z, Blau P, Kalisky Y, Shimony Y, Kikta MR (1998) "Excited- state absorption studies of Cr/sup 4+/ions in several garnet host crystals." IEEE journal of quantum electronics, 34(2), 292-299.

Clark G, Clark JGD (1986) Symbols of excellence: precious materials as expressions of status. Cambridge university press.

Chroma M, Pinkas J, Pakutinskiene I, Beganskiene A, Kareiva A (2005) "Processing and characterization of sol–gel fabricated mixed metal aluminates." Ceramics International, 31(8), 1123-1130.

Dong D, Xiao-Yu K, Jian-Jun G, Hui W, Kang-Wei Z (2005) Optical absorption and EPR study of the octahedral Fe 3+ center in yttrium aluminum garnet. Physical Review B, 72(7), 073101.

Dong B, Yang H, Cui Y, Yu L, Feng S (2007) "The magnetic properties of $BiY_2Fe_5O_{12}$ nanoparticles doped with Cr ions." Journal of materials science, 42(9), 3167-3171.

Dubnikova N, Garskaite E, Beganskiene A, Kareiva A (2011) "Sol–gel synthesis and characterization of sub-microsized lanthanide (Ho, Tm, Yb, Lu) aluminium garnets." Optical Materials, 33(8), 1179-1184.

Dubnikova N, Garskaite E, Pinkas J, Bezdicka P, Beganskiene A, Kareiva A (2010) "Sol–gel preparation of selected lanthanide aluminium garnets." Journal of sol-gel science and technology, 55(2), 213-219.

Eilers-Rethwisch M, Winter M, & Schappacher FM (2018). Synthesis, electrochemical investigation and structural analysis of doped $Li[Ni_{0.6}Mn_{0.2}Co_{0.2-x}M_x]O_2$ (x= 0, 0.05; M= Al, Fe, Sn) cathode materials. Journal of Power Sources, 387, 101-107.

Esparza-García AE, García-Hipólito M, Aguilar-Frutis MA & Falcony C (2002). Cathodoluminescent and photoluminescent properties of Al_2O_3 powders doped with Eu. physica status solidi (a), 193(1), 117-124.

Evans JG, Moyle PR, Bliss JD, Long KR (2006).US industrial garnet. US Department of the Interior, US Geological Survey, California.

Galoisy L (2013) "Garnet: From stone to star", Elements, 9(6), 453-456.

Garskaite E, Gibson K, Leleckaite A, Glaser J, Niznansky D, Kareiva A, Meyer HJ, (2006) "On the synthesis and characterization of iron-containing garnets ($Y_3Fe_5O_{12}$, YIG and $Fe_3Al_5O_{12}$, IAG)", Chemical physics, 323(2-3), 204-210.

Gasenkova IV, Mukhurov NI, Zhvavyi SP, Kolesnik EE, & Stupak AP (2017). Photoluminescent properties of nanoporous anodic alumina doped with manganese ions. Journal of Luminescence, 185, 298-305.

Grew ES, Locock AJ, Mills SJ, Galuskina IO, Galuskin EV, Halenius U (2013) "Nomenclature of the garnet supergroup", American Mineralogist, 98(4), 785-811.

Guillot, M, Feldmann P, Le Gall H, Fadly M (1978) "Molecular field coefficients of terbium, dysprosium and holmium iron garnets.", IEEE Transactions on Magnetics, 14(5), 909-911.

Hirata G, Perea N, Tejeda M, Gonzalez-Ortega JA, McKittrick J (2005) "Luminescence study in Eu-doped aluminum oxide phosphors.", Optical Materials, 27(7), 1311-1315.

Hreniak D, Stręk W, Mazur P, Pazik R, Ząbkowska-Wacławek M (2004) "Luminescence properties of Tb^{3+}: $Y_3Al_5O_{12}$ nanocrystallites prepared by the sol–gel method.", Optical Materials, 26(2), 117-121.

Hreniak D, Strek W (2002) "Synthesis and optical properties of Nd^{3+} doped $Y_3Al_5O_{12}$ nanoceramics.", Journal of Alloys and Compounds, 341(1-2), 183-186.

Hsu WT, Wu WH, Lu CH (2003) "Synthesis and luminescent properties of nano-sized $Y_3Al_5O_{12}$: Eu^{3+} phosphors.", Materials Science and Engineering: B, 104(1-2), 40-44.

Ilić S, Zec S, Miljković M, Poleti D, Pošarac-Marković M, Janaćković D, & Matović B (2014). Sol–gel synthesis and characterization of iron doped mullite. Journal of Alloys and Compounds, 612, 259-264.

Jou Yeong-chin, et al. (2007) "High-power holmium: yttrium-aluminum-garnet laser for percutaneous treatment of large renal stones.", Urology, 69.1: 22-25.

Jou YC, Shen JH, Cheng MC, Lin CT, Chen PC (2005) "Percutaneous nephrolithotomy with holmium: yttrium-aluminum-garnet laser and fiber guider—report of 349 cases.", Urology, 65(3), 454-458.

Katelnikovas A, Vitta P, Pobedinskas P, Tamulaitis G, Žukauskas A, Jørgensen JE, Kareiva A (2007) "Photoluminescence in sol–gel-derived YAG: Ce phosphors.", Journal of Crystal Growth, 304(2), 361-368.

Kareiva A (2011) "Aqueous sol-gel synthesis methods for the preparation of garnet crystal structure compounds.", Materials Science, 17(4), 428-436.

Kuwano Y, Suda K, Ishizawa N, Yamada T (2004) "Crystal growth and properties of $(Lu,Y)_3Al_5O_{12}$.", Journal of crystal growth, 260(1-2), 159-165.

Kim CS, Min BK, Kim SJ, Yoon SR, Uhm YR (2003) "Crystallographic and magnetic properties of $Y_3Fe_{5-x}Al_xO_{12}$.", Journal of magnetism and magnetic materials, 254, 553-555.

Kuklja MM (2000) "Defects in yttrium aluminium perovskite and garnet crystals: atomistic study.", Journal of Physics: Condensed Matter, 12(13), 2953.

Kumar GA, Lu J, Kaminskii AA, Ueda KI, Yagi H, Yanagitani T, Unnikrishnan NV (2004) "Spectroscopic and stimulated emission Characteristics of Nd/sup 3+/in transparent YAG ceramics.", IEEE journal of quantum electronics, 40(6), 747-758.

Leleckaite A, Kareiva A (2004) "Synthesis of garnet structure compounds using aqueous sol–gel processing.", Optical Materials, 26(2), 123-128.

Li X, Liu H, Wang J, Cui H, Han F (2004) "YAG: Ce nano-sized phosphor particles prepared by a solvothermal method.", Materials Research Bulletin, 39(12), 1923-1930.

Li J, Li JG, Liu S, Li X, Sun X, Sakka Y (2013) "Greatly enhanced Dy^{3+} emission via efficient energy transfer in gadolinium aluminate garnet ($Gd_3Al_5O_{12}$) stabilized with Lu^{3+}.", Journal of Materials Chemistry C, 1(45), 7614-7622.

Lu J, Ueda KI, Yagi H, Yanagitani T, Akiyama Y, Kaminskii AA (2002) "Neodmium doped yttrium aluminum garnet ($Y_3Al_5O_{12}$) nanocrystalline ceramics a new generation of solid state laser and optical materials.", Journal of alloys and compounds, 341(1-2), 220-225.

Malinowski M, Frukacz Z, Szuflińska M, Wnuk A, Kaczkan M (2000) "Optical transitions of Ho^{3+} in YAG.", Journal of alloys and compounds, 300, 389-394.

Marius M, Popovici EJ, Barbu-Tudoran L, Indrea E, Mesaros A (2014) "Cerium-doped yttrium aluminate-based phosphors prepared by wet-chemical synthesis route: Modulation of the luminescence color by changing the host-lattice composition.", Ceramics International, 40(4), 6233-6239.

Mathur S, Shen H, Leleckaite A, Beganskiene A, Kareiva A (2005) "Low-temperature synthesis and characterization of yttrium–gallium garnet $Y_3Ga_5O_{12}$ (YGG).", Materials research bulletin, 40(3), 439-446.

Matsubara I, Paranthaman M, Allison SW, Cates MR, Beshears DL, Holcomb, DE, (2000). "Preparation of Cr-doped $Y_3Al_5O_{12}$ phosphors by heterogeneous precipitation methods and their luminescent properties.", Materials research bulletin, 35(2), 217-224.

Muliuoliene I, Mathur S, Jasaitis D, Shen H, Sivakov V, Rapalaviciute R, Kareiva A, (2003). "Evidence of the formation of mixed-metal garnets via sol–gel synthesis.", Optical Materials, 22(3), 241-250.

Nagata S, Sasaki H, Suzuki K, Kiuchi J, Wada N (2001) "Specific heat anomaly of the holmium garnet $Ho_3Al_5O_{12}$ at low temperature.", Journal of Physics and Chemistry of Solids, 62(6), 1123-1130.

Nivaldo JT (2014) Chemistry: Structure and Properties, 1st edition, Pearson Education, Inc., Upper Saddle River, NJ.

Novak GA, Gibbs GV (1971) "The crystal chemistry of the silicate garnets.", American Mineralogist: Journal of Earth and Planetary Materials, 56(5-6), 791-825.

Pang M, & Lin J (2005). Growth and optical properties of nanocrystalline $Gd_3Ga_5O_{12}$: Ln (Ln= Eu^{3+}, Tb^{3+}, Er^{3+}) powders and thin films via Pechini sol–gel process. Journal of Crystal Growth, 284(1-2), 262-269.

Pavasaryte L, Katelnikovas A, Momot A, Reekmans G, Hardy A, Van Bael M, ... & Kareiva A (2019). Eu^{3+}-Doped $Ln_3Al_5O_{12}$ (Ln= Er, Tm, Yb, Lu) garnets: Synthesis, characterization and investigation of structural and luminescence properties. Journal of Luminescence, 212, 14-22.

Qu X, Cao L, Liu W, & Su G (2012). Sol–gel synthesis and luminescence properties of $CdSiO_3$: Mn^{2+}, Eu^{3+} phosphor. Journal of Alloys and Compounds, 533, 83-87.

Qu X, Cao L, Liu W, Su G, Wang P, & Schultz I (2012). Sol–gel synthesis of long-lasting phosphors $CdSiO_3$: Mn^{2+}, RE^{3+} (RE= Tb, Eu, Nd) and luminescence mechanism research. Materials Research Bulletin, 47(6), 1598-1603.

Ruan SK, Zhou JG, Zhong AM, Duan JF, Yang XB, Su MZ (1998) "Synthesis of $Y_3Al_5O_{12}$: Eu^{3+} phosphor by sol-gel method and its luminescence behavior.", Journal of alloys and compounds, 275, 72-75.

Shikao S, Jiye W (2001) "Combustion synthesis of Eu^{3+} activated $Y_3Al_5O_{12}$ phosphor nanoparticles.", Journal of alloys and compounds, 327(1-2), 82-86.

Si W, Ding C, Ding S (2014) "Synthesis and characterization of YAG nanoparticles by ultrasound-assisted and ultrasound-microwave-assisted alkoxide hydrolysis precipitation methods.", Journal of Nanomaterials, 218.

Singh V, Chakradhar RPS, Rao JL, Kwak HY (2010) "Green luminescence and EPR studies on Mn-activated yttrium aluminum garnet phosphor.", Applied Physics B, 98(2-3), 407-415.

Skaudzius R, Pinkas J, Raudonis R, Selskis A, Juskenas R, Kareiva A (2012) "On the limitary radius of garnet structure compounds Y3Al5− xMxO12 (M= Cr, Co, Mn, Ni, Cu) and $Y_3Fe_{5-x}Co_xO_{12}$ ($0 \leq x \leq 2.75$) synthesized by sol–gel method.", Materials Chemistry and Physics, 135(2-3),479-485.

Sugiyama M, Yanagida T, Fujimoto Y, Yokota Y, Ito A, Nikl M, Yoshikawa A (2012) "Basic study of Eu^{2+} doped garnet ceramic scintillator produced by spark plasma sintering.", Optical Materials, 35(2), 222-226.

Thirumalaisamy TK, Lakshmi Sri KJ, & Saravanan R (2011). Local structural analysis of Al_2O_3, Cr: Al_2O_3 and V: Al_2O_3 using Powder XRD. In Materials Science Forum (Vol. 671, pp. 131-152). Trans Tech Publications.

Vajargah SH, Hosseini HM, Nemati ZA (2007) "Preparation and characterization of yttrium iron garnet (YIG) nanocrystalline powders by auto-combustion of nitrate-citrate gel.", Journal of alloys and compounds, 430(1-2), 339-343.

Vaqueiro P, López-Quintela MA (1998) "Synthesis of yttrium aluminum garnet by the citrate gel process.", Journal of Materials Chemistry, 8(1), 161-163.

Veith M, Mathur S, Kareiva A, Jilavi M, Zimmer M, Huch V (1999) "Low temperature synthesis of nanocrystalline $Y_3Al_5O_{12}$ (YAG) and Ce-doped $Y_3Al_5O_{12}$ via different sol–gel methods.", Journal of Materials Chemistry, 9(12), 3069-3079.

Vetrone F (2005) Luminescence spectroscopy of Er^{3+} doped inorganic nanocrystals: an investigation into their upconversion properties, (Doctoral dissertation, Concordia University), Montreal, Quebee.

Wang D, Tie S, & Wan X (2015). White light emitting from YVO_4/Y_2O_3: Eu^{3+}, Bi^{3+} composite phosphors for UV light-emitting diodes. Ceramics International, 41(6), 7766-7772.

Wilson DM, Visser LR (2001) "High performance oxide fibers for metal and ceramic composites.", Composites Part A: Applied Science and Manufacturing, 32 (8), 1143-1153.

Yi X, Zhou S, Chen C, Lin H, Feng Y, Wang K, Ni Y (2014) "Fabrication of Ce:YAG, Ce, Cr: YAG and Ce: YAG/Ce, Cr: YAG dual-layered composite phosphor ceramics for the application of white LEDs.", Ceramics International, 40(5), 7043-7047.

Yuan L, Han A, Ye M, Chen X, Ding C, & Yao L (2017). Synthesis and characterization of novel nontoxic $BiFe_{1-x}Al_xO_3$/mica-titania pigments with high NIR reflectance. Ceramics International, 43(18), 16488-16494.

Zabiliūtė-Karaliūnė A, Dapkus H, Petrauskas RP, Butkutė S, Žukauskas A, & Kareiva A (2015). Cr^{3+} doped yttrium gallium garnet for phosphor-conversion light emitting diodes. Lithuanian Journal of Physics, 55(3).

Zatryb G, Podhorodecki A, Serafińczuk J, Motyka M, Banski M, Misiewicz J, & Gaponenko NV (2013). Optical properties of Tb and Eu doped cubic $YAlO_3$ phosphors synthesized by sol–gel method. Optical Materials, 35(12), 2090-2094.

Zhang JJ, Ning JW, Liu XJ, PanYB, Huang LP (2003) "A novel synthesis of phase-pure ultrafine YAG: Tb phosphor with different Tb concentration.", Materials Letters, 57(20), 3077-3081.

Zhang JJ, Ning JW, Liu XJ, Pan YB, Huang LP (2003) "Synthesis of ultrafine YAG: Tb phosphor by nitrate–citrate sol–gel combustion process.", Materials research bulletin, 38(7), 1249-1256.

Zhang S, Zhang P, Liu X, Yang Z, Huang Y, Seo HJ (2018) "A red-emitting phosphor of $Li_5La_3Ti_2O_{12}$: Eu^{3+} with garnet-like structure and nearUV/blue light excitation.", Journal of Luminescence, 203, 152-159.

Zhong HJ, Chen GH, Cui SC, Chen JS, Yang Y, Zhou CR, & Yuan CL (2015). Luminescence and energy transfer of Tm/Tb/Mn tri-doped phosphate glass for white light-emitting diodes. Journal of Materials Science: Materials in Electronics, 26 (10), 8130-8135.

Zhou YH, LinJ, Wang SB, Zhang H (2002) "Preparation of $Y_3Al_5O_{12}$: Eu phosphors by citric–gel method and their luminescent properties.", Optical Materials, 20(1), 13-20.

Zhou, Y., Lin, J., Yu, M., & Wang, S (2004) "Comparative study on the luminescent properties of $Y_3Al_5O_{12}$: RE^{3+} (RE: Eu, Dy) phosphors synthesized by three methods.", Journal of alloys and compounds, 375(1-2), 93-97.

Zhou Y, Lin J, Yu M, Wang S, Zhang H (2002) "Synthesis-dependent luminescence properties of $Y_3Al_5O_{12}$: Re^{3+} (Re= Ce, Sm, Tb) phosphors.", Materials Letters, 56(5), 628-636.

Zinatloo-Ajabshir S, Mortazavi-Derazkola S, Salavati-Niasari, M (2017) "Sono-synthesis and characterization of Ho_2O_3 nanostructures via a new precipitation way for photocatalytic degradation improvement of erythrosine.", International Journal of Hydrogen Energy, 42(22), 15178-15188.

7. CURRICULUM VITAE

Name SURNAME : **Seval KARAKUŞ**

Place and Date of Birth : **İstanbul 23.07.1989**

Universities

Bachelor's Degree : **Bolu Abant Izzet Baysal University**

e-mail : **karakusevall@gmail.com**

Address : **Mecidiyeköy mah. Kısmet sok. No:10/5 Şişli/İSTANBUL**

List of Publications : **"MANGAN KATKILI GARNET KRİSTALLERİNİN SENTEZİ, OPTİK VE YAPISAL ÖZELLİKLERİNİN İNCELENMESİ" , 5. Ulusal Anorganik Kimya Kongresi, 2015, Mersin.**